Studies on DNA, Complexed by Surfactants or Modified with Pyrene

Inauguraldissertation

zur
Erlangung der Würde eines Doktors der Philosophie
vorgelegt der
Philosophisch-Naturwissenschaftlichen Fakultät
der Universität Basel

von

Stephan Bürgi

aus Pratteln (BL)

Basel 2010

Genehmigt von der Philosophisch-Naturwisschenschaftlichen Fakultät auf Antrag von

Prof. Dr. Bernd Giese

Prof. Dr. Helma Wennemers

Basel, den 22. April 2008

Prof. Dr. Hans-Peter Hauri
Dekan

The work presented here was initiated and supervised by Prof. Bernd Giese at the Chemistry Department of the University of Basel, during the time period November 2000 to April 2008.

Contents

Summary

0.1 The Outline - Summary - Overview

1

0.1.1 The Hole Story of the Pyrene in DNA

T*. This nice story starts with the famous **T*** experiments of Giese *et al.*. There is a electron hole injection into DNA, forming a radical cation and the observation of the sequential hole transfer through the DNA. The major competition reaction is the trapping of the radical cation by water. It is known that certain cationic surfactants are able to comlex DNA. The complex can be dissolved in organic solvents. With this technique the aqueous environment could be exchanged by an alcohol.

Boss Pyrene. Boss found the cleavage of DNA to form the from **T*** known 3' and 5' fragments with his **10**. He found about 20% after 6 min of irradiation. The cleavage was restricted to the core sequence T**10**T. With different bases surrounding **10** there was no visable fragmetation after 6 min. He did in this cases not irradiate for longer! He also only irradiated double-strands. With new results of Boss, pyrene as a artifical RNA-like nucleobase in DNA got into our focus. So tried ET with own DNA analogon **14**. No ground state radical cation formation, but photoexcited pyrene with capability of charge separation. The question arose, how the influence of the OMe group is, and perhaps gain insight in the relevance of the neighboring bases. Why is T so relevant?

My pyrene Nucleoside. That's why we synthesized **11** and build the strand **s6** with the modification also between two Ts and the same sequence. Irradiation under the same conditions (buffer, temperature, lamb, cuvette) as Boss showed no fragmentation after 6 min. After 2 h 14% of the original amount of **s6** has fragmented to the expected (9% after 60 min), clearly identified 2 fragments. As DNA degrades also unspecifically, statistically, only a rough estimation of the amount of destroyed DNA independent of the modification can be done (*to be done. unmod. ds and modified ds. Told Giese: about 50% ; is the 14% about the amount missing between unmod. and modified?*).

Unclear is, how much the build 14% fragments are degraded themselves during the 2 h. So perhaps the real amount is higher. But surely not lower. When degraded, then both fragments about the same degradation expected, due to about same length. *check the destruction of shorter oligos, length of strand and fragments?*

Outlook: The irradiation of the monomer could bring insights into mechanism. Perhaps without sugar as suggested in Figure1.

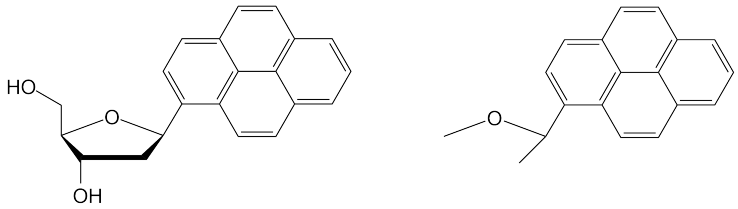

Figure 1: Possible molecules for control experiments and to gain mechanistical insights

As DNA has no substituent in position 2' at the sugar, but the modification of Boss has (methoxy) and this is the only structural difference, the reason for the clearly different results lies therein. In RNA, where a hydroxy group is at the 2' position, there are different sterical demands. T is therefore exchanged by U, that is lacking the methyl group. As Boss did use the natural DNA base T, the local secondary structure at his modification is altered (*check literature about U - dT in RNA or methoxy or hydroxy in DNA; influence of OMe in DNA, especially T; can the inventor of the **10** make a conformational calculation with OMe and without OMe? ; compair DNA to RNA structure ; distance between bases*). This sterical stress could be the reason for his results. The other nucleobases (A, C and G) are present in DNA and RNA. So when Boss put his **10** modification between those bases, there was enough space for the methoxy group and no conformational stress required an alteration of the secondary structure. Either the crucial distances have been changed to enable strand cleavage or a certain stacking arrangement of the neighboring Ts is enhanced, that leads to strand cleavage. The strand cleavage itself is most probably the consequence of a reaction of the photoexcited pyrene (no breaks without irradiation). Whatever the photoexcited pyrene does in the Boss case to induce the cleavage, it is slowed down i.e. less favorable in the **s6** case. Perhaps the CT (?) to the neighboring nucleobase is quenching the excitation and in the case of Boss, the nucleobases are not in range or something like that for this kind of quenching. Perhaps also a damage occurs, that is not visable in the HPLC chromatogram. In the Boss case, the reaction with the sugar or phosphate, whatever leads to the strand break, is not negligible and happens in observable amounts. Also a cleavage of the pyrene from the sugar is possible as one of the first steps (sugg. mech. Boss, no fragments with the pyrene found). Then the active sugar species could lead to strand breaks. There are also two possible scenarios concerning the relative amounts of 3' and 5' phosphate. Either the active species generates each time both fragments 1:1, or there are two pathways with one or two active

species which have about the same probability. This would have to be the case for Boss and my work. Can pyrene also act as a regioselective DNA cleavage site without the sugar moiety? (*add other questions, find differences between Häner and Boss strand*) Therefore a strand was used with the same sequence, changing as less parameters as possible in structure and irradiation provided by Häner.

Häner. The strand **s8** with the modification **15** between two phosphates was used. Irradiation for 60 min yielded in 70% cleavage (30 – 60% after 30 min, none after 10 min). The points of cleavage could be identified and are selectively around the pyrene concerning the amide bonds. The cleavage happens faster than in **s6** and slower than in **s5** . As we could show, the broken bonds are within the modification and not at the attached phosphates. So is the DNA crucial for the cleavage? We tested the monomer **15** for this purpose. It also breaks apart. After 40 min, 95% is destroyed (60% after 10 min). This is much faster than the same moity within the DNA. So the DNA hinders the bond cleavage of **15** when incorporated into **s8**The degree of hindering can be seen as measure for the different results when irradiating **s5**, **s6**, and **s8**.
The energy of the photoexcited pyrene could be quenched by the nearby nucleobases, when arranged in a nicely stacked manner. If this is energetically more favorable than the cleavage of the bonds then there is less strand cleavage. Or if a charge transfer is involved, the nearby bases are involved in the charge separation as showed by XYZ (ref Py-U work) and the less favorable transfer from or to a sugar or phosphate spot is not happening in the extend as it is in the disturbed system of Boss. *Question: ds / ss results. The ss should yield to higher cleaveage, when correctly arranged neighboring bases are missing. No differences expected, when the cleavage does not depend on the conformation. Then the methoxy group of Oli is directly involved in the process, and is strongly dependent on the conformation because only breaks at T**10**T .

Oli mechanism: Depyrenation could be the consequence of the photoexcitation. The resulting sugar species would yield either to 2 fragments sequentially or one of two fragments with compairable probability.

SDC. So the idea of the interesting properties of polyaromatics like photosensitization, fluorescence, the idea arose to build material of SDCs with polyaromatics on the end of surfactants and DNA as a linear scaffold. Nanowires because of redox properties. Severel complexes have been quantitatively formed, cmc and cytox of a surfactant determined, perhaps biological function like gene transfer, transportation through micelles, cell walls. Produced films with CTAB and electrospinning with 95% **26** and 5% CTAB.

Part I

Theoretical Part

Chapter 1

Charge Transfer Through DNA

1.1 Introductions

1.1.1 DNA

1.1.1.1 Structure

The story of 2'-deoxyribonucleic acid (DNA), carrying the hereditary information of all living cells, has begun in 1869, with the first crude purification of DNA from leucocytes by Friedrich Miescher.[2] DNA came into the researchers' focus in the early 1950s, when its molecular structure was elucidated.[3] In 1953, Watson & Crick succeeded in interpreting an X-ray scattering pattern of native DNA, and, together with previous results, proposed its structure to be a right-handed, double-stranded helix.[4] Three major types of DNA conformers exist: A-DNA, B-DNA and Z-DNA.[5] The B-DNA is the structure commonly adopted by DNA/DNA duplexes in the fully hydrated form. A-DNA is usually observed when DNA is dehydrated *in vitro*. Under high salt concentration, Z-DNA can be formed in G/C alternating DNA sequences. A- and B-DNA form a right-handed double helix, whereas Z-DNA forms a left-handed helix. DNA is a stable polymeric biomolecule, consisting of nucleotide monomer units linked together in a linear fashion like beads on a string. Each nucleotide monomer consists of three structural units. A 2'-deoxyribose (pentose sugar), one phosphate group and a nitrogenous heterocyclic base, called nucleobase (cf. Figure 1.1). The difference between the nucleotides lies in the nucleobase. In nature, four of them exist. In the double-strand they pair in two, which holds the DNA duplex together. Adenine (A) and guanine (G) are pyrimidines while thymine (T) and cytosine (C) are purines. A pyrimidine base always

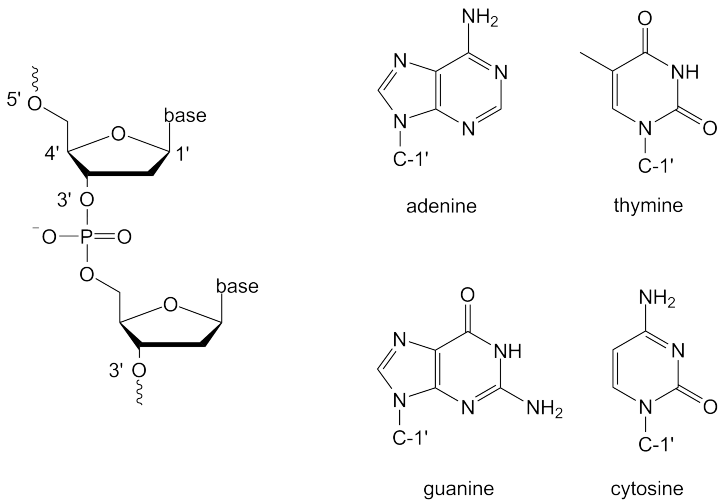

Figure 1.1: Building blocks of DNA. One nucleoside consists of a nucleobase, a sugar and a phosphate bridging two nucleoside.

pairs with a purine base and the natural Watson Crick pairing is G:C and A:T, as shown in Figure 1.2.

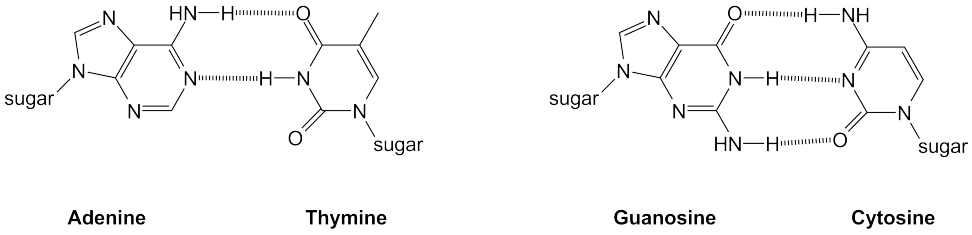

Figure 1.2: Watson Crick DNA base pairing

When the sequence of a strand corresponds exactly to the Watson & Crick base pair sequence of a second strand, they are complementary. Two complementary strands, arranged in an antiparallel fashion, meaning in opposite directions, build up a double-strand. The base pairs are stacked like sheets above each other, with a twist of 36° in B-DNA. They form the hydrophobic center of the helix. Their sequence determines the genetic code and is called the primary structure. The so-called 'backbone' consists of alternating sugars and phosphate groups. The latter are connecting the 3' and 5' position of two sugars. They build the outer sphere of the helix and form the major and the minor groove. The phosphoric acid -OH groups of the phosphodiesters are ionized at physiological pH since their pK_a values are around 2. This means, that DNA has a highly negatively charged surface. The distance between two negative charges is about 6.0 Å. The highly hydrophilic outside is responsible for the solubility in water (0.5 wt.%) and buffered aqueous solutions. The arrangement of the two antiparallel strands which form the helix is called secondary structure. In the case of the most common DNA conformer, the B-DNA, one turn consists of 10 base pairs with a total height of 34 Å and a diameter of 20 Å. The secondary structure

can be determined by circular dichroism (CD) measurements. DNA is insoluble in apolar solvents like lower alcohols e.g. methanol, ethanol or 2-propanol. This feature is applied for the purification of DNA by precipitation and will play an important role in the work concerning this thesis.[6]
The thermodynamic stability of a DNA double-strand, its ability not to part into single-strands with increasing temperature is an important measure for the quality of the base pairing, as hydrogen bonds and stacking are the most important forces to keep the double-strand together. Thermal denaturation experiments, where temperature is slowly increased, while the UV absorption at 260 nm is tracked, reveal the temperature, at which 50% of the strands are denatured (split into single-strands). This melting temperature (T_m) depends mainly on the number of base pairs and therefore on the length of the DNA strands and the surrounding buffer and salt concentrations. The reduction in π-stacking interactions among chromophores with increasing temperature are generally accompanied with a decrease in the absorbance intensity. This is called the hypochromic effect.[7,8]

1.1.1.2 An Easily Synthesizable Repeating Oligomer

From the design and synthesis point of view, DNA is an attractive system to work with nowadays because decades of previous work by many chemists have made it an easy molecule to assemble.[9,10] Automated synthesizers can routinely make oligomers (short DNA strands) in lengths approaching 100 nucleotides (100mer) with defined nucleobase sequence, and they can be adapted to incorporate unnatural monomers as well. Details can be found in Chapter 5.2.1. Moreover, because the synthesis is carried out by an iterative approach, the construction of a chain can also easily be carried out in a combinatorial fashion regarding the monomeric components. Finally, modern analytical methods have made characterization of modified oligomeric systems, even when highly charged like DNA, relatively straightforward.

1.1.1.3 Oxidative Damage and Mutations

Genetic information is stored in DNA sequences. Oxidative agents, such as reactive oxygen species (ROS), generated by ionizing radiation and endogenous oxidation processes, react with the deoxyguanosine residues in DNA, having the lowest oxidatation potential among all nucleobases, to form 8-oxo-7,8-dihydro-2'-deoxyguanosine.[11,12] ROS are species like oxygen radical anions ($O_2^{-\bullet}$), hydrogen peroxide, hydroxyl radicals ($^{\bullet}OH$), alkoxy and peroxy radicals. They are generated from molecular oxygen and can damage the DNA oxidatively. This is called oxidative stress. The damages are mostly repaired by enzymes and occur naturally about 10^4 times per cell and day. Unrepaired damage or modification of DNA bases may cause genetic mutation in semi-conservative replication processes of DNA. For instance, it is well known that damage on guanine like 8-oxo-7,8-dihydro-2'-deoxyguanosine (8-oxo-dG) among other oxidation products, leads to low fidelity in replication and enhances the probability of adenosine

incorporation instead of cytidine. Thus, the mutation from G:C base pairs into T:A base pairs occurs. Therefore, oxidative stress is an important mutagenic or carcinogenic lesion *in vivo* and is associated with as many as half of all human cancers.[13] It was found, that the actual oxidative damage leading to mutagenesis does not have to happen at the site of the attack by an oxidazing agent. Sequences of three Gs (GGG), called triple G sequences have a lower oxidation potential as G and are therefore more favoured for oxidation damage. G-rich sequences are often found in non-coding parts of the DNA, e.g. telomeres, regions at the end of chromosomes. A dislocation of a harmful oxidation to a non-coding domain is a desirable effect, since mutations in these regions do not lead to carcinogenesis. This protection mechanism is possible because of charge transfer inside the DNA.

1.1.2 Charge Transfer in DNA

In order to understand charge transfer in DNA, fundamental knowledge about DNA duplex helix structure is essential. The DNA backbone evolved to hold the flat aromatic DNA bases in a well-organized orientation.[10] In the double helical structure, the nucleobases are nearly perpendicular to the orientation of the backbone, and they stack on one another much like a roll of coins. In essentially all double-stranded nucleic acid structures, the bases are in direct $\pi - \pi$ van der Waals contact throughout the stack, so that the planes of the bases are separated by 3.4 Å, corresponding to the thickness of the π system in an aromatic ring.

Electron transfer (ET) or charge transfer (CT) are the most elementary and ubiquitous of all chemical reactions, playing a key role in many biological processes. Theoretical and experimental efforts initiated by Marcus in the late 1950s and continuing to the present day have provided a remarkably detailed description of CT reactions.[14] Charge transfer through DNA was studied by Giese and co-workers for several years now.[15,16] For the investigation of the migration of a charge in DNA, the charge has to be injected into the DNA. Giese *et al.* are able to generate an electron hole for the oxidative charge transfer as well as an extra electron for reductive electron transfer regiospecifically in a DNA strand.[17,18] The task of oxidative charge injection is performed by a radical cation, which is formed upon irradiation of the especially designed unnatural nucleoside $\mathbf{T}^*$, shown in Figure 1.3. This building block consists of the natural thymidine with a pivaloyl group replacing the 4' hydrogen. It can be incorporated into an oligonucleotide and pairs with adenine in the double-strand just like thymine. As the modification is located in the minor groove of the helix, it does not disturb the secondary structure.

The tertiary butyl ketone of $\mathbf{T}^*$ can undergo Norrish type I cleavage, yielding the C-4' radical **1**, a *tert*-butyl radical and carbonmonoxide (Scheme 1.1). This is achieved by irradiation with a 500 W Hg lamp in combination with a 320 nm cut-off filter to reduce unwanted damage of the DNA. The 4' radical **1** has the ability to induce a regioselective strand break. In the absence of radical traps, the 4' DNA radical is expected to undergo mainly spontaneous heterolytic cleavage of a β-bond. There are two CO bonds,

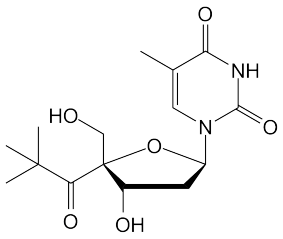

*Figure 1.3: **T*** nucleoside with 4' pivaoyl modification*

both phosphodiesters, for this reaction available. The 3' leads to a 5'–phosphate (**2**) and the radical cation **4** whereas the 5' leads to a 3'–phosphate (**3**) and the radical cation **5**. Both ways involve a cleavage of a backbone bond and are therefore strand breaks. This phosphate heterolysis was originally proposed by von Sonntag and Schulte-Frohlinde in 1975.[19] It was confirmed by others and our group.[16]

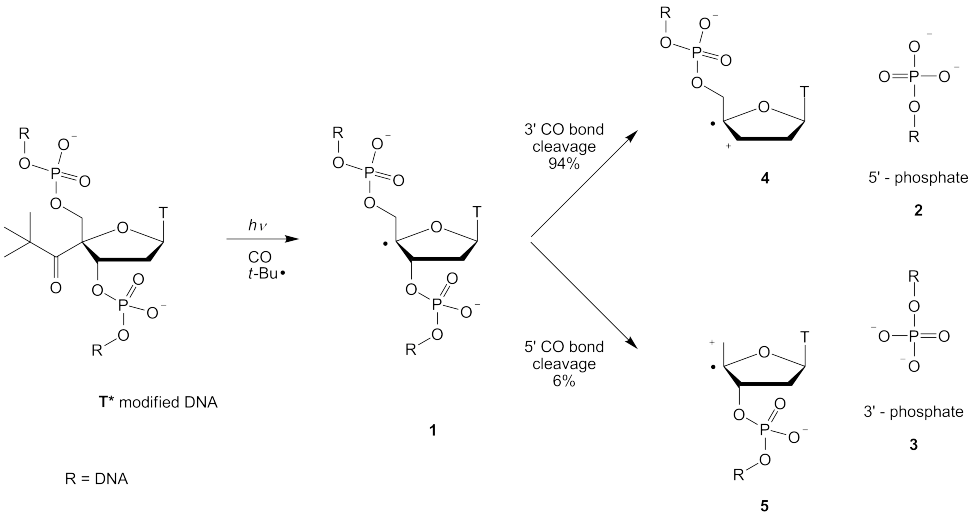

*Scheme 1.1: Site-selective formation of the radical cation **4** from **T*** by irradiation. First Norrish type I cleavage, then β-elimination of a phosphate by phosphorester bond cleavage.*

Dussy investigated the difference in rates for the β-elimination to form the 5'–phosphate **2** or the 3'–phosphate **3** in detail.[20] He found that the secondary 3'–CO bond cleaves about 15 times faster than the primary 5'–CO bond. In other words, 94% of the cleavage yield 5'–phosphate and **4** and 6% yield 3'–phosphate and **5**. This finding fits also well with the observation that in the first case a more stable secondary carbocation is formed primarily.

The stabilization of the negative charge on the leaving phosphate influences the rate of the bond cleavage.[21] By this, the polarity of the medium, the solvent and the presence of cations should play a role concerning the reaction speed.

The generated radical cation **4** can now be reduced by an electron via charge transfer (CT) from a nearby

electron donor or trapped by water (cf. Scheme 1.2). In natural DNA the charge transfer partner is

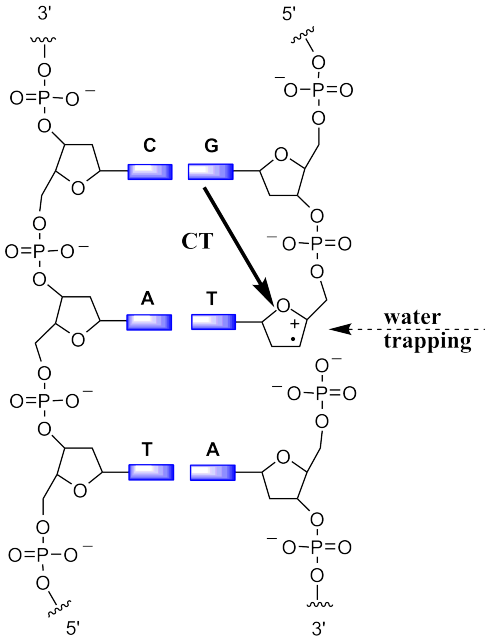

Scheme 1.2: Charge Transfer in DNA with ***T*****. The radical cation has two major competing reactions. Charge transfer (CT) from an electron donor or trapping with water.*

favourably a G and the radical cation **4** is converted to the enolether **6** (cf. Scheme 1.3).[16] If **4** is attacked by a nucleophile, namely water or a hydroxyl anion, a second β-elimination is induced and the 3'–phosphate **3** or the ketoaldehyde **7** is generated. Thus, the presence of enolether indicates charge transfer and the presence of **3** or **7** indicates trapping of the radical cation **4** by water.

After this electron transfer, the oxidized guanine in turn has two possibilities: Either the radical is trapped by water, or another guanine in its surrounding donates an electron to become the new active species and so on. In the latter case electrons are hopping from G to $G^{\bullet+}$ through the DNA. The analysis of irradiation experiments was done by product quantification using RP-HPLC. In the case of hopping experiments, Giese *et al.* used radioactive ^{32}P labelling in combination with poylacryl amide gel electrophoresis (PAGE).[22]

As a measure for the ability of the radical cation **4** to undergo charge transfer, the relative rate constant for charge transfer ($k_{CT,rel}$) was introduced.[23,24] It describes the charge transfer relative to the competing water trapping reactions. Assuming, the charge transfer obeys first order kinetics and the competing water reaction *pseudo*-first order kinetics (excess of water), the relative rate constant can be calculated using Equations 1.2. The CT product is enolether **6** and the water trapping products are the 3'–phosphate **3** and the ketoaldehyde **7** (cf. Equation 1.1).

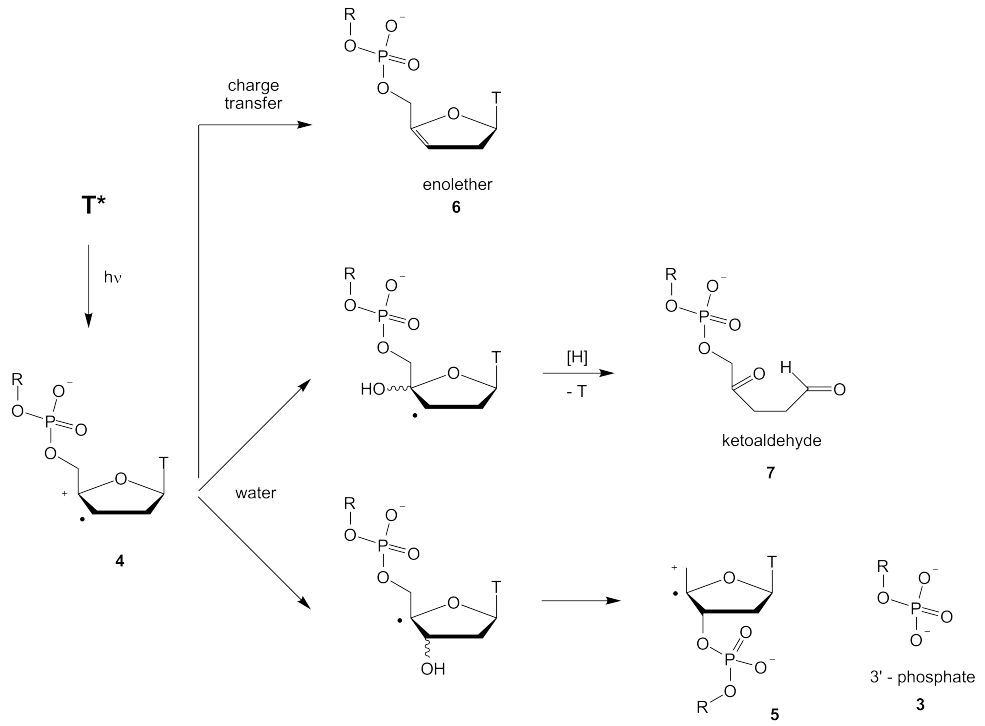

Scheme 1.3: Reactions of the $\mathbf{T}^*$ *radical cation* ***4*** *with a charge transfer partner or water.*

$$k_{CT,rel} = \frac{k_{CT}}{k_{\text{water trapping}}} = \frac{[\text{enolether } \mathbf{6}]}{[\text{3'–phosphate } \mathbf{3}] + [\text{ketoaldehyde } \mathbf{7}]} \tag{1.1}$$

The starting compound for the competition is the radical cation **4**. The amount of **4** is almost equal to the amount of formed 5'–phosphate **2** . Therefore, as the products of the two reaction pathways (charge transfer and water reaction) are known, the sum of the products of the water reactions can be exchanged by the difference of formed 5'–phosphate and formed charge transfer product **6**, resulting in Equation 1.2.

$$Assumption : [\text{3'–phosphate } \mathbf{3}] + [\text{ketoaldehyde } \mathbf{7}] = [\text{5'–phosphate } \mathbf{2}] - [\text{enolether } \mathbf{6}]$$

$$k_{CT,rel} = \frac{[\text{enolether } \mathbf{6}]}{[\text{5'–phosphate } \mathbf{2}] - [\text{enolether } \mathbf{6}]} \tag{1.2}$$

The C-4' radical **1** is the only known furanosyl radical which leads to strand cleavage under anaerobic conditions, meaning in the absence of reactive oxygen species (ROS).[20] Thus, irradiation experiments were performed in the absence of oxygen. Oxygen, which is present in untreated aqueous solutions can form ROS when irradiated. They would influence the system by making side reactions and therefore must be excluded.

The charge transfer reaction partner of the radical cation **4** is an electron donor. Guanine has the lowest

oxidation potential among the natural DNA bases (1.49 – 1.58 vs. SHE) and is therefore the first choice to transfer an electron to a C-4' deoxyribose radical cation.[16,11] The driving force or free reaction energy $\Delta G°$ of an electron transfer reaction is an essential measure for its velocity. It can be enlarged by lowering the oxidation potential of the electron donor. This can be achieved by exchanging the guanosine nucleoside by 7-deazaguanosine (**dG**^{z}), depicted in Figure 1.4.[11] It features the same hydrogen-bonding pattern for base pairing in DNA with thymine and does not disrupt the DNA structure significantly. It's oxidation potential is according to calculations about 0.38 V lower than the one of guanine and is therefore a better electron donor.[12] 7–Deazaguanine has also been applied by other groups as acceptor in charge transfer studies.[25,26,27]

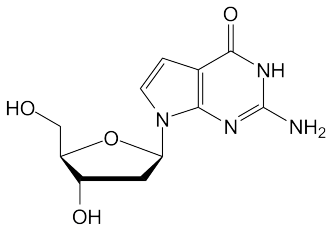

*Figure 1.4: 7-Deazaguanosine (**dG**^{z}), an alternative electron donor.*

1.1.3 Surfactant-DNA Complex (SDC)

DNA has a variety of interesting structural properties. One of them is the DNA secondary structure. In its natural environment, the DNA forms a B-helix, reminiscent of a rod-like barrel. All phosphodiesters, connecting the nucleobases, carry one negative charge each. One negative charge per nucleotide add up to 20 negative charges per turn for the double-strand. The resulting polyanionic DNA backbone is one of the best natural scaffolds for arranging organic molecules in a regular, predictable way.[10]
The term *surfactant* is a blend of 'surface acting agent'. Surfactants are usually organic, amphiphilic compounds, meaning they contain both, hydrophobic groups ('tails') and hydrophilic groups ('heads'). Therefore, they are soluble in both, organic solvents and water. The term surfactant was coined by Antara Products in 1950. Surfactants reduce the surface tension of water by adsorbing at the liquid–gas interface. They also reduce the interfacial tension between oil and water by adsorbing at the liquid–liquid interface. Many surfactants can also assemble in the bulk solution into aggregates. Examples of such aggregates are vesicles and micelles. The concentration at which surfactants begin to form micelles is known as the critical micelle concentration (cmc). In a micelle, the tails are in the core and the heads maintain favorable contact with water. Surfactants are often classified into four primary groups; anionic, cationic, non-ionic, and zwitterionic (dual charge). Surfactants are applied in a lot of fields like detergents (e.g. sodium dodecyl sulfate, sodium lauryl sulfate), fabric softeners (DMDTAB, CTAB), emulsifiers, paints, adhesives,

anti-foggings, Ski wax, foamings, herbicides, insecticides, antimicrobial agent (DMDTAB, CTAB), phase-transfer catalysts, hair conditioners and antiseptics (e.g. cetylpyridinium chloride) and for gene delivery.[28,29,30] Cationic surfactants are often covering negatively charged surfaces (fabric softeners, Ski wax, etc.). Widely spread pH independent polar head groups are permethylated ammonium salts. As hydrophobic tails, saturated alkyl chains are very common. Two prominent examples of this composition, dimethylditetradecylammonium bromide (DMDTAB) and cetyltrimethylammonium bromide (CTAB, *cetyl* is equal to *hexadecyl*), also known as Cetavlon, are depicted in Figure 1.5.

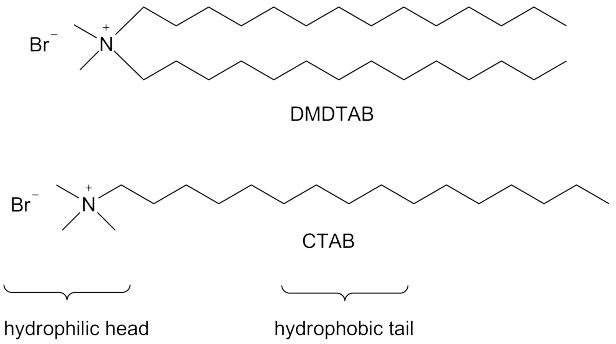

Figure 1.5: The cationic surfactants DMDTAB and CTAB

When a monocationic surfactant like CTAB or DMDTAB is combined with DNA in aqueous solution, the hydrophilic heads are attracted by the DNA through electrostatic interactions with the polyanionic scaffold (Coulomb forces), whereas the hydrophobic tails of the surfactants interact among each other through van der Waals forces.[31,32] The surfactants replace the present cations (mostly sodium cations) and bind cooperatively due to the tail's van der Waals forces to the DNA. The self-assembled surfactant-DNA complex (SDC), which is formed spontaneously, consists of one surfactant molecule per phosphodiester group of the DNA and precipitates quantitatively from aqueous solutions. The precipitation can be explained by the hydrophobic cylindrical sphere around the DNA, build by the alkyl chains. As this complex precipitates quantitatively when enough surfactants are present, purification and removal of inorganic salts (mostly sodium from the DNA and bromide from the surfactant) can be performed by simply washing the precipitate with water. The calculated structures from Smith in Figure 1.6 illustrate the self-assembly process.[33] The combining of surfactants (depicted as micelle) and the helical DNA, results after cooperative binding in a rod-like, spherical structure.

After drying, the SDC can be dissolved in methanol, other lower alcohols or dimethylformamide (DMF). The B-DNA secondary structure can be retained in dissolved SDCs in certain cases. For instance when using the surfactants CTAB or DMDTAB and methanol or 2-propanol as solvent. This was known from literature and was confirmed by circular dichroism (CD) measurements, described in the Experimental Part.[34]

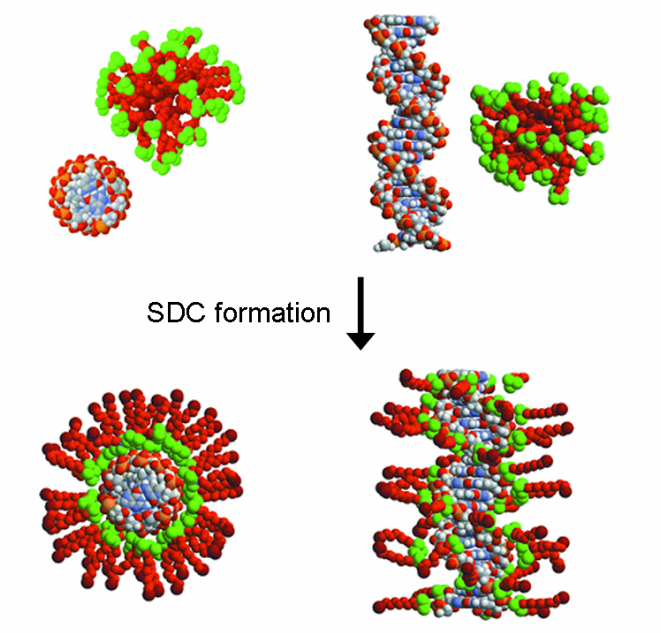

Figure 1.6: The formation of a SDC as top (left) and side view (right). Before (on top) and after the cooperative binding of the surfactants.

Water is essential for the B-DNA conformation. About seven water molecules are suggested to be acco-ciated with the non-bridging oxygens of the phosphodiesters in uncomplexed DNA in solution.[35] In the minor groove the adenine residues and the thymine residues appear responsible as the anchoring points for the minor groove spine of hydration. Additional layers of ordered water were reported. A similar spine does not appear to exist in the minor groove of dG–dC rich sequences. When drying, there are still some crystal water molecules left inside the grooves. Feig estimated the amount of remaining crys-tal water in a B-DNA-like surfactant-DNA complex to 10 molecules per base pair.[36] This water is very restricted and closely packed inside the grooves.

DNA can be liberated again from inside a surfactant-DNA complex.[37] Therefore, the surfactants have to be replaced by smaller, non-agglomerating cations, like sodium and stablilized by mobile, monovalent anions. Release of DNA is driven by the increasing enthropy of the surfactant and the different solubili-ties of surfactants and DNA.[38,39] Concentrated salt solutions like 3 M sodium chloride or water/ethanol mixtures were applied. The best release buffer for short oligonucleotides in the range of 20 nucleotides was evaluated to be 70% 2-propanol, containing 0.1 M sodium acetate (cf. Chapter 1.3.7).

When genomic DNA is complexed with CTAB, the water insoluble product can be separated form the aqueous solution and the DNA subsequently released again from the complex. This process was origi-nally used to isolate DNA from biological samples.[40] The 'CTAB method' was first described in 1959 and is still a common DNA isolation technique.[41,42] DNA, complexed in SDCs were observed to be

resistent to DNA decomposing enzymes, thus, surfactants have a biologically protective function. Also the chemical stability of DNA against degradation during storage can be significantly enhanced by wrapping the DNA in surfactants (forming SDCs). Other fields of application for SDCs are gene transfer, gene therapy (the insertion of DNA fragments into cells) or nanomaterial science (discussed in Chapter 4).[43,44]

1.2 Motivation

One way to expand the knowledge about the charge injection and charge transfer in DNA using $\mathbf{T}^*$ is to change the environment. All investigations performed so far were in buffered aqueous solutions with a high salt concentration of 100 mM sodium chloride. The complexation of DNA with cationic surfactants allow investigations in the absence of small, mobile cations and anions and with a minimal amount of water. As charge seperation occurs after the irradiation of $\mathbf{T}^*$, mobile ions and the solvent have to rearrange and optimize solvation. Ammonium groups of surfactants have less degree of translatorial freedom than sodium ions as they are restrained by the hydrophobic tails, which interact with each other, leading to different rearrangement properties. The role of the SDC is to reduce the amount of available water by exchanging it with alcohol and to change the mobility and kind of cations, stabilizing the polyanionic DNA backbone. Thus, we want to compare irradiations of $\mathbf{T}^*$ modified oligonucleotides in buffer and the corresponding surfactant-DNA complex in alcohol. As surfactant, we chose the well-known two-tailed DMDTAB.

1.3 Experiments

1.3.1 A Typical Irradiation Experiment

The way from the idea of irradiating a modified DNA double-strand as surfactant complex to the results is described here as an overview. The several steps are explained in details later on. The injector system $\mathbf{T}^*$ was synthesized and incorporated into an oligonucleotide. This strand was annealed with its counter strand to form a double-stranded helix in the aqueous irradiation buffer. About 15% was removed to serve as analytical reference (strand ratio before irradiation). The surfactant DMDTAB was dissolved in buffer, and the oligonucleotide solution was added to the surfactant solution. During the addition, the instantly formed surfactant-DNA complex (SDC) precipitated. After centrifugation, the supernatant, containing buffer salts and sodium bromide from the complexation, was removed. To control the nearly quantitative precipitation, the absorption at 260 nm of the supernatant was measured, as DNA absorbs at this wavelength. The solid SDC pellet was washed with nanopure water, to remove remaining buffer

and salts, and subsequently dried in vacuo. Also the washing solution was tested at 260 nm to be able to detect any loss of DNA. Now, the dry pellet was dissolved in methanol or 2-propanol over night. Argon was bubbled through the solution to remove dissolved oxygen and the irradiation was carried out. The irradiated solution was dried in vacuo. Washing several times with a release buffer dissolved and removed the surfactants, leaving the oligonucleotides behind as undissolved pellet. The dried pellet was redissolved in nanopure water and injected into a RP-HPLC with UV detection. The collected samples were analysed by MALDI-ToF and quantified based on their RP-HPLC peak integrals.

1.3.2 T* Synthesis and Incorporation into an Oligonucleotide

The **T*** compound, a modified thymidine, is stable as free diol and can be stored at -18°C. It was synthesized after known procedures or purchased.[24] For the incorporation into an oligonucleotide, two additional reaction steps were required. The primary 5' alcohol of **T*** was protected by dimethyltrityl to yield 71% of **8**. The secondary alcohol function was transformed to the phosphoramidite using 2-cyanoethyl-*N,N*-(diisopropyl)-chlorophosphoramidite and Hünig's base as shown in Scheme 1.4 in 75% yield. The resulting **9** is sensitive to humidity and cannot be stored for a long time (days).

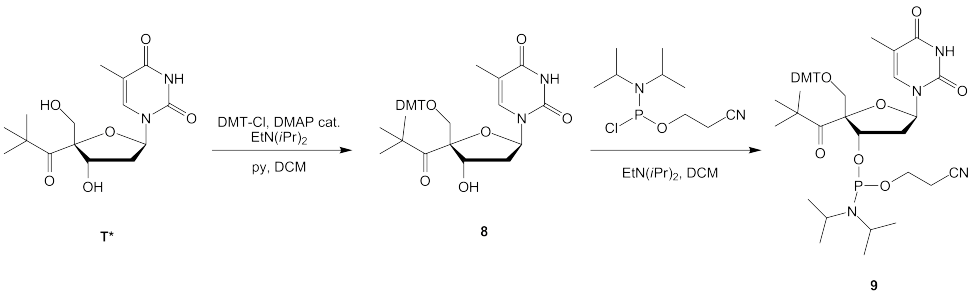

*Scheme 1.4: **T*** finalizing syntheses steps for incorporation into an oligonucleotide*

The incorporation into three different sequences was done by solid-phase phosphoramidite chemistry on a DNA synthesizer, with elongated coupling time of 10 min for the modifications. The second modification **dG^z**, depicted in Figure 1.4, was purchased as phosphoramidite and also incorporated using the automated process with an elongated coupling time of 10 minutes in high yields. The corresponding counter strands have additional nucleosides on both ends, which do not participate in base pairing (dangling ends). Firstly for analytical reasons because of longer retention time in the HPLC and secondly for a better annealing of the double-stranded part. They were purchased at Microsynth and repurified by RP-HPLC prior to use.

1.3.3 Selection of Strand Sequences

For the charge injection and charge transfer experiments, the injector **T*** is placed in the middle part of the oligonucleotides. The relative position of the electron donor dG or **dG**^{z} to the injector is of big importance for the experiments. Also the absence of unwanted donors like other dGs or GGG sequences has to be regarded. To compare the obtained results with already existing observations, the sequences were chosen according to known strands.
The first strand to investigate (**s1**) features as central sequence 5'-G**T***-3' in the middle of the 20mer. This strand was already investigated by Meggers.[23] The distance between the **T*** and the nearest dG is 7.3 Å. Its counterstrand **cs1** is complementary, bearing an adenine opposing the **T*** and features the additional base triplet 'CTT' as dangling end on both sides. The strands are shown below. As Meggers used the same conditions for the irraditations and the same analytical approach with comparable devices, his results are of direct interest.

s1: 5'-TGC ATC ATT G**T***T ATC AGA GC-3'
cs1: 3'-CTT ACG TAG TAA CA A TAG TCT CG TTC-5'

Beside dG, also **dG**^{z} was chosen to function as electron donor for the **T*** radical cation. Thus, in **s2**, the two modifications **T*** and **dG**^{z} were incorporated. The sequence was chosen to compare the results directly with those of Biland, who investigated the identical strand.[24] Its counter strand **cs2** is complementary, featuring an adenine opposing **T***, a cytidine opposing **dG**^{z} and two thymidine triplets as dangling ends on both sides. The strands are shown below.

s2: 5'-TGC ATC ATT **G**^{z}**T***T ATC AGA GC-3'
cs2: 3'-TTT ACG TAG TAA C A A TAG TCT CG TTT-5'

For structural investigations and as reference, an unmodified analogue to **s1**, called **s3**, was employed. The injector **T*** was replaced by a normal thymidine. Although the complementary counter strand **cs3** is identical to **cs1**, it was denoted differently to enhance comprehensibility. The strands are shown below.

s3: 5'-TGC ATC ATT G**T**T ATC AGA GC-3'
cs3: 3'-CTT ACG TAG TAA C**A**A TAG TCT CG TTC-5'

1.3.4 Irradiation of T* Strands: Procedure

Irradiations of the **T*** double-strands **s1/cs1**, **s2/cs2** and **s3/cs3** in aqueous buffer served as a reference for the surfactant-DNA complex irradiations. The experiments were performed as follows: 1 nmol of annealed double-strand was used in 240 mL 20 mM sodium citrate buffer, containing 100 mM sodium chloride at pH 5.0 (4.2 μM). For every experiment, 15% of the solution was removed and injected into the HPLC as a reference for the ratio of the two strands in double-strand experiments and to check the purity. Oxygen was removed from the sample by bubbling argon through the solution for 10 min. This ensures the absence of oxygen to avoid ROS formation unter the irradiation conditions (cf. Chapter 1.1.1.3). Irradiations were performed in an airtight disposable plastic cuvettes with a 500 W Hg lamp for 6 minutes at 5°C. The spectrum of the lamp was limited by a 320 nm cut-off filter (>320 nm). After the irradiation, the sample was subjected to RP-HPLC. As detection, DNA was monitored at 260 nm. Samples were collected and analysed by MALDI-ToF mass spectroscopy. Assignment of the compounds was done by comparing HPLC retention times with reference injections and mass analysis results. For quantification of HPLC results, the integrals of the signals were divided by the molar extinction factors of the corresponding molecules. The results are summarized together with the results of the irradiations of the surfactant-DNA complexes in Chapter 1.3.8.

1.3.5 Formation of Surfactant-DNA Complex

When surfactants are wrapped around DNA, the resulting surfactant-DNA complex (SDC), is often soluble in lower alcohols. The B-DNA helical structure of the enclosed DNA is not altered. Thus, the formation of a SDC enables the investigation of DNA in salt-free alcoholic solutions. To produce the surfactant-DNA complex, a solution of double-stranded oligonucleotide and a solution of corresponding amount of the surfactant DMDTAB (10% molar excess) in 20 mM sodium citrate buffer, containing 100 mM sodium chloride was provided. To calculate the appropriate amount of surfactant, the following consideration has to be made: One surfactant carries one positive charge. A 20mer oligonucleotide, like **s1**, carries 19 negative charges from the intervening phosphodiesters. The 26mer counter strand **cs1** carries 25 negative charges. Therefore 1 nmol of double-stranded oligonucleotide corresponds to 44 nmol of surfactant. By adding the dissolved oligonucleotides slowly to the surfactant solution, the surfactants bind cooperatively, replacing the sodium cations and the formed SDC precipitates immediately. By this order of addition it is ensured that all negative charges are paired with a surfactant (in excess) before the SDC precipitates. The supernatant was removed after centrifugation and the pellet washed with nanopure water to remove remaining salts, namely sodium chloride. To control the precipitation, UV absorption at 260 nm (A_{260}) of the supernatant was measured and compared with A_{260} of the initial oligonucleotide solution. By this means, the loss of oligonucleotide during complexation could be determined in all cases and all experiments to be less than 2%.

The control of the supernatant is a proof that the complexes are one on one by charge, meaning not more than one surfactant per phosphate. If more surfactant would bind, because of van der Waals forces among the tails, there would not be enought surfactants at the end for the last strands entering the solution. Those strands would therefore be left uncomplexed and be detected in the supernatant. In control experiments, the amount of surfactant was set to exactly the same amount as the oligomers (1.0 eq. in charge). Also without any excess of surfactant, no oligomers were found in the supernatant by means of UV analysis. The resulting pellet, containing pure SDC, was dried using a speed-vac and was ready to be dissolved in methanol or 2-propanol over night for irradiation experiments.

1.3.6 Proof of Structure

Circular dichroism spectroscopy (CD) is a useful tool in detecting the overall secondary structural alteration in DNA helical conformation because CD spectra shows chirality changes in optically active molecules.[45,46] B-DNA has a specific CD spectrum with maxima at 220 and 279 nm, minima at 208 and 250 nm and zero-crossing at 230 and 264 nm. Apart from revealing the secondary structure of nucleic acids and oligonucleotides, circular dichroism spectroscopy is a useful technique to establish the successful base pairing of a modified strand to its counterpart, which is mirrored by the secondary structure. The CD spectrum of the unmodified double-strand **s3/cs3** in the irradiation buffer served as reference. It shows clearly the B-DNA conformation. The CD spectrum of the same double-strand, complexed with DMDTAB as surfactant-DNA complex in 2-propanol was equal. The same accounts for the complexation with the sufactant CTAB and methanol as solvent. Therefore, during irradiation the double-strand within the surfactant complex is expected to be in a B-DNA conformation.

1.3.7 Release of Oligonucleotides from SDC

After irradiation, the products were analysed by RP-HPLC. Therefore, the complexes of surfactant and DNA had to be dissociated. To release the oliogonucleotides and their fragments, the alcohol (solvent) was first removed in vacuo. To the dry SDC, 70% 2-propanol, containing 0.1 M sodium acetate (release buffer) was added followed by vortexing and centrifugation.[37] In this way the dissolved surfactants could be removed by removing the supernatant. The resulting oligonucleotide pellet can, after drying, be dissolved in water and was ready for HPLC analysis.

To determine the reliability of the release of oligonucleotides from the complexes, the complexes had to be formed first, because a direct comparison of SDC and released oligonucleotides is not possible. Thus the release was tested, by comparing the amounts of oligonucleotides before complexation with the amounts of oligonucleotides after the release by UV absorption (A_{260}). As described in Chapter 1.3.5, loss of oligonucleotides during formation of the complex according to A_{260} of removed supernatant is less than 2%, taking all experimental errors in account. The tested DNA for the release comprised

genomic size DNA and oligonucleotides with 26 (**cs3**), 20 (**s3**) and 11 (**s4**) nucleosides. Being complementary to **cs3**, the 11mer **s4** has about the length of the expected $\mathbf{T}^*$ irradiation fragments (shown below).

s4: 5'-TGC ATC ATT GT-3'
s3: 5'-TGC ATC ATT GTT ATC AGA GC-3'
cs3: 3'-CTT ACG TAG TAA CAA TAG TCT CG TTC-5'

The evaluated loss in release is negligible for oligonucleotides with length down to 20. It is about 1 – 3% after abstraction of the losses in formation but increases significantly for the shorter **s4** strand up to 18%. As all irradiation fragments have almost the same length, a significant difference in loss among them is not expected. Therefore the fragments can be compared among each other.
Several known release buffers were tested (details to be found in the Experimental Part). The best results were obtained with 70% 2-propanol containing 0.1 M sodium. This release buffer was especially adapted for short oligonucleotides by exchanging ethanol with 2-propanol, based on a known release buffer.[37] The high alcohol content is responsible for the dissolving of the surfactants. The water contents of 30% inhibits the dissolving of the surfactant-DNA complex. In summary, the release buffer breaks apart the surfactant-DNA complex by dissolving the surfactant. The complex and the resulting, desired free oligonucleotides stay undissolved.

1.3.8 Irradiation, Results and Discussion

To change the aqueous medium of the $\mathbf{T}^*$ strands and to exclude sodium ions during irradiations, we applied the surfactant-DNA complex technique. The overall experimental procedure is described in Chapter 1.3.1. The required formation of the complex before the irradiation and release of the encapsulated oligomers after irradiation was performed as described in the previous Chapters 1.3.5 and 1.3.7.
Experiments with the two $\mathbf{T}^*$ modified double-strands **s1/cs1** and **s2/cs2**, both as SDCs dissolved in alcohol and as free double-strands in water were performed. The double-strand **s1/cs1** with the central sequence -G$\mathbf{T}^*$- was already investigated by Meggers.[23] The **s2/cs2** double-strand with $\mathbf{dG}^z$ as electron donor was tested by Biland.[24]

s1: 5'-TGC ATC ATT G$\mathbf{T}^*$T ATC AGA GC-3'
cs1: 3'-CTT ACG TAG TAA CA A TAG TCT CG TTC-5'

s2: 5'-TGC ATC ATT $\mathbf{G}^z\mathbf{T}^*$T ATC AGA GC-3'
cs2: 3'-TTT ACG TAG TAA C A A TAG TCT CG TTT-5'

Both SDCs were irradiated in methanol, and **s1/cs1** additionally in 2-propanol to explore the influence of the chosen alcohol. As reference, the complementary, unmodified double-strand **s3/cs3** revealed the relevance of the charge injector $\mathbf{T}^*$ in the above mentioned experiments.

An amount of 1.0 nmol $\mathbf{T}^*$ strand was used for all experiments. Reference injections with 1.0 nmol unirradiated strand determine the expected integral (100%) of the $\mathbf{T}^*$ strand and were compared with the irradiated sample HPLC chromatogram. In double-strand experiments, the counter strand also functions as pseudo internal standard and can be used to confirm the calculations. The amount of stand cleavage was calculated by substracting the remaining amount of the $\mathbf{T}^*$ strand found in the HPLC from the expected 100% employed. This contains the assumption, that all of the $\mathbf{T}^*$ strand signal vanishing, is caused by strand cleavage and not by other theoretically possible reactions. All SDCs were formed with the surfactant dimethylditetradecylammonium bromide (DMDTAB). All samples were irradiated at 5°C for 6 minutes, using a 320 nm cut-off filter.

Photolysis of the 4'-pivaloylsubstituted nucleotide $\mathbf{T}^*$ in single- and double-stranded DNA generates strand breaks (for details cf. Schemes 1.1 and 1.3). A simplified overview is given in Scheme 1.5. After the formation of the C-4' radical **1**, an anaerobic C-4' radical-induced β-bond cleavage as initial step takes place. This can happen in two directions. In the aqueous buffer system (H_2O), 94% of the cleavages yield the 5'–phosphate **2** and 4% the 3'–phosphate **3**.[16] There are two major competing reactions concerning the resulting radical cation **4**. On one side, there is charge transfer, yielding the enolether **6** and on the other side, a trapping reaction with water can occur. This yields either the 3'–phosphate **3** or the ketoaldehyde **7** (cf. Chapter 1.1.2). The charge injection step as well as the water trapping reactions yield the same **3**. To destinguish the two phosphates in the discussion, they are denoted 3'–phosphate$_{inject}$ as product from the charge injection and 3'–phosphate$_{trap}$ as water trapping product. The observed 3'–phosphate **3** represents the sum of 3'–phosphate$_{inject}$ and 3'–phosphate$_{trap}$ (cf. Equation 1.3).

$$\text{3'–phosphate } \mathbf{3} = \text{3'–phosphate}_{inject} + \text{3'–phosphate}_{trap} \tag{1.3}$$

The ketoaldehyde, one product of water trapping reactions, was not identified in any experiment. The difficult identification was already known from Meggers. Also no products resulting from radical cation **5** were detected.

In some experiments, the sum of all fragments was significantly lower than the amount of cleaved target strand. Mathematically, these two amounts should be equal. The difference is attributed to losses in the release step. As the 5'–phosphate, 3'–phosphate and enolether have a comparable length and no relevant discrimination between these fragments is expected during release, their amounts were compared among each other. The estimated error range for all values of yields is ±10%. A representive RP-HPLC chromatogram with all identified fragments from SDC irradiations is shown in Figure 1.7

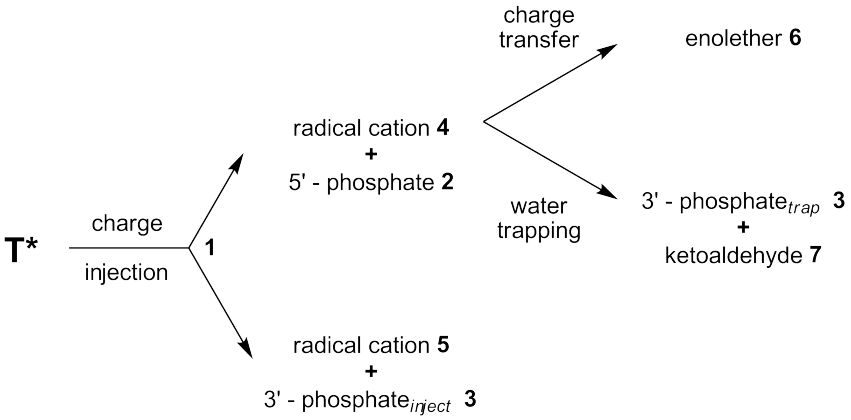

*Scheme 1.5: Simplified overview of the **T*** irradiation.*

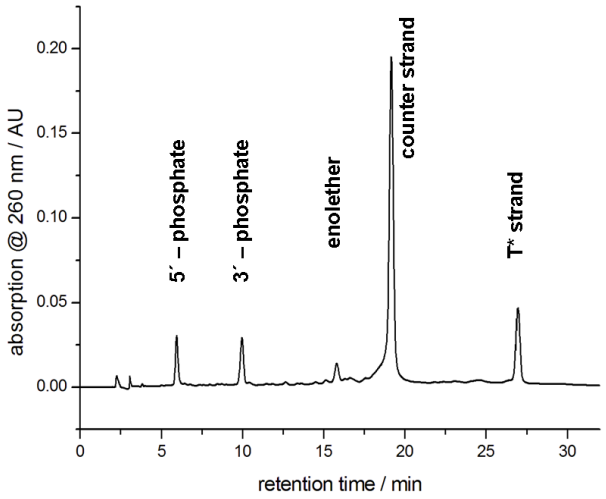

*Figure 1.7: RP-HPLC with the fragments formed after irradiation of double-strand **s1/cs1** as surfactant-DNA complex in methanol.*

The irradiation results of SDCs and corresponding free oligonucleotide irradiations are summarizing in Table 1.1. The central sequence is indicated in 5'–3' direction. Amounts of formed products are given in relative ratios. The ratio of charge transfer to water trapping is represented by $k_{CT,rel}$ and was calculated using Equation 1.2 on page 1.2.

strands	central sequence	medium	formed products **2** : **3** : **6**	$k_{CT,rel}$
s1/cs1	**–GT***–	SDC in MeOH	3 : 1 : 2	2.0
s1/cs1		SDC in 2-PrOH	1 : 2 : –	–
s1/cs1		free in H_2O	2.2 :1.0: 1	0.85
s2/cs2	**–G**^{z}**T***–	SDC in MeOH	1.3 : 1 : 0.5	0.63
s2/cs2		free in H_2O	13.7: 1 : 12.5	10.7

*Table 1.1: Summarized **T*** irradiation results. The relative rate constant $k_{CT,rel}$ was determined with Equation 1.2. The central nucleobase sequences are indicated in 5'–3' direction.*

Irradiation of SDC **s1/cs1** in methanol yielded the same fragments (5'–phosphate **2**, 3'–phosphate **3** and enolether **6**) as the irradiation of the free double-strand in water. The charge injection as well as the charge transfer are therefore occuring in the SDC and yield the same products. The quantitative results of the irradiations performed in water are in aggreement with the results of Meggers.[23] This reference proved our strands and setup to be comparable to the ones of Meggers. 80% of **s1** were cleaved inside the SDC and 65% were cleaved in uncomplexed oligonucleotides in buffer. The charge injection step was therefore more effective in the SDC than in the free double-strand (80% compared to 65%). The relative rate constant $k_{CT,rel}$, described in Chapter 1.1.2 and calculated using Equation 1.2 increased thereby from 0.85 to 2.0. As $k_{CT,rel}$ describes the ratio of charge transfer to the trapping of the formed radical cation **4**, charge transfer is faster in the SDC system than in free double-strands. The amount of observed 3'–phosphate equals the expected amount of water trapping. Thus, when irradiating the SDC, mainly 5'–phosphate **2** was produced in the charge injection step. This is similar to the irradiations in water yielding 94% **2** and 6% 3'–phosphate$_{inject}$ (**3**) during charge injection.

To explore the solvent dependency of the reaction, we made the same experiment with SDC **s1/cs1** in 2-propanol with surprising results. The charge injection, being 50 – 70% in the SDC was similar to the irradiations in water, but the charge transfer product enolether **6** was not produced. The solvent 2-propanol inhibited charge transfer completely. When **s1/cs1** was irradiated as surfactant-DNA complex in 2-propanol, the RP-HPLC analysis showed more (double the amount) 3'–phosphate than 5'–phosphate. This result can only be explained by a change in ratio at the charge injection step. Assuming the amount of build enolether and ketoaldehyde are negligible, we calculated the ratio of 5'–phosphate **2**: 3'–phosphate$_{inject}$ **3** to be 67:33. This is a shift towards the thermodynamic less favorable

3'–phosphate$_{inject}$ (detailed equations in the Experimental Part).

The results from the irradiations of the double-strand **s2/cs2** , having the central sequence 5'–**G**^{z}**T***–3', in buffer are equal to the ones of Biland, applying the same conditions. The formation of 5'–phosphate **2**, 3'–phosphate **3** and of the enolether **6** was confirmed. The charge injection in the SDC, being 60 – 80%, was similar to the one in the free double-strand. The $k_{CT,rel}$ of buffer and methanol experiments were calculated using Equation1.2. In the buffer, the relative rate constant was 10.7 (confirmed by results of Biland) and in methanol 0.63. The charge transfer in the SDC (0.63) was slower than in the corresponding irraditaion of the free oligonucleotides in water (10.7) and also slower than in SDC **s1/cs1** (2.0) The observed charge transfer rate was unexpectedly low. The electron donor dG in the **s1** strand was substituted in **s2** with the 'better' electron donor **dG**^{z} (lower oxidation potential). This should have made charge transfer faster than in the **s1** strand. In contrast, $k_{CT,rel}$ dropped from 2.0 to 0.63. Thus, the surrounding surfactants and methanol as solvent slowed down charge transfer in **s2/cs2**. We calculated the ratio of 5'–phosphate : 3'–phosphate$_{inject}$ at the charge injection to be 84:16.

Compairing the ratios of 5'–phosphate **2**: 3'–phosphate$_{inject}$ **3**, we observed a correlation between drop of charge transfer rate and decreasing 5'–phosphate formation. Both phenomena are attributed to local conformation changes.

1.4 Summary

Oligonucleotides and the cationic surfactant DMDTAB have the ability to agglomerate. When surfactants replace the mobile sodium cations, the formed complex is no longer water soluble, but can be dissolved in methanol or 2-propanol. The overall conformation of the double-strand is not affected significantly by this additional shell when dissolved in methanol or 2-propanol and retains the B-DNA-like structure, as proven by circular dichroism measurements.

The injector system **T*** was synthesized and incorporated into oligonucleotides. The modified strands (**s1** and **s2**) were annealed with their counter strands (**cs1** and **cs2**), bearing an adenine (A) opposite to the injector. The double-strands were irradiated in water (free) and as surfactant-DNA complex (SDC), with DMDTAB as surfactant, in methanol and 2-propanol.

After irradiation, **T*** injects a positive charge into DNA by creating a radical cation. This charge injection, was shown to work with high yields in surfactant-DNA complexes. The radical cation migrates through the DNA by charge transfer or gets trapped by water, yielding strand breaks. This was also confirmed in SDCs as the corresponding fragments were observed. The analysis of the charge injection and the competition between charge transfer and water trapping was done by quantitative product comparison.

Charge transfer in SDC **s1/cs1** in methanol with dG as electron donor was faster than in the free double-strand in water. The missing mobile sodium cations and methanol as solvent enhance charge transfer.

In **s2/cs2**, the electron donor dG was replaced by **dG**^{z}. The lower oxidation potential was expected to enhance charge transfer even more. Against expectations, charge transfer was reduced. It was not only slower relative to the free oligonucleodide experiments in water, but even slower compared to dG as donor in SDC **s1/cs1**. We attribute the reduced charge transfer to unfavorable local changes in conformation around **dG**^{z}. The solvent 2-propanol inhibited charge transfer completely in SDC **s1/cs1** and promoted 3'–phosphate$_{inject}$ formation at the charge injection step. Both phenomena can be explained by conformational changes. Our observations lead to the conlusions, that the local structure at the reaction site is more important than the influence of the cations. Surfactant-DNA complexes promote charge transfer over water trapping when the conformation is conserved.

Chapter 2

Pyrene as C-Nucleosides Incorporated in DNA

2.1 Introductions

2.1.1 2'-Methoxy-β-1'-pyrenyl-C-nucleoside (10), Results of Boss

During his PhD thesis in the Giese group, Boss synthesized and incorporated 2'-methoxy-β-1'-pyrenyl-C-nucleoside **10** in DNA oligomers (cf. Figure 2.1).[47] Instead of a nitrogen-bonded nucleobase, the sugar of this unnatural nucleoside carries a carbon-bond pyrene (C-nucleoside). The deoxyribose sugar, present in DNA nucleosides is replaced by a ribose, like in ribonucleic acid (RNA). The 2' hydroxy group missing in DNA is additionally methylated to form a 2' methoxy substituent.
For the formation of a double-strand with the strands carrying the modification, Boss chose complementary strands bearing an abasic site (**Ab**) on the opposite position of the modification for structural reasons, that will be explained later in Chapter 2.1.2.2. Five additional thymidines on each side of counter strand **cs5** were added to function as dangling ends.

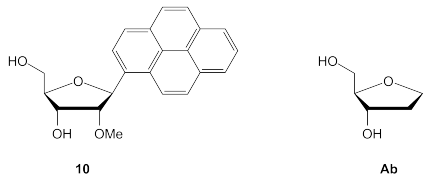

*Figure 2.1: The pyrene C-nucleoside **10** examined by Boss, featuring a methoxy group at the 2' position on the left side and the counterpart in double-stranded oligonucletide, the abasic site (**Ab**) on the right.*

Boss initially used pyrene as electron donor, replacing dG, for the **T*** hole transfer system of Giese (cf. Chapter 1). Among the expected fragments from the **T*** experiments, he discovered fragments that could

not be explained by known **T*** induced fragmentations. Thus he synthesized strands with **10** as the only modification.

The irradiation of the double-strand in which **10** is incorporated between two Ts (single–strand **s5**) revealed strand cleavages on both sides of the modification, yielding two identified fragments, denoted as **s5** 5'– and **s5** 3'–phosphate (cf. Figure 2.2). After 6 minutes, with conditions equal to **T*** irradiations

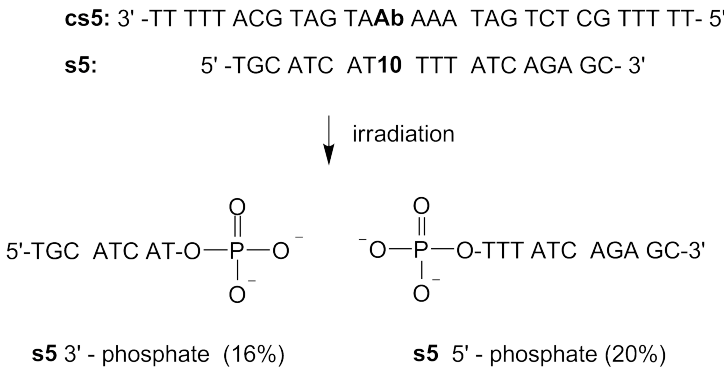

Figure 2.2: Pyrene induced strand cleavage discovered by Boss

applied in Chapter 1.3, 55% of the **s5** strand was cleaved. About 20% **s5** 5'–phosphate and about 16% **s5** 3'–phosphate were identified as products. There were no fragments identified containing the pyrene moiety. Interestingly, strands with core sequences -T**10**C-, -C**10**T-, -C**10**C-, -G**10**G- and -A**10**A- did not break during the 6 minutes of irradiation. So the two Ts enclosing the pyrene nucleoside are crucial for the fast strand cleavage observed. As experiments with longer irradiation times have not been made, it cannot be ruled out, that the strand cleavage also occurs with the other core sequences, only much slower. Also single-strand experiments have not been performed. The effect of the modification on the local structure of the B-DNA is not known. CD spectra are not available.

2.1.2 2'-Deoxy-β-1'-pyrenyl-C-nucleoside (11)

2.1.2.1 Structure

The first synthesis of the pyrene 2'-dexoynucleoside, denoted **11**, and first investigations have been done by Kool *et al.* in 1997 (cf. Figure 2.3). The C-nucleoside is stable under standard conditions and the oligonucleotides can be stored at -18°C for several months. The correct incorporation into DNA was confirmed by ^{1}H NMR of the T**11**T trimer.

The excitation wavelength of **11** at about 350 nm ($\varepsilon_{346} = 1500\,\mathrm{M^{-1}cm^{-1}}$) is far apart from DNA absorption band at 260 nm (**11**: $\varepsilon_{260} = 8600\,\mathrm{M^{-1}cm^{-1}}$), which makes selective excitation feasible. Figure 2.4 shows the UV/vis spectrum of the modification incorporated in the 20mer oligonucleotide used for our investigations as double-strand. DNA itself has very limited absorption around 350 nm, thus unwanted

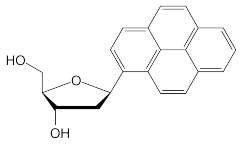

*Figure 2.3: Pyrene deoxyribose nucleoside **11***

excitation of the other bases is minimized. Observations around 350 nm enables pyrene specific analysis of experiments.

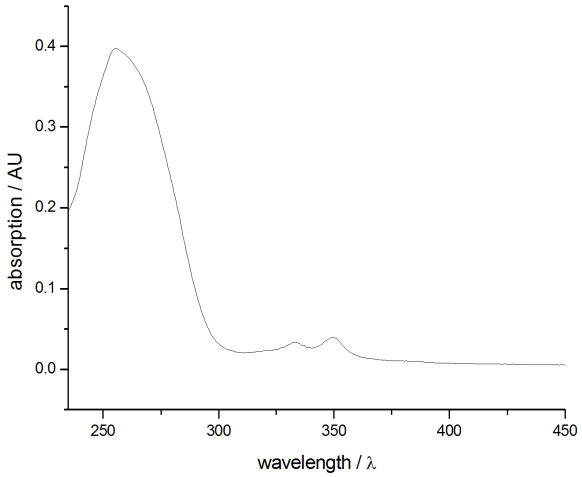

*Figure 2.4: Double-strand with incorporated **11***

2.1.2.2 Deoxynucleoside 11 – Pairing with Abasic Site in DNA

In natural DNA, the pairing of the nucleobases determines the secondary structure. Only when every guanine has a cytidine and every adenine has a thymine on the corresponding position of the counterstand, the B-DNA secondary structure can be adopted. This represents the native Watson & Crick base pairing (G≡C, A=T). The B-DNA conformation is well-defined and most of its properties, like distances and angles are known. When a nucleobase is exchanged by a synthetical compound, it is therefore desirable to preserve the defined secondary structure as good as possible. When the unnatural deoxynucleoside **11** is incorporated in DNA, its counterpart on the other strand of a double-stranded DNA has to be chosen carefully. Pyrene is sterically more demanding than a natural nucleobase. Thus, when the pyrene of the nucleoside **11** is located inside the stack, the space, left for the opposing base is not big enough for one of the natural nucleobases. In fact, the pyrene surface area of 108 $Å^2$ (one side) occupies about the same space as a whole pair of natural nucleobases need for stacking (115 $Å^2$).[48,49] Taken this sterical

problem in account, Kool, who investigated the nucleoside **11**, has chosen the so-called abasic site (**Ab**) as counterpart. Its structure is depicted in Figure 2.1 and is based on tetrahydrofuran. As it possesses no nucleobase, the whole space for the base pairing is available for the pyrene. The abasic site occurs naturally in DNA. It is a frequent DNA lesion, caused by the loss of a nucleobase due to cleavage of the *N*-glycosidic bond.[50] If not repaired by enzymes, mutations during replication and thereafter cancer or cell death can be the results. The artifical base pair consisting of **11** and an abasic site as counterpart is already known for more than ten years.[51] Several structural investigations revealed its ability to replace a natural DNA base pair. In the Watson & Crick pairing of natural nucleobases, not the stacking but hydrogen bonding is the most important force for the stablility of the double-strand. The DNA bases do not stack very strongly relative to many common organic aromatic molecules. For example, benzene itself stacks better than three of the four DNA bases, and naphthalene even better.[48] It was believed, that for the coherence of the two strands, strong hydrogen bonds are essential in all cases. As pyrene is not able to form any hydrogen bonds, it was first expected to destabilize the DNA double-strand. The investigation of this 'base pair' by Kool *et al.* showed, that hydrogen bonds are not absolutely required for stabilization of a base pair within the double helix and stacking alone can maintain the stability.[52] The **11**:**Ab** pair was the first described artificial base pair replacement, stabilizing DNA only by stacking interaction and without any hydrogen bonds.[52,53]

Thermal denaturantion temperature (melting temperature, T_m) of a 15mer (oligonucleotide containing 15 nucleotides) having the base pair A:T in the middle dropped from 43°C to 41°C when that base pair was exchanged by the modification pair **11**:**Ab**. This data numbers the influence on the double-strand stability of **11**:**Ab** about equal to an A:T pair.[54] When an abasic site is placed opposite a natural nucleobbase, a strong destabilization is observed. This finding underlines the matching of **11** and **Ab**. The pyrene nucleside **11** not only compensates the destabilizing effect of **Ab**, the combination of the two even enhances the double-strand stability almost by the same amount as an A:T pair. Also circular dichroism measurements (CD) approve the local B-DNA structure to be intact.

The knowledge about the pairing and behaviour in DNA led to biological investigations. Kool *et al.* discovered in 1997 that nonpolar base mimics, including **11**, could be replicated by polymerase enzymes, refuting the long–held and widespread belief that Watson & Crick hydrogen bonds were the main arbiters of base pair synthesis by these enzymes. Since then, it has become accepted that steric and geometric effects in the polymerase active site may be more important than hydrogen bonding.[55] The triphosphate of **11** was found to be specifically inserted by DNA polymerases opposite sites that lack DNA bases (abasic sites).[10] The efficiency of this process approaches that of a natural base pair and the specificity is 100-fold. Using this propertiy they sequenced abasic lesions in DNA. Another example is the investigation of the active site of T7 DNA polymerase. When the thymidine photoproduct dimer T_T, a known DNA lesion, is *inside* the active site, an adenosin is incorporated as opposing base. When it is *outside*,

the active site is empty and resembles an abasic site. In this case, **11** is incorporated selectively. In this manner, sequence dependencies have been examined.[56]

2.1.3 Pyrene Radical Cation

The induction of selective strand breaks by the pyrene nucleoside **10** of Boss are so far not explained. A suggested mechanism involves a fast reversible charge separation inside the DNA with the formation of an intermediate pyrene radical cation ($Py^{\bullet+}$). The theoretical background for the suggested mechanism is provided by Wagenknecht and Netzel.[57] Based on the relative redox properties, intercalated pyrene derivatives could initiate both, oxidative hole transfer to guanines ($E(Py^{\bullet+}/Py)$ = 1.5 V, vs. SHE), and reductive electron transfer to thymines ($E(Py/Py^{\bullet-})$ = -2.3 V, vs. SHE in DMF).[58] Both charge transfer assignments are proven by picosecond transient absorption experiments using the described Wagenknecht nucleoside or benzo[a]pyrenyl-2'-deoxyguanosine conjugates, respectively.[58] In order to avoid this dual charge transfer behaviour of intercalated pyrene derivatives and favourize the reductive charge transfer, Wagenknecht chose to attach the pyrenyl group to the nucleobase uracil in order to place it outside the DNA base stack. This extended nucleoside was investigated as monomer in water. Excitation of the pyrene moiety at 340 nm leads to an intramolecular electron transfer (ET), which yields the corresponding uracil radical anion and the pyrenyl radical cation ($Py^{\bullet+}$ – $dU^{\bullet-}$).[59,60] The intramolecular ET is an ultrafast process, the contact ion pair $Py^{\bullet+}$ – $dU^{\bullet-}$ can already be observed a few picoseconds after excitation in water (cf. Scheme 2.1).[61]

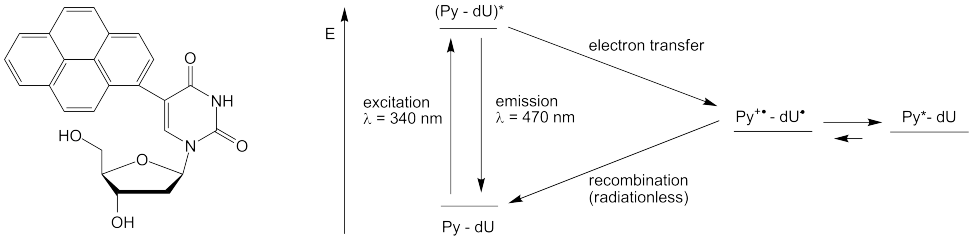

Scheme 2.1: 5-Pyrenyl-2'deoxyuridine nucleoside of Wagenknecht (left) and the ultrafast reversible injection of negative charge into a the nucleobase uracil (simplyfied, right)

This charge transfer (CT) assignment has been proven previously by Netzel et al.[62] In the nucleoside, the two chromophores are linked covalently by a single C–C bond, thus resulting in strong electronic coupling between them as a result of direct π-orbital overlap.[59,60,61] As a result of this specific mode of interaction between pyrene and the attached chromophore, the observable formation of strongly fluorescent intramolecular CT states may be considered as intramolecular exciplexes (excited complexes). These exciplex states contain locally excited (Py* – dU) and CT charge separated contact ion pair ($Py^{\bullet+}$ – $dU^{\bullet-}$) contributions. Moreover, the charge separated species that is initially formed ($Py^{\bullet+}$ – $dU^{\bullet-}$) is not fluorescent and equilibrates with the fluorescent locally excited form Py* – dU.

The excitation has been performed using a 75 W Xe lamb with a cut-off filter (> 305 nm).
Photoexcited Py* allows the reduction of C and T (U).[63,64] The oxidation potential versus standard hydrogen electrode (SHE) of pyrene to form the radical cation, $E(Py^{\bullet+}/Py)$, is 1.5 V.[63,59] For the photoexcited pyrene, the oxidation potential is assumed to be $E(Py^{\bullet+}/Py^*) = 1.85$ V. The corresponding reactant, uracil in the Wagenknecht experiments, exhibits a potential of $E(dU/dU^{\bullet-})$ = -1.10 V. [64] Quantitative estimates of the electrochemical reduction potentials of nucleosides are difficult to obtain, the reduction potentials of T is the same as for C and is almost equal to the one of dU, $E(T/T^{\bullet-}$ and $dC/dC^{\bullet-})$ = -1.09 V.[58] When 5-Pyrenyl-2'deoxyuridine nucleoside is incorporated in DNA, the injection of a negative charge into uracil was shown to induce electron transfer inside the DNA.
Also other groups like Majima *et al.* confirm the pyrene radical cation formation and charge transport in DNA.[65,66]
In this context, also the direct interaction of the pyrene with nucleobases is of interest. Exciplex (excited complex) formation between pyrene and nucleobases, in particular guanine, has been described by Arai *et al.*.[67,68] They attached a pyrene to the C-5 position of a single guanine base via a alkylether linker and observed a large Stokes shifted emission in the fluorescence spectrum compared with 1-hydroxymethylpyrene. This stacking may change the oxidation or reduction potential locally within the DNA and influence charge transfer reaction, if they occur.

2.2 Motivation

With pyrene induced strand breaks found by Boss, pyrene as an artifical nucleobase in DNA got into our focus. The strand breaks are not primarily induced by a ground state C-4' radical like in the case of **T***, but by a photoexcited pyrene, covalently attached in the middle of the DNA. The question arises, whether the strand breaks with the RNA-like nucleoside, possessing a methoxy group at the 2' position of the sugar, can also be observed with the 2'-deoxy version **11**, that is structurally closer to the natural DNA building blocks. Also the finding, that the nucleoside has to have two thymidines as neighbours to result in fast photoinduced strand cleavage is of interest. As the corresponding DNA nucleoside **11** and its structure inside the DNA is already known in literature and synthetically available, we wanted to compare it with **10** of the Boss system.

2.3 Synthesis of 11 and Incorporation into an Oligonucleotide

The synthesis pathway and procedures have been combined from several sources and optimized.[51,69] For the substitution on Hoffer's chlorosugar at the 1' position with 1-bromopyrene using boron trifluoride etherate, a slightly modified procedure from Seitz was used as shown in Scheme 2.2.[69,70] This

yielded 62% of the desired β-anomer **12**. An efficient method for epimerization of the, as by-product obtained, undesired α-anomer to the β-anomer by acid-catalyzed equilibration was applied to increase the yield (not depicted).[51] The geometry of the anomeric substitution is derived from ^{1}H NOE experiments by Kool *et al.*.[51] The simultaneous deprotection of the 3' and 5' position of **12**, to form the free diol **11**, was done with sodium methoxyde as base in 79% yield. To obtain the asymmetry required for the incorporation in DNA the 5' alcohol function was etherified using 4,4'-dimethoxytrityl chloride in basic conditions, yielding 76% of **13**, and the 3' alcohol function was modified with the precursor of the phosphate linkage as a phosphoramidite, producing **14** in 88% yield. This was done by using 2-cyanoethyl-*N,N*-(diisopropyl)-chlorophosphoramidite and Hünig's base.

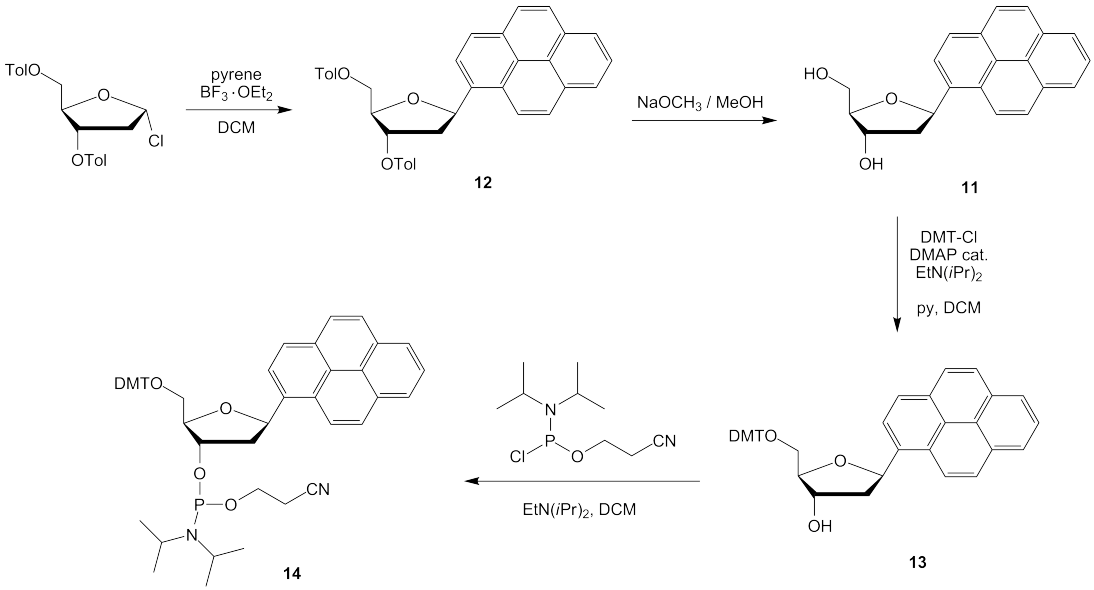

*Scheme 2.2: Synthesis overview of the polyaromatic C-nucleoside **11**.*

The resulting DNA synthesizer compatible nucleoside building block could be successfully incorporated in good yields according to trityl monitoring into an oligonucleotide via automated solid-phase synthesis. The oligo was cleaved from the solid support and purified first with the last trityl protection still intact. After deprotection, a second RP-HPLC purification was performed and the mass confirmed with MALDI-ToF MS. Detailed description can be found in the experimental part.

For double-strand experiments and measurements, the corresponding counter strand **cs6** was purchased and repurified. At the position of the modification **11**, an abasic site (**Ab**) was choosen and 3 and 4 Ts were added on the oligo as dangling ends to encrease hybridisation.

The following 20mer, called **s6**, carrying the modification **11** was synthesized, below the corresponding couter strand **cs6**.

s6: 5'-TGC ATC AT**11** TTT ATC AGA GC-3'

cs6: 5'-TTT ACG TAG TA**Ab** AAA TAG TCT CG TTT T-3'

To control the correct annealing of the double-strand, thermal denaturation measurements were performed. The resulting T_m = 54°C in irradiation buffer confirmed its stability. Circular dichorism experiments (CD) were compared to references and the B-DNA secondary structure was attested.

2.4 Irradiation Experiments

The pyrene containing strand **s6** was irraddiated either as single-strand or as double-strand. In the latter case, **s6** was annealed with the corresponding counter strand **cs6**. About 1 nmol was dissolved in 240 mL 20 mM sodium citrate buffer, containing 100 mM sodium chloride at pH 5.0 (4.2 µM). Oxygen was removed from the sample by bubbling argon through the solution for 10 min. This ensures the absence of oxygen to avoid formation of reactive oxygen species (ROS) unter the irradiation conditions (cf. Chapter 1.1.1.3). Irradiations were performed in an airtight disposable plastic cuvettes with a 500 W Hg lamp with a 320 nm cut-off filter at 15°C. The expected **s6** 5'– and **s6** 3'–phosphates were purchased, repurified and injected separately to serve as retention time reference. For every experiment, 15% of the solution was removed before treatment with argon and injected into the HPLC as a reference for the ratio of the two strands in double-strand experiments and to check the purity. DNA was monitored at 260 nm and the pyrene containing strands and fragments simultaneously at 346 nm. For quantification of HPLC results, the integrals of the signals were divided by the molar extinction factors of the corresponding molecules.

The samples were irradiated for 40 min or 120 min. Up to 40 min, there is no significant damage of the strands. After 120 min the HPLC chromatogram reveals several damages. The damages can be split in two categories. Firstly there is a statistical, not regio specific degradation of the strands. This leads mainly to broadening of the signals. As a consequence, integration and therefore quantification of the remaining strands is difficult and the accuracy is reduced. Secondly the pyrene induced strand cleavage products, as expected from the Boss experiments, could be identified. As their retention time (t_R) is much shorter than the ones of the strands and the statistically produced products, they can be analysed with ease. These **s6** 5'– and **s6** 3'–phosphates were identified in three ways. Firstly, the HPLC peaks at 260 nm (DNA) show no signal at 346 nm, meaning no pyrene present in the strands. Secondly, the retention times correspond to the reference injections of the same fragments. Thirdly, the found masses in the MALDi-ToF are exactly as calculated. Both phosphates are almost equal in amounts. Within the experimental error, a slightly higher amount of **s6** 3'–phosphate can be assumed. In Figure 2.5, a HPLC chromatogram after 120 min of irradiation is depicted. The starting strands (**s6** and **cs6**) and the fragments **s6** 5'– and **s6** 3'–phosphate are labeled. Totally, about 55% of **s6** has been destroyed. One part is

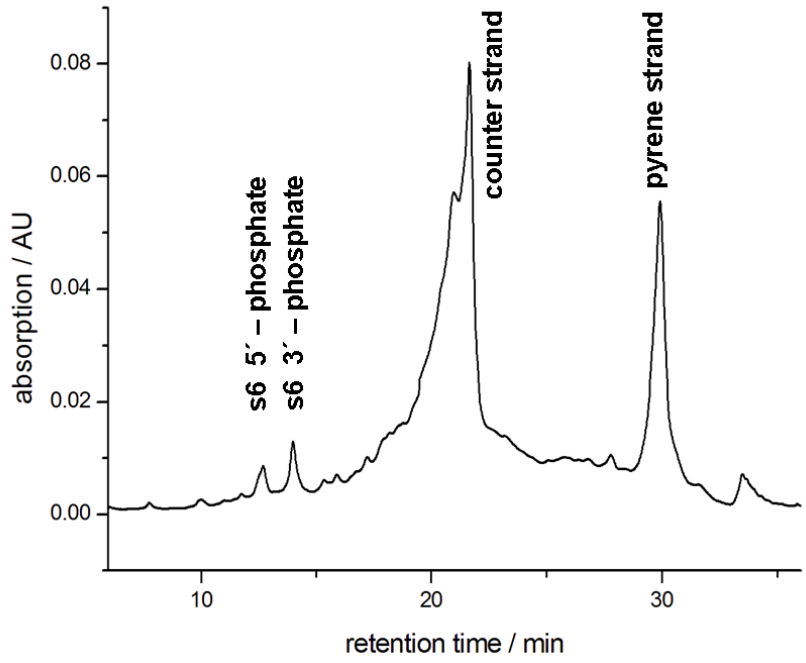

*Figure 2.5: Chromatogram after irradiation for 120 min of the double-strand **s6/cs6**. The remaining strands and the pyrene induced fragments are labeled.*

the statistical damage, that is estimated to be about 41% according to reference irradiations. As a reference the double-strand **s7/cs7** (T instead of **11**, A instead of **Ab**) was irradiated for 2 h (strands shown below). Both strands produce fragments that are grouped around the peak of the strands in the HPLC. But there are no relevant amounts of fragments in the range, where the strand break phosphates are found.

s7: 5'-TGC ATC AT**T** TTT ATC AGA GC-3'
cs7: 5'-TTT ACG TAG TA**A** AAA TAG TCT CG TTT T-3'

Theoretically, all formed products are also subjected to statistical damage themselves. The statistical degradation of DNA strands during irradiation is strongly dependent on the length of the strands. As the strands resulting from pyrene induced strand cleavage (8mer and 11mer) are about half the length of the starting strand (20mer), the statistical degradation is assumed to be negligible. The finding that the signals of the two phosphates are sharp and do not exhibit shoulders like the starting strand, the assumption seem to be confirmed. The amounts of **s6** 3'–phosphates are nearly the same, the calculation yields almost same results.
If all pyrene induced strand breaks yield **s6** 5'– and **s6** 3'–phosphate, and the damage of these products themselfes during the irradiation is negligible, at least 14% of the irradiated **s6** has been cleaved around

the pyrene moiety (cf. Equation 2.1). If other products were also formed or the phosphates were suffering degradation, the amount of pyrene induced strand cleavage would be higher. The statistical damage on the counter strand yields to a signal, that cannot be used for calculation of strand ratios in a suitable manner.

$$\textit{Strand cleavage} = \frac{\textit{formed 3'–phosphate}}{\textit{remaining } \mathbf{s6} + \textit{formed 3'–phosphate}} \tag{2.1}$$

The results of the two irradiation times are summarized in Table 2.1. The irradiation results for single- and double-strands were comparable within the experimental error.

retention time	mass	amount after 40'	amount after 120'	assignment
12.6'	2465	2.4%	14%	**s6** 3'–phosphate
13.8'	3411	1.9%	12%	**s6** 5'–phosphate
21.6'	8450	96%	–	**cs6**
29.9'	6158	91%	45%	remaining **s6**

*Table 2.1: Summarized results of the pyrene induced strand break of **s6**. The assignment was made according to t_R and MALDI-ToF*

2.5 Summary

Pyrene was sucessfully introduced into a β-C-nucleoside and incorporated in the middle of an DNA oligomer in good yields. For structural reasons the abasic site was chosen as counterpart in a double-strand. The unchanged B-DNA conformation with the unnatural base pair is known from literature and could be confirmed by CD measurements and thermal denaturation experiments. An unmodified double-strand, having the same sequence and with a T instead of the pyrene nucleoside and an A instead of the abasic side, was considered as reference. The double-strand was irradiated with a 500 W Hg lamp equipped with a 320 nm cut-off filter at 15°C. Excessive irradiation durations of 1-2 hours lead to degradation of the strands. The amount of destroyed pyrene modified strand (**s6**) ranges from 9 - 55% for irradiations form 40' to 120'. Among the products are two prominent fragments, both in 12% and 14% yield. They could be identified by MALDI-ToF mass analysis and comparision of HPLC retention times with synthesized references to be **s6** 5'–phosphate and **s6** 3'–phosphate. The irradiation yielded in slightly more **s6** 3'–phosphate than **s6** 5'–phosphate. The difference is reproducible but small (Δ = 2%) and lies within the experimental error range.

2.6 Discussion

This discussion is focused on the comparison of the irradiation results of the **s6** strand and the results of Boss (**s5** strand). The regioselective strand breaks by $\mathbf{T}^*$ of Giese *et al.* were initiated by the chemical

generation of a sugar radical in ground state, followed by charge transfer (cf. Chapter 1). In contrast, the pyrene induced strand breaks are based on photoexcitation of pyrene.
The sequence of the oligonucleotide **s6** is identical with the sequence of **s5**, where Boss has observed the pyrene induced strand breaks. As the only chemical difference is the lacking 2' methoxy group at the modified nucleoside, the significantly different irradiation yields must be caused by this methoxy group. An unsubstituted 2' position, like in **11**, is typical for the deoxyribose sugars of DNA. The methoxy substituent of **10** resembles more the 2' hydroxy substituent of RNA ribose sugars (cf. Figure 2.6). In

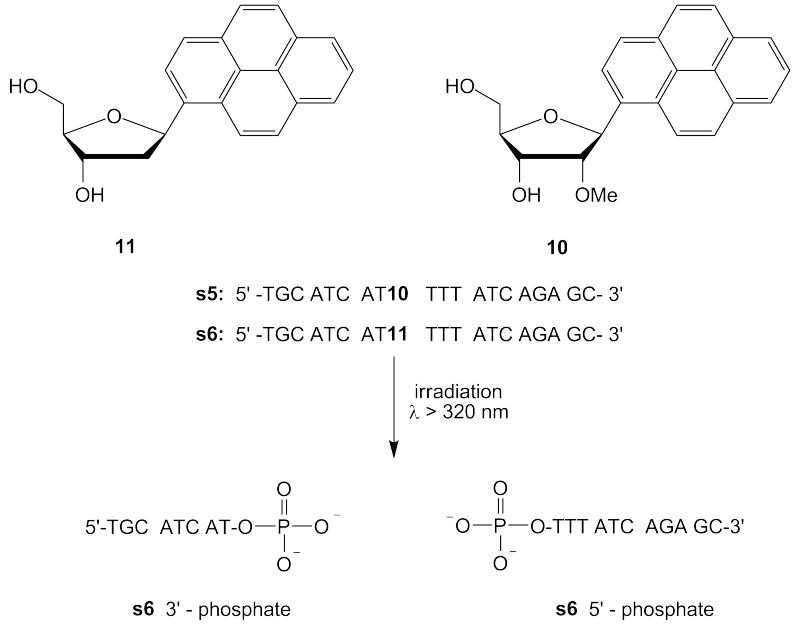

Figure 2.6: Overview over the compared artificial nucleosides and the resutling specific irradiation products.

RNA, where a hydroxy group is at the 2' position of the sugar, there are different sterical demands. The deoxynucleoside T is therefore exchanged by the nucleoside U, that is lacking the methyl group (cf. Figure 2.7). The other nucleobases (A, C and G) are present in DNA and in RNA. Like all nucleosides, their sugars carry a hydroxy group at the 2' position (ribose) in RNA and are unsubstituted in DNA.
When irradiating up to 40 min, the **s6** strand does not exhibit any degradation. After longer irradiations, like 120 min, the **s6** strand clearly cleaves. The **s5** strand already produced 20% strand breaks after 6 minutes. The identified strand break fragments of the **s5** strand, denoted 5'–phosphate and 3'–phosphate, could also be observed as strand break fragments of the **s6** strand (cf. Figure 2.6). We identified slightly more 3'–phosphate than 5'–phosphate. The difference is small and it is unclear, whether it is relevant, as the difference lies within the experimental error range. The relative ratio is in contrast to Boss experiments, where there was slightly more 5'–phosphate (20%) than 3'–phosphate (16%) as explained in Chapter 2.1.1). The modification themselfes (**10** and **11**) are not part of any observed fragments. This

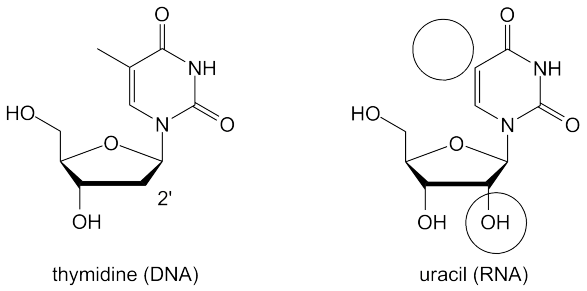

Figure 2.7: Comparison between the DNA and the RNA buiding blocks T and U. Differences are the methyl group at the base and the hydroxy group at the sugar, both marked with a circle.

can be explained by a detachment of the pyrene as a consequence of the irradiation. Based on the similar amounts of both phosphates and the missing pyrene moiety we conclude, that both fragments are produced in the same reaction sequence.

As we observed, the methoxy nucleoside **10** leads to faster strand cleavage than the 2' deoxynucleoside **11**, if the pyrene nucleosides have thymidines as neighbours.

The strands do not form the specific fragments without irradiation and also not when a unmodified control strand is irradiated. The photoexcitation of the pyrene is therefore considered to be a crucial step. The charge separation, postulated by Wagenknecht and described in Chapter 2.1.3, could be the next step after the photoexcitation. In this process, an adjacent nucleobase may serve as electron donor, while the photosensitizer pyrene acts as excited state oxidant.

The methoxy group of **10** influences the local secondary structure of the strand. This alteration could expose the pyrene more to the surface in the methoxy case. Pyrene could unwantedly be flipped outside the stack. Spontaneous flipping out of nucleobases from the helical stack in solution are known and occur on milisecond time scale (approx. $50\,\mathrm{kJ{\cdot}mol^{-1}}$).[71] A hint for a pyrene, flipping outside of the stacked nucleobases in DNA (and not in RNA) was given by Pedersen in 2002.[72,73] As pyrene has to be excited by light to produce strand breaks, a better exposure would speed up the reaction. This is in agreement with the observed results.

Conformational stress can produce sterical tension. The methoxy group of **10** resembles to the nucleosides of RNA. In RNA, the nucleobase thymidine is replaced by uracil to avoid sterical tension. From the conformational point of view, thymidine is more restricted inside the B-DNA than other nucleobases. Being hydrophobic, the methyl group is forced to a certain position in the major groove in the DNA strand. This restriction results in a more stable structure. If the local environment is disturbed, as it probably is with the pyrene nuceoside **10**, the methyl group can cause sterical tention instead of stabilisation. When two Ts are adjacent to the methoxy substituted **10**, the stress, produced by the methyl groups of T may be much bigger than when other nucleobases are adjacent (-C**10**C-, -A**10**A- etc.). Therefore the strand breaks can occur more easily in -T**10**T-. The missing sterical stress in the **s6** strand would explain the

slowed down strand breaks. As mentioned in Chapter 2.1.1, Boss did not irradiate the other sequences (-C**10**C-, -A**10**A- etc.) for more than 6 minutes. As **10** has not two Ts as neighbours in these sequences, their local conformation is probably more like the -T**11**T- structure. Perhaps they would exhibit a similar behaviour like the **s6** strand and also degrade after longer irradiation. An altered conformation due to the methoxy group could also lead to changes of oxidation potentials, as the oxidation potentials of nucleobases are sensitive to their environment.[74] For example, the one of guanosine is lowered by the formation of its Watson & Crick base pair with cytosine.[75] This changes, being different for the **s6** and the **s5** strand, could also be the reason for the different results.

When the adjacent nucleobases are arranged in a nicely stacked manner like in -T**11**T-, where strand breaks occur slower than in -T**10**T-, the energy of the photoexcited pyrene could be quenched by the nearby nucleobases as a competing reaction.

To answer the question, whether pyrene also acts as a regioselective DNA cleavage site without the sugar moiety, another pyrene building block was incorporated into an olignucleotide. This approach is described in the next Chapter.

Chapter 3

Pyrene Diamide Incorporated in DNA

3.1 Introductions

3.1.1 Structural Informations

Häner and his group from the University of Bern are working on artificial DNA base surrogates.[76,77] They employ polyaromatic compounds as center, for instance phenanthrene, phenanthroline or pyrene.[68,78] The type of modified DNA of our interest, to investigate its ability to produce strand breaks, is based on the use of extended aromatic systems with non-nucleosidic linkers.[79] The positions 1 and 8 of pyrene

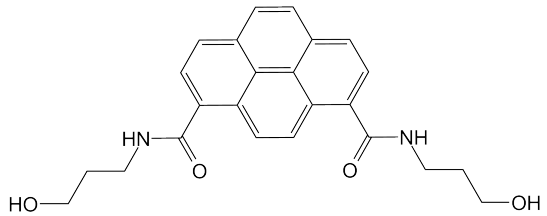

15

*Figure 3.1: The pyrene derivative **15** of Häner.*

are connected to γ-hydroxypropyl linkers via a amide functions (cf. Figure 3.1). Häner implemented the investigated molecule **15** in the middle of a 19mer oligonucleotide between two phosphate groups, replacing a nucleoside in the middle. In terms of the DNA backbone, the molecule replaces the sugar connection between two phosphates. Also strands with the modification at the terminal position have been under investigation. There the pyrene exhibits a stabilizing effect as it can lay on top of the stacked bases.[77]

In this system, the stacking properties can be considered as the main factor for stabilization of secondary structures like it is in the case of **11**, as discussed in Chapter 2.1.2.2.[79] Due to their hydrophobic nature, stacking interactions of pyrene–base and/or pyrene–pyrene type are expected to play an important role

not only in duplex but also in single-strands in polar medium.

For the formation of a double-strand, a suitable counterpart to the pyrene diamide **15** had to be chosen. As pyrene is sterically more demanding as a natural nucleobase, its counterpart has to be smaller than in usual base pairing. Häner chose therefore the abasic site (**Ab**) like Kool did for his pyrene nucleoside **11** (cf. Chapter 2.1.2.2).

The circular dichroism (CD) spectra of an oligomer bearing a **15** moiety as a double-strand with **Ab** as counterpart on the other strand, are in good agreement with that of a typical B-DNA structure.[5,77] The spectroscopic investigations support a duplex, in which the polyaromatic residue is arranged in an interstrand-stacked fashion without destabilizing the DNA duplex nor altering its overall B-type structure.[80] The minimum, maximum and the zero-crossing of the modified duplexes correlate very well with the ones of the unmodified DNA duplex (250 nm, 280 nm and 260 – 265 nm, respectively). Also the thermal denaturation experiments (T_m) and cumputer based calculations confirm the structure and stability of the abasic site pairing with **15** inside an oligonucleotide.[81,82]

Langenegger tested several linker length to determine the maximal thermodynamic stability of the double-strand.[5,77] The length of the linkers determine the degree of freedom of the pyrene and the local backbone. He placed 2 – 5 methylene groups between the amide and the phosphate. The differences in melting temperature arising from changing the length of the linker in a 19mer was about 2°C. This means, that the linker length in this case is not very relevant. The highest thermodynamic stability was achieved with four methylene groups. He compared the stability with the strand, where the pyrene nucleoside is exchanged by an adenosine opposing the abasic site.

3.1.2 Synthesis of the Pyrene Diamide 15 and its Incorporation into DNA

The synthesis of the building block and the incorporation into an oligonucleotide has been performed by coworkers of Häner.

For the incorporation, the alcohol groups were modified on one side with a dimethyltrityl (DMT) protection group and on the other side with a standard phosphite function. The resulting building block has the same attachment points as the phosphoramidite of **11** or **T***. The oligonucleotide was prepared via automated oligonucleotide synthesis by a standard synthetic procedure and purified by reverse phase HPLC and characterized by electrospray ionisation time-of-flight (ESI-TOF) mass spectrometry.[79] Incorporation of **15** proceeded without any difficulties with coupling yields being equal to those of unmodified nucleotide bases. Before usage, the mass has been confirmed by MALDI-ToF MS. The Scheme 3.2 show the local structure of the incorporation and the chosen nucleotide sequence **s8**. The sequence of the bases was chosen to be exactly like the sequences in **s5** (Chapter 2.1.1) and **s6** to maximize comparablitiy. The counter strand for double-strand experiments contains an abasic site opposing **15** and 5 Ts on both sides as dangling ends.

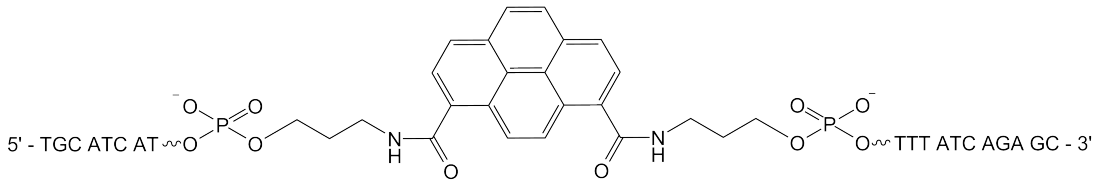

*Figure 3.2: Sequence and core structure of **s8**.*

The fluorescence properties of pyrene and the clearly distinguishable emission of the excited pyrene dimer have led to application as structural probes.
In particular, it was shown by Häner that interstrand stacked pyrenes (one pyrene in each strand opposing each other) give rise to excimer (excited dimer) formation according to changes in fluorescence.[77] Due to the large bathochromic shift of the excimer fluorescence – up to 100 nm compared to the fluorescence of the monomer – adjacent pyrene systems are of interest for applications in materials research as well as in genetic diagnostics. The stacking and the flourescence properties were used by Häner for creating a molecular beacon.[83]

3.2 Motivation

As we concluded, by comparing the experiments with **s5** and **s6**, the more B-DNA-like structure in the latter case slows down the strand cleavage. So the question arises, what will happen, if a pyrene was introduced with a much higher conformational freedom. A pyrene, attached between two propyl groups seemed to be suitable for answering that question. Also the importance for the strand cleavage of the sugar in the pyrene nucleoside could perhaps be revealed. The pyrene diamide of Häner can be incorporated into DNA and does not destabilize the B-DNA double-stranded helix when paired with the abasic site. It was chosen as candidate for the investigations.

3.3 Pyrene Diamide as Oligonucleotide Modification

3.3.1 Irradiations

The focus in these irradiations is the modification **15** inside the oligonucleotide sequence **s8**. The nucleobase sequence is identical to the one of **s5**, containing **10** and **s6**, containing **11**, to optimize the comparability of the results. For double-strand formation the counter strand **cs8** has 5 T's on both sides and a abasic site (**Ab**) opposing **15**. The investigated **s8** has been irradiated as single-strand and as double-strand, annealed with **cs8**.

s8: 5' –TGC ATC AT**15** TTT ATC AGA GC– 3'

cs8: 3' –TT TTT ACG TAG TA**Ab** AAA TAG TCT CG TTT TT– 3'

The irradidation conditions are very similar to those of **s6** irradiation to increase the comparability. 1.0 nmol have been used for each irradiation. When irradiated as double-strand, 1.1 nmol counter strand were added and annealed. The aqueous citrate buffer was degassed, using argon. About 15% of each sample has been removed to serve as reference. The samples were irradiated for 10, 30 and 60 min at 15°C. Analysis was performed by RP-HPLC using 260 nm and 346 nm UV light as detection. The DNA bases are pyrene are absorbing at 260 nm. At 346 nm only pyrene absorbs. This enables to destinguish between pyrene containing fragments and fragments without pyrene. The peaks have been collected separately and subsequent MALDI-ToF mass analysis enabled fragment assignment.

As reference, unmodified control strands with a T instead of the pyrene linker and an A instead of the abasic site (**s7/cs7**) are mostly stable under the irradiation conditions as double- and as single-strands. After 60 min, unspecific degradation occured, but none of the characteristic fragments from irradiations with the modified strand were formed. As control double-strand, the ones applied in Chapter 2.4 were used.

The shortest irradiation time chosen for **s8/cs8** was 10 min. No strand degradation could be observed in the double-strand as well as in the single-strand. The amounts after irradiation are equal to the amounts before irradiation.After 30 min, the amount of detected intact **s8** is 40 – 65% . That means 35 – 60% was damaged or cleaved. About 70% of the disappeared **s8** amount could be found as defined fragments. The fragments occur in comparable amounts.

After **s8/cs8** irradiation for 60 minutes, again, single- and double-strand experiments gave similar results. When comparing the integral of the remaining **s8** after 60 min and the corresponding integral before irradiation, 68 – 72% has been damaged or cleaved. 73 – 95% of the disappeared **s8** was found as defined, characterized fragments. The fragments occur in comparable amounts.

The irradiations of 30 and 60 min show several peaks resulting from degrading starting material that can be precisely integrated or an approximation of the integral is reasonable. We observed three peaks around t_R 13 – 15 min and two peaks, that is not very good resolved at t_R 34 min, if one detects at 260 nm. After longer irradiation, the strands start to degrade at statistical positions. This also happens to the same extent with the unmodified control strands (**s7/cs7**). The resulting fragments have a similar retention time in the HPLC and are grouped around the starting strand, like already observed and described in Chapter 2.4. Quantifications are difficult in these areas of the chromatogram. The amount of destroyed **s8** can be estimated from the HPLC chromatogram. Both simultaneously recorded wavelength are suitable (260 nm and 346 nm). This redundancy was used as a control for calculations. The chromatograms recorded at 260 nm were used to find the products of the irradiation. The peaks were collected separately and masses

were determined by MALDI-ToF. The assignment, whether a fragment contains pyrene or not can be seen when comparing the chromatograms recorded at 346 nm, as unmodified DNA does not absorb at this wavelength, only pyrene does.

Every pyrene induced strand break, results in a 5' fragment paired with a 3' fragment. They were always detected in equal amounts. HPLC signals in the range of 2 – 4 min are assigned to artefacts of the used HPLC buffer.

In Figure 3.3, the irradiation (right side) and reference (left side) HPLC chromatograms recorded at 260 nm (top) and 346 nm (bottom) are displaid. The above mentioned group of peaks are zoomed as inset (right top and bottom).

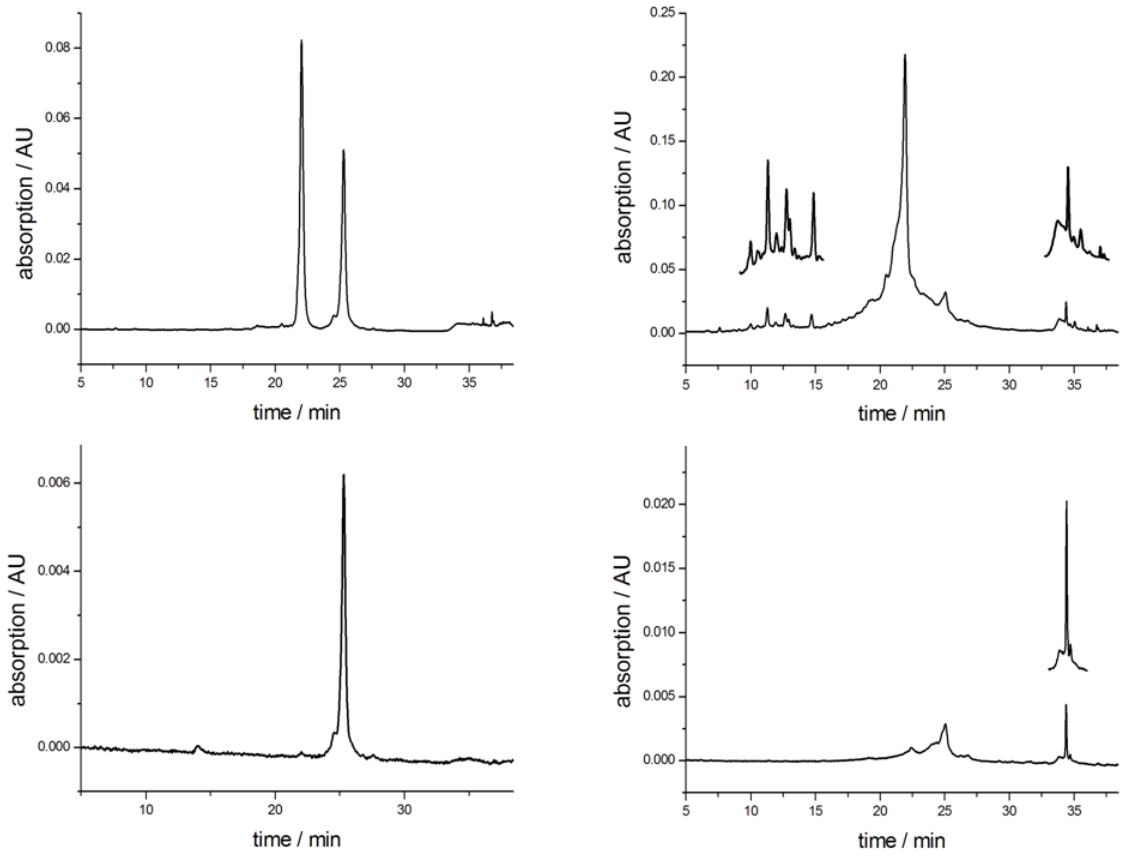

*Figure 3.3: 260 nm and 346 nm irradiation (60 min) and reference HPLC chromatograms of double-strand **s8/cs8**.*

In Figure 3.4 the breaking sites are indicated with lines perpendicular to the broken bonds. Fragments starting at the 5'-end are labeled with an '**f**' and numbers. The corresponding 3' fragment have the same f-number plus a 'prime'. All the indicated fragments are confirmed by mass analysis (MALDI-ToF). The masses were calculated with an proton at the position of the broken bond. All masses were confirmed. A complete list can be found in the Experimental Part. The fragment **f6'**, resulting of the bond cleavage

between **f6** and **f6'**, could not be confirmed by its mass. This might have analytical reasons and will not be discussed in detail.

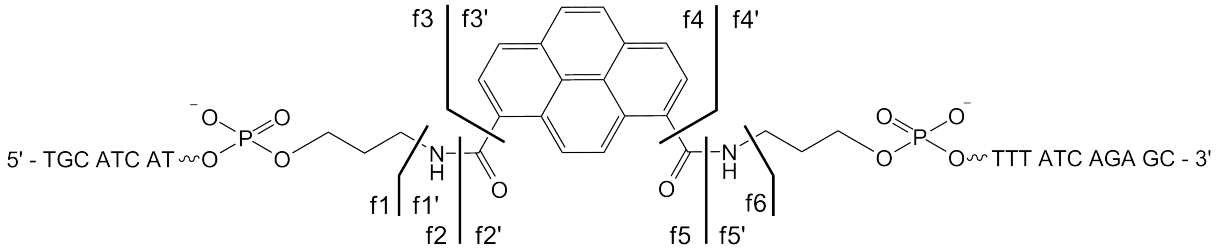

*Figure 3.4: Observed fragmentation points of **s8***

The fragments can be allocated to the peaks of the HPLC chromatogram recorded at 260 nm, as depicted in Figure 3.5. The braces indicate an uncertainty in allocation. The large peak at 23 min represents the counter strand **cs8**. Here, the statistical degradation can be seen as shoulders and broadening of the peak at the base. Before the irradiation, the signals of the two employed strands are baseline separated (cf. Figure 3.3, top left).

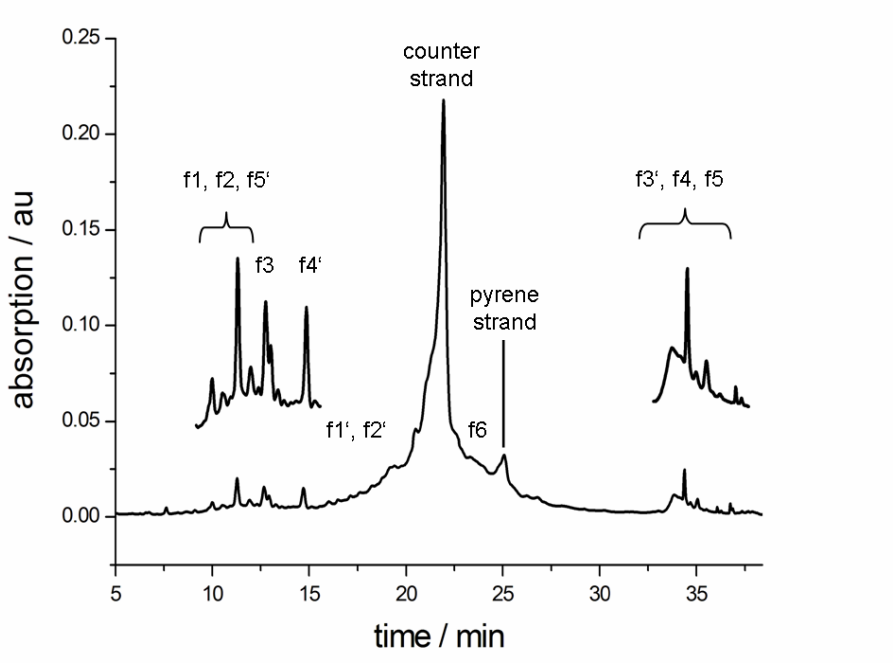

*Figure 3.5: Fragments of **s8** assignment according to mass*

In Figure 3.6, the damage of **s8** from 0 min over 30 min to 60 min irradiation is shown. The reference (0 min) is the lowest line and the upper ones are with increasing irradiation time. The chromatogram, recorded at 346 nm, only shows the employed strand **s8** and pyrene containing fragments. This property

was used as control for the assignment of the fragments according to their mass. As the strand at 23 min vanishes from the chromatogram, broadening occurs on both sides. Also a prominent couple of peaks arises at about 32 min (fragments **f3'**, **f4** and **f5**).

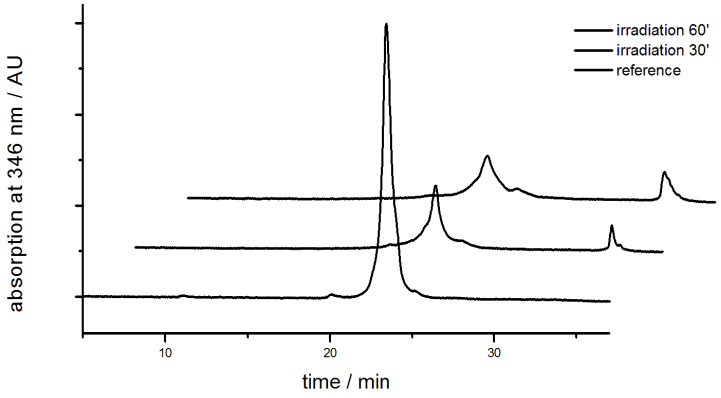

*Figure 3.6: Degradation of **s8** at different times.*

The results will be summarized and discussed at the end of the following Chapter 3.4.
The points of cleavage in the case of the Häner strands are all close to the pyrene. The phosphorester bond did not break. The question arises, whether the DNA with its nucleobases and defined secondary structure is necessary for the bond cleavages around the pyrene. If the free diol **15** would be irradiated in solution, this question should be answered in the next Chapter.

3.4 Pyrene Diamide as Free Diol

3.4.1 Irradiations

The diamide **15** represents the core structure of **s8**. Irradiation of **15** would show, whether the DNA environment actually plays a role in the cleavage. Whether due to sterical stress or electronic interaction like e.g. charge transfer. In the following irradiations, there are no nucleobases nor phosphorester bonds present, that can act as reaction partners. The compound shown in Figure 3.7 was received from the Häner group and was used without further purification. The compound is 95.6% in purity, according to HPLC analysis at 346 nm.

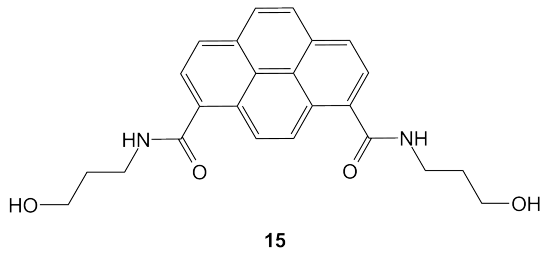

*Figure 3.7: Compound **15**, the core of the strand **s8** as free diol.*

The irradiation conditions have been identical to the one of the **s8** irradiations. The diamide **15** was dissolved in 0.1 M citrate buffer, containing 100 mM sodium chloride (pH 5.0). The buffer was filtered using a 0.45 µm syringe filter to ensure quality. The concentration has been determined by measuring the optical density at 260 nm by using the estimated molar extinction coefficient $\varepsilon_{260} = 8600\,\mathrm{M^{-1}cm^{-1}}$ for the pyrene motif yielding in a 0.6 µM solution. The irradiation was done with a 500 W Mercury lamp and a 320 nm cut-off filter. All experiments were done at a constant temperature of 15°C. The irradiation times were 10 min or 40 min. The experiments have been tracked and analysed by RP-HPLC, recorded at 346 nm. For analytical reasons, a different RP-HPLC solvent gradient was applied.

Before each irradiation, about 10% of the solution has been removed and injected as reference. The analysis of the experiments has been done using the integrated HPLC chromatograms. The integrated areas of the peaks are quantitatively comparable among each other, as all products have similar molar extinction factors.

The results of the irradiation performed with **15** can be summarized as follows: The molecule **15** (t_R = 15.6 min) is photosensitive and breaks apart during irradiation. After 10 minutes, about 60% and after 40 minutes of irradiation 95% were decomposed. No masses of the observed signals could be measured using ESI or MALDI-ToF. There were no differences in the result whether the solution was degassed

or not. Thus the presence or absence of oxygen did not influence the results of the experiments. One peak (10.4 min) appears during the irradiation and features an increasing integral over time. This is the only observed stable product. The following estimation about the amounts can be made. After 10 min 0.2% and after 40 min 0.7 – 1.5% of the starting material was transformed into this new compound. As the masses could not be determined, no assignment was possible. Roughly, after irradiation, the overall integral is constant. Thus the integral of the remaining **15** plus all the integrals of the other peaks (irradiation products) equals the amount of starting material. As the pyrene aromatic system is the only chromophore, and the overall integral is constant, it can be assumed, that the pyrene aromatic system itself is not destroyed during irradiation in relevant amounts.

3.4.2 Summary

In summary, strand **s8** was irradiated as single- and double-strand. The strand **s8** contains the modification **15** between two phosphates. In the double-strand, an abasic site was incorporated opposite the pyrene moiety in the counter strand. The pair functions as a base pair replacement without major distortions to the DNA conformation. Irradiation for 60 min yielded in 70% cleavage (30 – 60% after 30 min, none after 10 min). The points of cleavage could be identified by MALDI-ToF mass analysis and are selectively in close proximity around the pyrene concerning the amide bonds. The phosphorester bonds were not cleaved. Thus the 5'– and 3'–phosphates of **s5** and **s6** (containing pyrene as C-nucleoside) were not produced. No major differences in irradition results for single- and double-strands were observed. Unmodified strands with a T instead of the pyrene linker and an A instead of the abasic site (**s7/cs7**) were irradiated as control experiments. None of the fragments assigned to pyrene induced strand cleavage were detected. The bond cleavage in the strand **s8** was therefore clearly triggered by photoexitation of the pyrene moiety. The irradiation of the free diol **15** was performed the same way as the irradiation of the strand **s8**. After 10 min, 60% and after 40 min, 95% of **15** was destroyed. Fragments could not be identified. According to HPLC integration calculations, the pyrene chromophore itself was not destroyed during the irradiation. We have compared the irradiations of the strand **s8** with the irradiations of the free pyrene diamide diol **15**. The degradation of **15** is faster when irradiated as free diol. Therefore we conclude, that charge transfer reactions with nucleobases are not responsible for the **s8** strand breaks. The surrounding DNA slows down the degradation of the pyrene moiety.

Chapter 4

Polyaromatic Surfactants Complexed with DNA

4.1 Introduction and Motivation

Due to the repetitive, well-defined arrangement of their building blocks, nucleic acids and related types of oligomers are ideal objects for the designed construction of larger assemblies and architectures.[77,84] Tertiary structures in nucleic acids are also becoming better understood. DNAs are even capable of being assembled into designed structures that undergo controllable motions, much like molecular machines.[10,85] We wanted to use the established technique of SDC formation to produce novel nanomaterials. A calculated version of a SDC is shown in Figure 4.1.

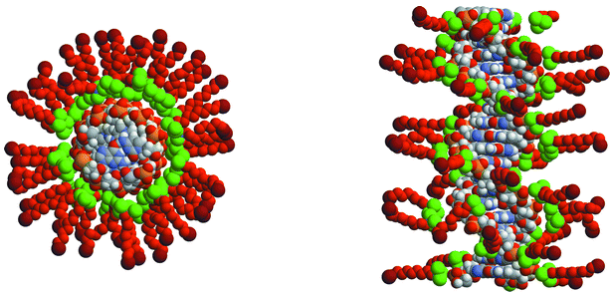

Figure 4.1: Calculated structure of an SDC with aliphatic surfactants. A model of a surfactant-DNA complex (SDC). The surfactants surrounding the DNA (in blue and grey) are shown with hydrophobic tails in red and cationic head groups in green. Left: top view, right: side view.

The alignment of small particles to form a big structure is called bottom-up assembly. As the DNA delivers the linear (actually spiral) scaffold, a kind of nanowire can be produced. DNA can attract and

arrange cations. When potentially conducting cations like polyaromatic compounds are used, electrons may be hopping from one aromatic stepping stone to another, forming a nanosized molecular wire. The drawing in Figure 4.2 illustrates the idea.

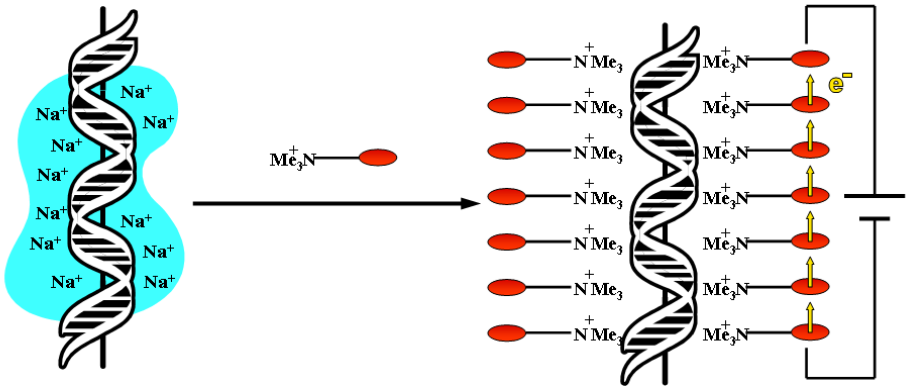

Figure 4.2: Draft of the motivation for the project

This new approach may open a whole new field in nanoelectronics, where carbon-nanotubes currently are the dominating species.[86] If a significant charge migration can be observed, the fibers could be applicable in electrical circuits. The metal-free composition and the low production costs would inherently be more interesting than silicon based structures. The measurement of conductance of biomolecules is a very difficult task.[87] The main problem is to establish a sufficient contact between the electrodes and the molecules. The measurements of conductance is not part of this thesis. The question to be answered was: Can aromatic compounds be attached non-convalently to DNA using surfactant-DNA complexes and is it possible to produce nanostructured materials?

4.2 Experiments

4.2.1 Investigated DNA

For the investigation of surfactant-DNA complexes with material science background, the DNA was required to be readily available in gram scale. As the DNA was used as scaffold, the second requirement was the double-stranded structure. We have chosen two kinds of DNA. Genomic DNA and DNA fragments in the 0.5 kbp scale (kilo base pair scale).

We used commercially available genomic DNA, isolated from salmon or herring testes. Genomic DNA is a fragile molecule. 'Small' DNA with less than 10^4 base pairs (10 kbp) can be vortexed without damage. Larger DNA with 10 – 30 kbp survives gently shaking. Any longer DNA is very fragile. For quantification and calculation, an average ε_{260} = 8300 $M^{-1}cm^{-1}$ per base and therefore per negatively charged phosphate was used. To confirm the double-stranded structure, melting experiments were per-

formed. When working with genomic DNA, the temperature has to be kept low. The molecule can break apart and the double-strand can be denatured (separated in two single-strands). Once denatured, the double-strand cannot be annealed anymore because of its length and the broad mixture of strands in solution.

For our experiments we also wanted DNA fragments with a defined length. One easyly accessible and low priced way is to sonicate genomic DNA. The ultrasound breaks the DNA in fragments of 400 – 500 base pairs with high fidelity. The theoretical lower limit in breaking up DNA with ultrasound is defined by its persistence length of about 140 – 150 base pairs (50 nm).[88] This was done in collaboration with Fabienne Hamburger from the Bickle group at the University of Basel. To confirm the conserved double-strand structure, we measured the melting point in buffer and observed a clear transition at 60°C (melting curve shown in the Experimental Part). So the structure is not harmed by ultrasound treatment. The fragments were purified from buffer and salt by preciption in 70% 2-propanol. The sonification was performed in three times for 20 seconds with cooling with ice inbetween. The sonication has to be kept short in time to avoid temperature increases in the sample which would mean denaturation. The length of the fragment was controlled by 1.2% agarose gel, using a 1 kbp and a 100 bp ladder for comparison.

4.2.2 Functionalized Surfactants

4.2.2.1 Choice of Surfactants

For the formation of surfactant-DNA complexes and their application, we have chosen different surfactant structures. The requirements for all compounds to serve as surfactant were already discussed in Chapter 1.1.3. The leading structure is composed of three parts. A permanently positive charged head attaches to the polyanionic backbone of the DNA non-covalently. A hydrophobic tail is responsible for cooperative binding due to hydrophobic interactions between the surfactants. It also serves as spacer between the DNA and the functional group, attached at the end of the tail. As aliphatic alkyl chain surfactant for testing we used CTAB (already described in Chapter 1.1.3), shown in Figure 4.3.

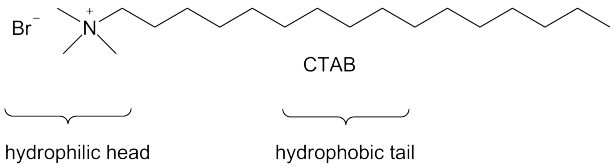

Figure 4.3: The aliphatic surfactant CTAB with a trimethylammonium head and a hexydecyl tail.

Pyrene was the first choice as aromatic functionality to be transformed into a surfactant. Other functional groups such as anthracene, which shows a higher solubility and has a lower oxidation potential (1.41 V vs. SHE) than pyrene (1.5 V vs. SHE) can also be attached. Therefore, anthracene is a better candidate to

function as a charge carrier for instance in the surfactant-DNA complex.

4.2.2.2 Synthesis of Surfactants

All surfactants were synthesized with the final step being the introduction of the trimethylammonium group. For all compounds the same procedure was applied. The substituted alkylbromide was converted quantitatively with fiftyfold excess of trimethylamine in ethanol at 55°C to the corresponding trimethylammonium bromide salt (cf. Scheme 4.1). After drying, no additional purification of the powder was required.

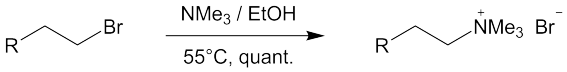

Scheme 4.1: Quantitative formation of trimethylammonium bromides from alkyl bromides. ***R*** *represents aromatic alkyl substituents.*

The attachment of the alkyl chain as bromide to the nitrogen of 1,8-naphthalimide to form **16** was achieved with potassium carbonate in *N,N*-dimethylformamide (DMF). Subsequent amination yielded **17** (cf. Scheme 4.2) The corresponding reaction for carbazole to yield **18** as phase-transfer reaction with tetrabutylammonium iodide (TBAI) in a 1:1 mixture of 50% sodium hydroxide and benzene was done with the same 1,8-dibromooctane. After amination, **19** was obtained as pure product.

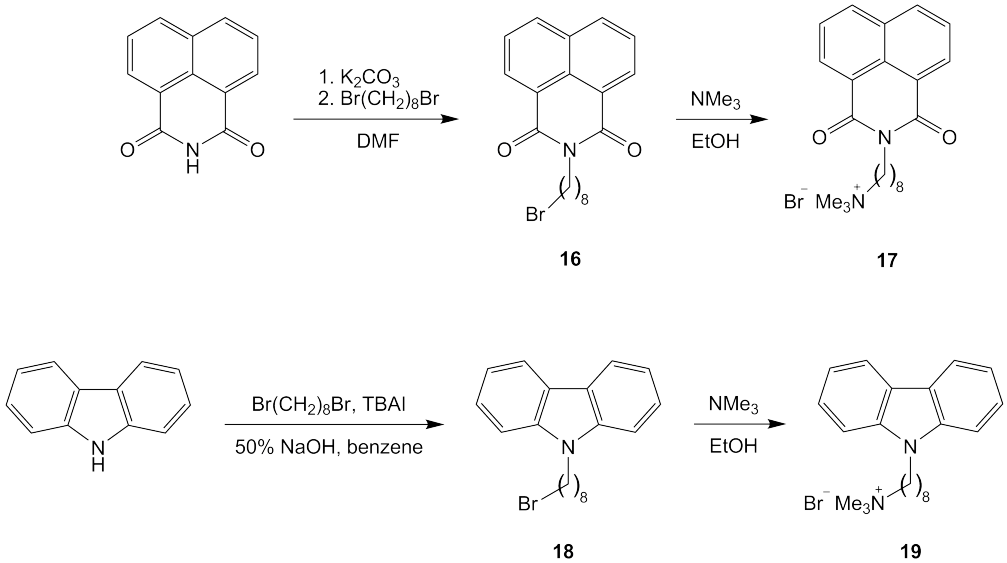

Scheme 4.2: Alkylation of 1,8-naphthalimide and carbazole to yield ***16*** *and* ***18****. Followed by amination with trimethylamine to yield* ***17*** *and* ***19****.*

The substitution of the alcohol function of 9-hydroxymethyl anthracene with 1,6-dibromohexane in DMF was initiated by quantitative deprotonation using sodium hydride at -78°C. The resulting bromide **20** was

provided with a positive charge to yield **21** (cf. Scheme 4.3).

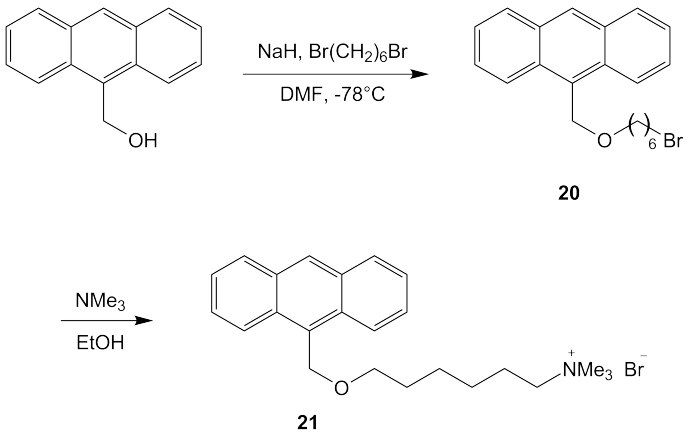

*Scheme 4.3: Alkylation of 9-hydroxymethyl anthracene to yield **20** and subsequent amination to form **21**.*

All substitutions of aromatic bromides were performed by lithiation of the aromatic compound and subsequent alkyation by providing the appropriate bromide. When using dibromoalkanes, almost no double substitution was observed as side reaction. Also the use of excess dibromoalkane prevented such a reaction for statistical reasons. For the lithiation, *n*-, *s*- or *t*-butyl lithium was used in tetrahydrofurane (THF). The temperature for the lithiation was set to -78°C and for the substitution in most cases an increase to about -10°C was required. In this way, the anthracene derivatives with decreasing alkyl chain length **22** (n=8), **23** (n=6) and **24** (n=4) were synthesized. Careful purification by flash-chromatography was required in all cases. Detailed descriptions are provided in the Experimental Part. Subsequent amination yielded the surfactants **25** (n=8), **26** (n=6) and **27** (n=4) (cf. Scheme 4.4).

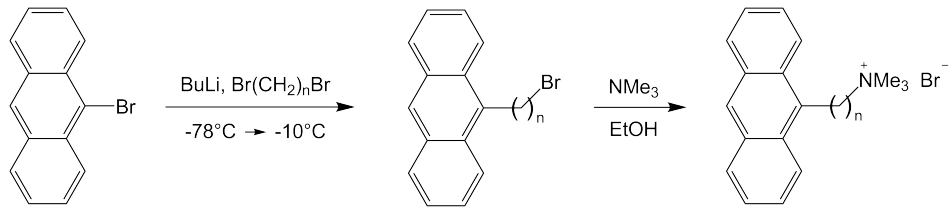

*Scheme 4.4: Alkylation of 9-bromoanthracene with different alkyl chain lengths and subsequent amination yielded the surfactant series **25** (n=8), **26** (n=6) and **27** (n=4).*

With 9,10-dibromoanthracene, the alkylation by lithiation was done twice. The first step with 1-bromobutane yielded **28** and the second with 1,8-dibromooctane **29**. The resulting alkyl bromide was substituted with trimethylamine to form **30** (cf. Scheme 4.5).

Surfactants, bearing pyrene at the hydrophobic end were synthesized in analogy to the anthracene surfactants. Two different alkyl chain length were chosen for the reaction with 1-bromopyrene. Using

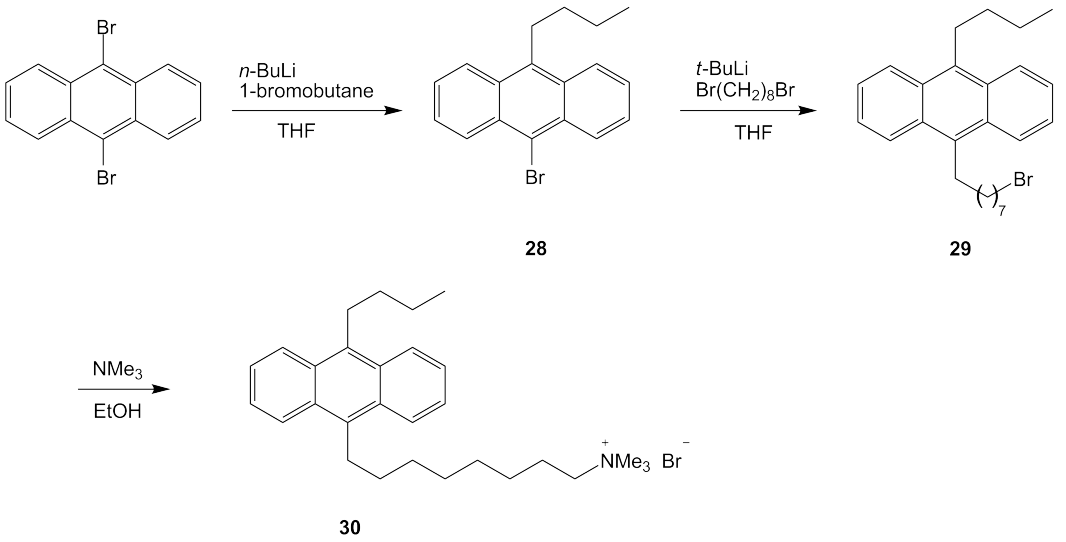

*Scheme 4.5: Two subsequent lithiation and alkylation, followed by amination produced **28**, **29** and finally **30**.*

1,12-dibromododecane or 1,8-dibromooctane the alkyl bromides **31** or **32** resulted. Standard amination with trimethylamine yielded the white salts **33** (dodecyl chain) and **34** (octyl chain) as pure compounds (cf. Scheme 4.6).

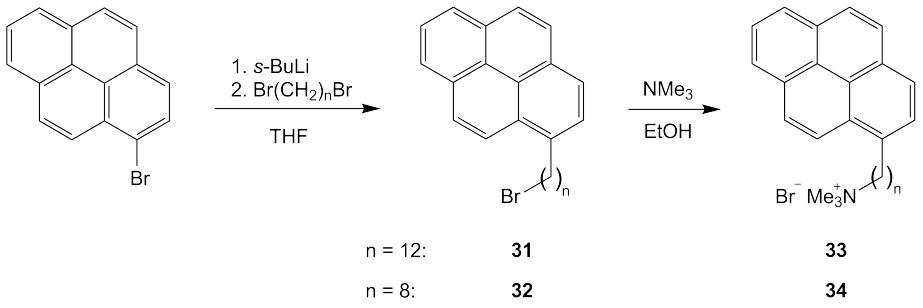

*Scheme 4.6: Alkylation of 1-bromopyrene with two different alkyl chain lengths and subsequent amination yielded the pyrene modified surfactants **33** (n=12) and **34** (n=8).*

The ether formation to obtain **35** and **36** (and subsequently **37** and **38**) was done by quantitative deprotonation of the alcohol umbelliferone using sodium hydride in DMF followed by addition of the appropriate dibromoalkane (cf. Scheme 4.7).

For the phthalimide derivative **39** and nonyl trimethylammonium bromide (**40**), the alkyl bromide precursors were commercially available. The substitution of the bromide with trimethylamine in ethanol yielded directly the desired surfactants (cf. Scheme 4.8).

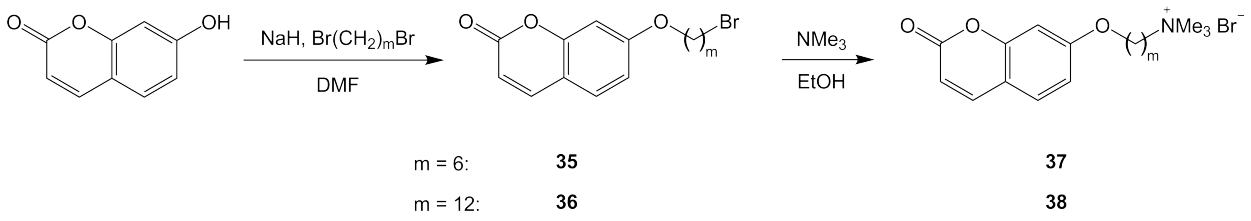

*Scheme 4.7: Etherification of umbelliferone and amination to form **37** via **35** and **38** via **36**.*

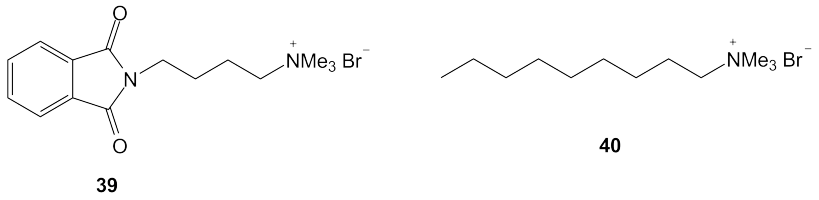

*Scheme 4.8: The phthalimide derived surfactant **39** and the only aliphatic surfactant synthesized **40** were directly formed from commercially available alkyl bromides.*

4.2.2.3 Optical Tweezers

In cooperation with Sudhir Husale under the guidance of Martin Hegner (NCCR, Institute of Physics, University of Basel) a further feature of surfactants interacting with DNA was studied using optical tweezers. In these experiment, single DNA molecules can be investigated. The setup with laser and buffer filled fluid chamber is sketched in Figure 4.4

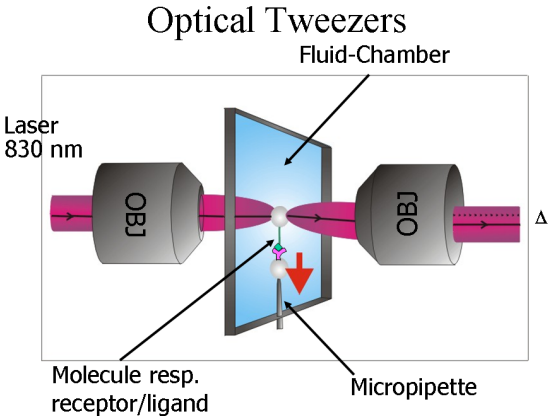

Figure 4.4: Optical Tweezers - the setup.

One strand of the approx. 7.4 kbp DNA is attachted between the bead, the other strand is annealed. The 5'–end of the attached strand is covalently bound via an amino function to one bead. The opposing 3'–end is modified with biotin. The second bead carries streptavidin on its surface, that binds non-covalently to

biotin. The DNA beads were trapped by the laser (focused by objectives) and the free biotinylated DNA end was attached to a streptavidin bead, which was held by suction on a micropipette. The micropipette enables to control the motion of the second bead. By pulling apart two polystyrene beads, they are able to stretch out a single double-stranded DNA molecule inbetween. Consequent force feedback experiments reveal informations about the effects of added surfactants on the DNA conformation and mechanical behaviour.[89] The force feedback is measured, when the double-strand is denatured, as the beads are pulled apart. Based on his experiments, Husale suggested that short chain surfactants, which do not induce any condensation, could lie down on the DNA surface and directly interact with the DNA grooves through hydrophobic–hydrophobic interactions. In contrast, long chain surfactants could have their aliphatic tails pointing away from the DNA surface.[89,90] As our surfactants are modified at the end, we have tested the double substituted anthracene surfactant **30** as a representative (depicted in Figure 4.5). It has shown normal 'melting' behaviour of the DNA like without any surfactant present. Thus, no groove binding to DNA occurs and the tails are oriented towards the solution.

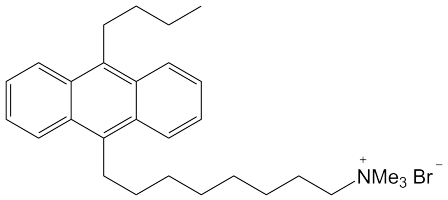

*Figure 4.5: 9,10-Disubstituted anthracene surfactant **30**.*

4.2.3 SDC Formation

Surfactant-DNA complexes were formed by adding a solution of DNA to a solution of surfactants (1.2-fold excess in charges) while shaking. The process was already used for the $\mathbf{T}^*$ experiments and is described there (cf. Chapters 1.1.3 and 1.3.5). The surfactants in Figure 4.6 formed a quantitative precipitate with genomic DNA as well as with DNA fragments. The precipitates could be isolated by centrifugation and removing of the solvent. After drying they were ready for dissolving experiments.
No precipitation after the combining of the surfactant and DNA solutions was formed with the surfactants **39**, **27** and **40**, depicted in Figure 4.7. Similar surfactants do form precipitates. The anthracene surfactant **27** has the shortest tail in the series of **25** (eight CH_2 groups), **26** (six CH_2 groups) and **27** (four CH_2 groups). We attribute the missing precipitation with **27** to weak van der Waals forces between the tails. Also the aliphatic nonyl-trimethylammonium bromide (**40**) (eight CH_2 groups plus methyl group) with its shorter tail does not precipitate DNA, while CTAB (fifteen CH_2 groups plus methyl group) does. Here, one limitation for the construction of surfactants is revealed. The linker between functional group and polar head, or the tail in aliphatic surfactants has to have a certain length.

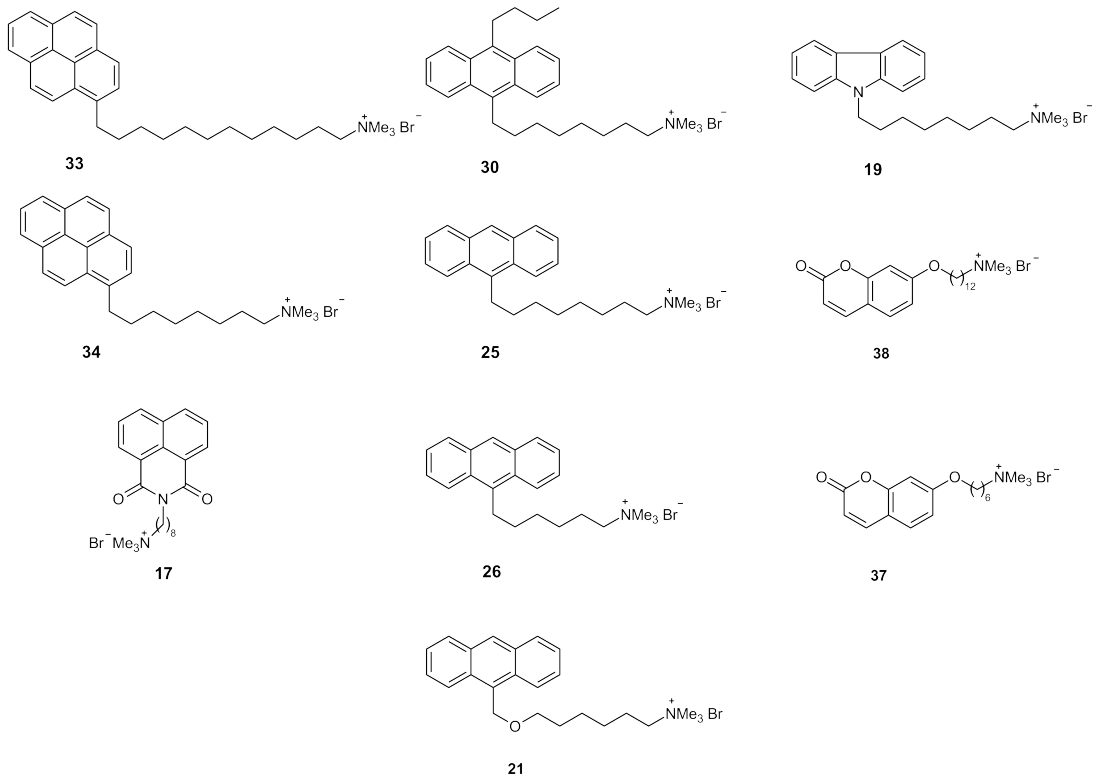

Figure 4.6: Surfactants that produced a precipitated SDC

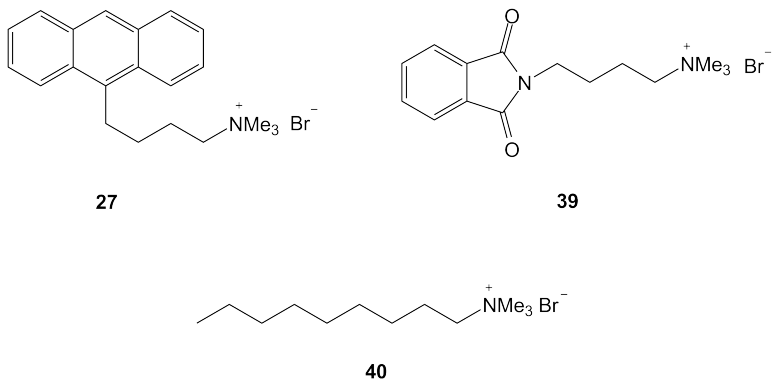

Figure 4.7: Surfactants that do not produce a precipitating SDC

4.2.4 Dissolving Funtionalized SDCs

The surfactant-DNA complex with the surfactant CTAB or with other aliphatic surfactants are readily dissolvable in methanol, ethanol, 2-propanol, dichloromethane or THF. Therefore we did not expect any difficulites in dissolving also complexes with polyaromatic surfactants.
8-(Pyren-1'-yl)-octyl-trimethylammonium bromide and DNA was precipitating well as amorphous powder, as expected, but the formed complex could only be dissolved in benzyl alcohol. However, the very limited solubility can be interpreted as a hint towards a special orientation of the surfactants within the complex. The pyrenes probably form a π-stacked and well-ordered arrangement along the DNA. Solvation can be regarded as dilution of the compound with solvent molecules. Therefore, an aromatic solvent is required to overcome the stacking interactions and to dissolve the complex. Benzyl alcohol turned out to be able to dissolve all successfully formed SDCs. And it was the only possible solvent for all aromatic surfactant-DNA complexes. A list of solvents that did not work is given in the Experimental Part and contains basically every common solvent.

4.2.5 SDC Material Formation

One of the most promissing ways of producing material with defined shapes is to dissolve the SDC and use the drying process for the structuring. Therefore, the solvent has to fulfill certain requirements. Fist of all it has to be volatile. On the other hand, if the evaporation is too fast, only powders are obtained, like with THF. Suitable solvents for this kind of material formation are methanol or ethanol. Genomic DNA was complexed with aliphatic surfactant CTAB. This was done easily in 100 mg scale. The applied technique for film formation was already described in literature.[34] The CTAB-DNA complex was dissolved in methanol (40 mg/mL). The solution was placed in a rectangular container, made from Teflon covered aluminium foil. By slow evaporation of the solvent methanol (or ethanol) at room temperature, transparent and stable macroscopic films are obtained, which can be manipulated without special precautions (cf. Figure 4.8).
Not only films, but also fibers can be produced with this complex. From a highly concentrated viscous solution of CTAB-DNA complex in methanol, fibers were obtained by dipping a pointed tip into the solution and slowly pulling it out again. Methanol evaporates during the tip is pulled out, leaving the concentrated SDC behind as fiber between tip and solution with a length of several centimeters and diameters in the micrometer range. This was possible, because methanol has a low boiling point of 65°C and is volatile. None of the complexes formed with modified surfactants were soluble in methanol, ethanol or any other volatile, suitable solvent. We have tried to form films with the complex of **34** and DNA fragments or genomic DNA, dissolved in benzyl alcohol. The solvents boiling point of 206°C excluded fiber formation in the way described above and films could not be produced. Reducing the pressure (down to 22 mbar) or increasing slowly the temperature (up to 150°C) always yielded in powders. A technique

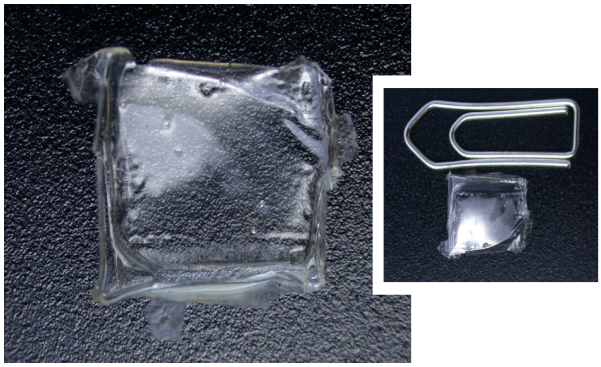

Figure 4.8: SDC film containing genomic DNA and CTAB as complex. A paper clip shows the size of the film.

called electrospinning seemed to be the right way.

4.2.6 Electrospinning

4.2.6.1 The Electrospinning Technique

One access to polymeric nanoscale materials offers the electrospinning process. It was patented by Antonin Formhals in 1934.[91] About 50 patents for electrospinning polymer solutions were filed in the past 60 years. In this technique, a polymer solution is transformed into fibers with diameters in the order of 10 – 1000 nm.[92] The technique is well established and was applied to a variety of organic polymers before. The high specific surface area and small pore size of electrospun nanofibers make them interesting candidates for a wide variety of applications. For instance nanofibers with a diameter of 100 nm have a ratio of geometrical surface area to mass of approximately 100 m^2/g.

The electrospinning process involves the application of a strong electrostatic field in the range of 1 kV/cm to a capillary connected with a syringe (with syringe pump) containing a polymer solution (depicted in Figure 4.9).[93,94]

When the voltage surpasses a threshold value (several kilovolts), the electrostatic forces overcome the surface tension of the pendant droplet of the polymer solution at the capillary tip. The formed conical shape known as the Taylor cone is the origin of the ejected fine charged jet traveling in air. The solvent begins to evaporate immediately after the jet is formed on a time scale well below the second-range. Therefore, only volatile solvents are suitable. Furthermore, the jet is strongly elongated during electrospinning due to the acceleration in the direction of the counter electrode. This leads to a dramatic increase of the jet surface within milliseconds. The result is the deposition of a thin polymer fiber on a substrate located above the counter electrode.[95] In this manner whole mats of electrospun polymers can be build. The deposition rate of fibers is in the order of several meters per second.

The following parameters and processing variables affect the electrospinning process: System parameters

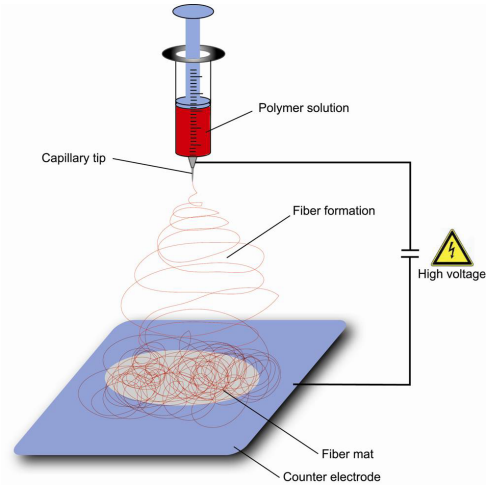

Figure 4.9: The electrospinning technique. A jet of polymer solution is accelerated by an electric field. As the solvent evaporates, thin fibers are formed.

such as molecular weight, molecular weight distribution and architecture (branched, linear etc.) of the polymer and solution properties (viscosity, conductivity and surface tension), and process parameters such as electric potential, flow rate and concentration, distance between the capillary and collection screen and finally ambient parameters (temperature, humidity and air velocity in the chamber).[92] For instance, the polymer solution must have a concentration high enough to cause polymer entanglements yet not so high that the viscosity prevents polymer motion induced by the electric field. The solution must also have a surface tension low enough, a charge density high enough, and a viscosity high enough to prevent the jet from collapsing into droplets before the solvent has evaporated.

4.2.6.2 Electrospinning of CTAB/DNA Complexes

In collaboration with Markus Rudisile from the Wendorff group at the University of Marburg (Germany), we were the first to elecrospin surfactant-DNA complexes. A series of solvents are suitable for electrospinning. Water, methanol, ethanol, 2-propanol, dichloromethane, chloroform, formic acid, acetic acid, hexafluoro-2-propanol, THF, acetone, trifluoroacetic acid, CCl_4, CS_2 and mixtures work. Also hydrocarbons as additives are known.[93]

A CTAB / genomic DNA SDC was provided as 2.5 wt.% solution in methanol. From this solution, we successfully formed nanofibers using the electrspinning technique. Scanning electron microscopy (SEM) pictures are shown in Figure 4.10 and 4.11. The labels 'A' and 'B' indicate the position of the zoomed pictures in Figure 4.10, the frame corresponds to the size. In Figure 4.11, two structural varieties are shown. Depending on the spinning parameters, the fiber surface is smooth, branched or it reminds of 'beads on a string'. The 'beads' are halfway formed droplets during the electrospinning.

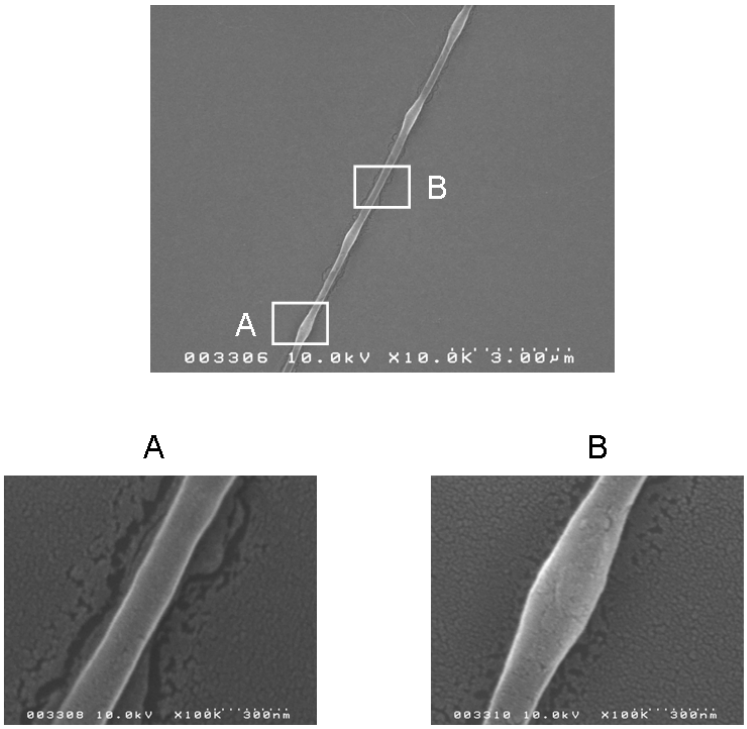

Figure 4.10: SEM pictures of the CTAB/DNA complex. The pictures A and B on the bottom are zoomed from picture on top.

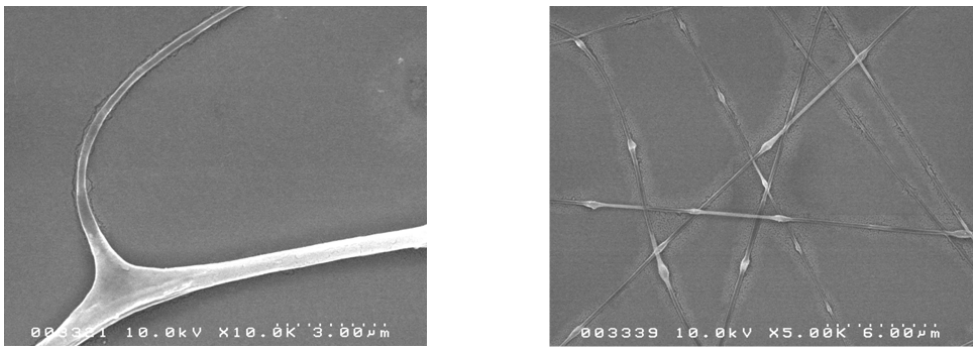

Figure 4.11: SEM pictures of the CTAB/DNA complex. A smooth branched fiber (left) and the 'bead on a string' structure (right).

4.2.6.3 Electrospinning Functionalized SDC

For electrospinning, volatile solvents are required. None of the functionalized surfactants synthesized, formed complexes that were readily soluble. As the electrospinning of CTAB / genomic DNA SDC was working very well, we doped this complex by exchanging a part of the CTAB surfactants by the anthracene modified surfactant **26** (shown in Figure 4.12) .

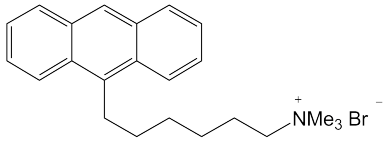

*Figure 4.12: 6-(Anthr-9'-yl)-hexyl-trimethylammonium bromide (**26**) was used to be mixed with CTAB for complexation and electrospinning.*

Starting with a molar ratio of 5:95 (**26** : CTAB), we increased the amount of **26** stepwise. All formed comlexes were soluble in methanol, when dichloromethane was added. a SDC of 100% **26** was not soluble in a broad variety of methanol : dichloromethane mixtures. The highest possible content of **26** to form a dissolvable SDC was 95 mol.%. A SDC with 95 mol.% **26** and 5 mol.% CTAB was produced. This complex turned out to be soluble in a methanol : dichloromethane 9:1 mixture. A 0.5 wt.% solution of this mixed surfactant SDC was successfully electrospun to fibers.

Obtained fibers with a branch on the lower right side are shown in Figure 4.13. The fibers in the 5000-fold magnified optical microscope picture have diameters of 300 – 700 nm.

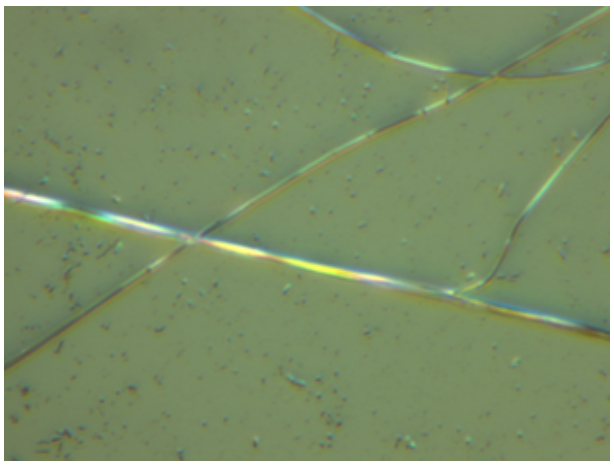

*Figure 4.13: 5000-fold magnified optical microscope of fibers from SDC with 95% anthracene surfactant **26**.*

4.3 Summary

The goal of this project was to produce nano-structured self-assembling solid materials. To form these functional materials, functionalized surfactants were aligned in a rod-like structure by using DNA as the central scaffold. A series of surfactants were synthesized. The structure consists of a head and a functionalized tail. The head, a trimethylammonium group, is pH independent positively charged. The tail is composed of a aliphatic spacer and an aromatic functional group. Ten surfactants were successfully complexed with DNA to form a surfactant-DNA complex. Optical tweezers experiments of one representative surfactant suggest, that the aromatic moiety does not interact with the DNA grooves and is therefore oriented towards the solution. Surfactant-DNA complexes (SDCs) were successfully electrospun into fibers for the first time. The SDC of aliphatic surfactant CTAB and DNA was chosen to establish the technique. One complex with 95 wt.% of the anthacene bearing surfactant **26** and 5 wt.% CTAB was electrospun to fibers with diameters of several hundred nanometers, which can now serve as working basis for a new field of chemically modified, well structured polymeric nanomaterials, bearing a DNA core.

Part II

Experimental Part

Chapter 5

Material and Methods

5.1 Devices and Materials

5.1.1 Photolysis and Irradiation Setup

Device: Oriel 68810 photolysis stand equipped with an Osram HBO 500 W/2 L2 highpressure mercury arc lamp and 320 nm lowpass filter (2 mm thick) by Schott (WG–320) (Figure 5.3). The device used was further equipped with an Oriel 6123 IR cutoff filter and a thermostatically cooled sample holder set to 5°C for T^* experiments and to 15°C for all others. At given wavelength of the filter (320 nm) light transmittance is about 50%. The UV light was focused to the centre of the sample holder using an additional Schott UG–1 UV bandpass filter and a sample of bright–white paper, which shows visible fluorescence when excited at 325 nm. Figure 5.1 shows the photolysis device and Figure 5.2 the unfiltered spectrum of the mercury arc lamp.

5.1.2 ^{1}H NMR Spectroscopy

Spectra were either recorded on a Varian Gemini VXR 400 with 400 MHz or a Bruker DRX 250 with 250 MHz. The chemical shifts (δ) are given in ppm relative to tetramethylsilane ($\delta = 0.00$) or are referring to the partially deuterated nuclei of the used solvents (7.26 for $CDCl_3$, 2.50 for DMSO-d_6 and 3.31 for MeOH-d_4).[96] All spectra are interpreted by first order, and the coupling constants (J) are given in Hertz (Hz). The chemical shift of signals featuring defined multiplicity were determined by the arithmetic mean of the signal lines. Therefore the following abbbreviations were used: s = singlet, d = doublet, t = triplet, q = quartet, quint. = quintet, m = multiplet and their combinations. The numbering of the protons are analogous to the proton numbers resulting from the name of the compound. Aromatic protons are labelled with 'Ar' subscript. Assignment of protons was accomplished by calculation or comparison with reference spectra (*e.g.* `http://www.aist.go.jp`)

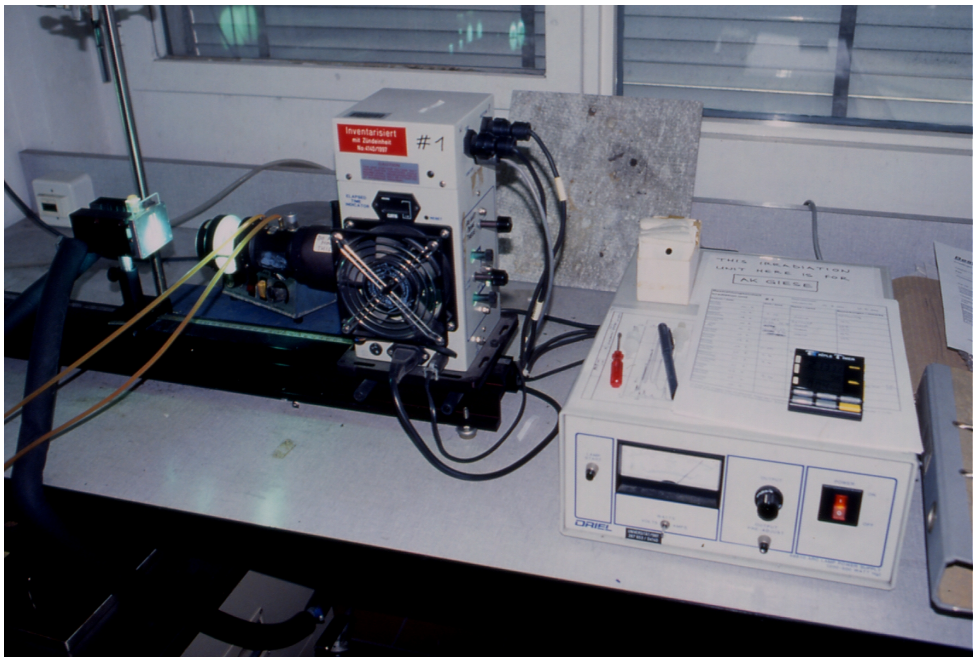

Figure 5.1: Photolysis Device

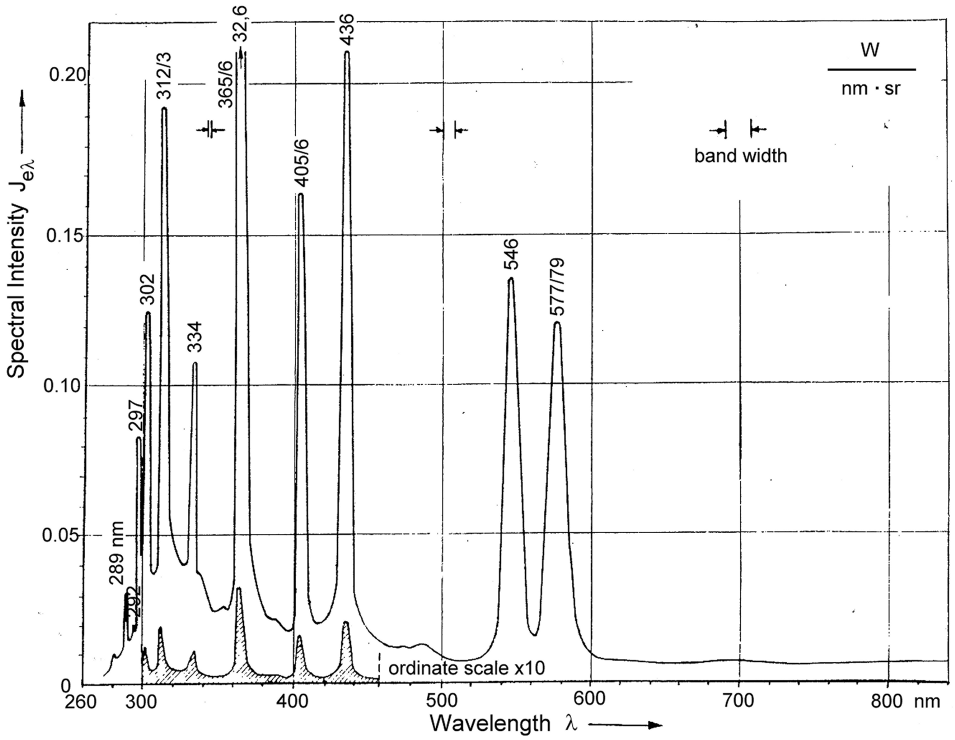

Figure 5.2: Unfiltered mercury arc lamb spectrum

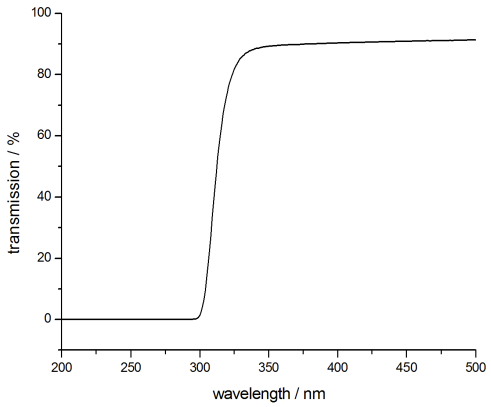

Figure 5.3: 320 nm lowpass filter transmission

5.1.3 ^{13}C NMR Spectroscopy

Spectra were either recorded on a Varian Gemini VXR 400 with 101 MHz or a Bruker DRX 250 with 62.9 MHz using proton broad-band decoupling. The chemical shifts (δ) are given in ppm referring to the solvent signals (77.16 for $CDCl_3$, 39.52 for DMSO-d_6 and 49.00 for MeOH-d_4). The following abbreviations were applied for carbon characterization: p = primary, s = secondary, t = tertiary and q = quaternary, C_{Ar} = aromatic carbon atom. The numbering of the carbon atoms are analogous to the carbon atom numbers resulting from the name of the compound.

5.1.4 Infrared Spectroscopy (IR)

The spectra were recorded on a Perkin-Elmer 1600 FT–IR. They were aquired by overlapping four scans and substraction of a background scan to eliminate the CO_2 bands. Liquids were measured as thin film between sodium chloride plates, solids as potassium bromide pressings. The wavenumbers ($\tilde{\nu}$) are indicated as cm^{-1}. Strong absorbing bands are marked as 's'.

5.1.5 Mass Spectroscopy

5.1.5.1 EI and FAB

Samples were measured by Dr. H. Nadig at the Department of Chemistry (University of Basel) using a VG70-250 or a Finnigan MAT 312 mass spectrometer. The ion generation was achieved by a ionization energy of 70 eV at approx. 200 °C(EI, elecron–ionization) or via fast–atom bombardment (FAB) using xenon atoms, 3-nitrobenzyl alcohol as matrix and sodium chloride as additive. Data are given in atomic mass units per charge (m/z) followed by the relative intensity of the signal in parentheses.

5.1.5.2 Electrospray Ionisation (ESI)

Samples were measured on a Finnigan MAT LCQ octapole mass spectrometer as a 0.1 mg/mL solution in methanol (if not indicated else). Data are given in atomic mass units per charge (m/z) followed by the relative intensity of the signal in parentheses.

5.1.5.3 MALDI–ToF

Samples were measured on a Vestec Voyager Elite or a PerSeptive Biosystems Voyager-DE PRO mass spectrometer using the MALDI-ToF (matrix–assisted laser desorption ionization time–of–flight) method. 2,4–Dihydroxyacetophenone was used as a matrix. Probe desorption and ionization was induced by a N_2–LASER (337 nm, 3 ns pulses, 0.2 mJ per pulse, acquisition of 10 to 100 pulses). The signals are referred to the unfragmented, single negatively charged molecule ions $[\text{M-H}]^-$. Data are given in atomic mass units per charge (m/z). Argumentum baculinum![97]

5.1.6 Elementary Analysis (EA)

The elementary analyses were carried out by W. Kirsch at the Department of Chemistry (University of Basel) using a Leco CHN-900 for the detection of carbon, hydrogen and nitrogen and a Leco RO-478 for oxygen detection. The values are indicated in percent by weight.

5.1.7 UV/vis Spectroscopy

Spectra were recorded on a Perkin-Elmer Lambda Bio 40 spectrophotometer, featuring a PTP-6 peltier unit for temperature control. Samples were measured in quatz glass cuvettes from Hellma or, if feasible, disposable PMMA cuvettes from Semadeni providing a pathlength of 1 cm. Normal parameters were scan rate 120 nm/min, slit width 2.0 nm and measuring interval 0.5 nm, if not indicated else.

5.1.8 Melting Points (mp)

Melting points of organic compounds were measured on a Büchi 530 or a Hund Wetzlar V200 in degree Celsius and are uncorrected.

5.1.9 Chromatography

5.1.9.1 Thin Layer Chromatography (TLC)

TLCs was performed with aluminium-baked 0.2 mm thick Merck silica gel 60 F_{254} plates. The compounds were detected by one of the following means:
— Fluorescence quenching detection at 254 nm or 366 nm;

— Dipping into a solution of 3 g potassium permanganate, 5 mL 5% sodium hydroxide, 20 g potassium carbonate and 300 mL water and subsequent heating;
— Dipping into a solution of 10 g ceric (IV) sulfate tetrahydrate, 25 g ammonium molybdate tetrahydrate, 100 mL concentrated sulfuric acid and 900 mL water and subsequent heating.
Retention factors (R_f) are indicated with the corresponding solvent mixture in brackets.

5.1.9.2 Flash Column Chromatography

Flash Column Chromatography was performed under pressure ($\sim$ 1.5 bar) using Merck silica gel 60 (particle size 40 – 63 µm, 230 – 400 mesh). Solvents were of at least technical grade and distilled prior to use. The indicated mixture ratios are in volumes.

5.1.9.3 Reversed–Phase High Performance Liquid Chromatography (RP–HPLC)

Purifications and analytical runs were performed on a Hewlett-Packard 1050 Series chromatograph or on a Water Alliance 2690 Separation Module with a 2680 Dual Mode Detector adjusted to 260 nm and 364 nm. Columns for reversed–phase HPLC were Merck LiChroSpher 100 (RP–18e, 5 µm, 125 $\times$ 4 mm at a flow of 1.0 mL·min^{-1}). Eluents were acetonitrile 190 (Romil) and 0.1 M aqueous triethyl-ammonium acetate (TEAA) solution, purchased as 1.0 M stock solution from Fluka, diluted with nanopure water.

5.1.10 Electrospinning at Marburg

The device in Figure 5.4 and 5.5

5.1.11 Chemicals

Reagents and chemicals were obtained from Fluka, Aldrich, Acros and J.T.Baker and were in general used without further purification. Water: Barnstead, ultrapure water system or deionized water for reaction work-up.

5.1.11.1 Genomic DNA

SIGMA, Sodium Salt, Type XIV, from Herring Testes, Na content: 6.2%, water content: 4.5%, ε_{260}=6600 M^{-1}cm^{-1} or SIGMA, sodium salt from Salmon Testes, Na content: 6.2%

5.1.12 Further Instruments

Centrifuges (Eppendorf 5415C and 5415D), Thermomixer (Eppendorf 5436), Vortex (Bender & Hobein Vortex Genie 2)

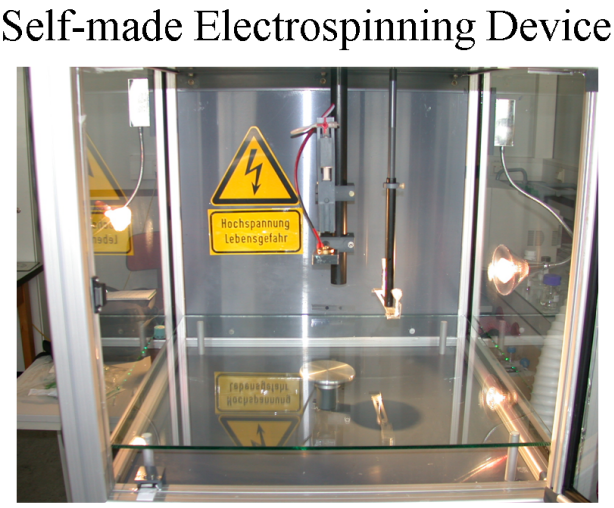

Figure 5.4: Self-made apparatus for electrospinning, located at Marburg

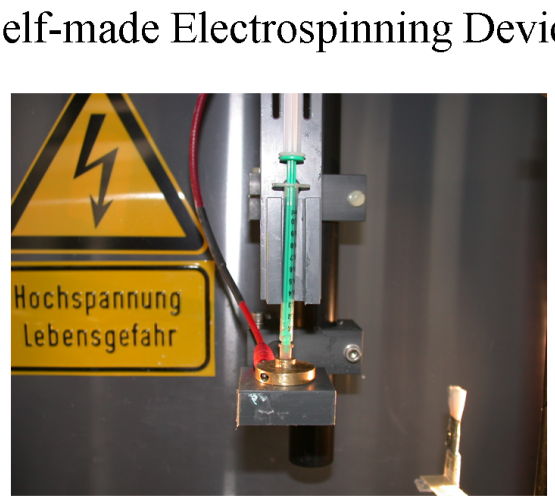

Figure 5.5: Close-up of self-made apparatus for electrospinning, located at Marburg

5.2 Methods

5.2.1 Synthesis of Oligonucleotides

Synthetic oligonucleotides are usually built up in 3' to 5' direction and the first building block is covalently bound to the solid phase via a base–labile succinyl linker. The connection to the solid phase is via an amide bond and the 5' hydroxy group is protected by an acid–labile dimethoxytrityl (DMT) ether. Generally, the solid phase has a loading density of 20 to 30 mmol of the starting nucleotide per gram of solid phase. Solid phase amino functionalized borosilicates (CPG - controlled pore glass) are widely used, which offer a range of pore widths from 500 to 2000 Å. Solid phase material featuring a pore width larger than 1000 Å is of particular advantage for longer oligonucleotides (> 30mers). Preloaded flow–through columns for automated DNA syntheses span a synthesis scale range from 40 nmol up to 10 mmol. For this work, only 500 Å pore width CPG columns in 0.2 mmol and 1.0 mmol synthesis scale were used. The monomeric nucleotide building blocks carry temporary protection groups, which get cleaved before each coupling step. They also contain permanent protection groups for the amino functions of A, C and G, as well as for the phosphite function, which are only cleaved after completion of the oligonucleotide synthesis. The DMT group is used for the protection of all 5 ' hydroxy groups. The amino groups of A, C, and G are protected as amides or amidines, and the phosphites are protected by the 2–cyanoethyl group. The first step of oligonucleotide synthesis is the deprotection of the terminal DMT group by 2% trichloroacetic acid. The following, tetrazole–activated nucleotide then couples with this free hydroxy group. The amidite building blocks are added in approximately 20–fold excess for the coupling steps. In the next step, unreacted 5 ' hydroxy groups are capped in a fast and quantitative reaction as acetates, in order to terminate any further synthesis of fault sequences. The subsequent oxidation of the labile P(III) compound to the phosphate is achieved by reaction with a iodine/water/pyridine mixture. With the cleavage of the DMT group the next synthesis cycle starts. The amount of cleaved trityl cation is monitored photometrically or conductometrically, as this serves as a scale for coupling efficiency. Upon completion of the synthesis, the oligonucleotide is manually cleaved off the solid phase by treatment with 30% aqueous ammonia solution at 55°C for 8 hours. All permanent protection groups are also cleaved in this step with exception of the terminal DMT group (Scheme 5.2.1).

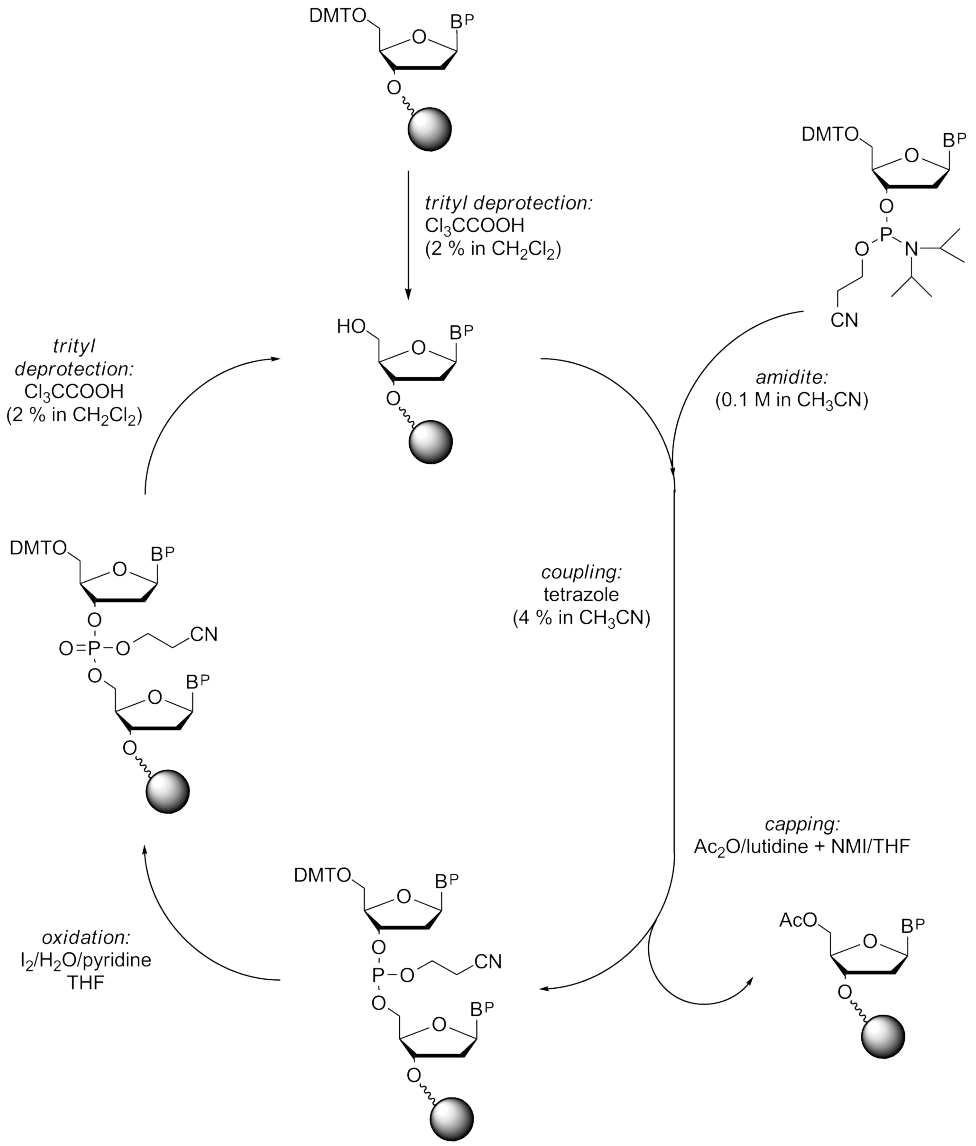

Scheme 5.1: Automated Oligonucleotide synthesis

DNA syntheiszer manual LB 3078.

5.2.2 Purification of Oligonucleotides

Commercially available oligonucleotides were ordered 'trityl-off' and PAGE purified. All strands were repurified with RP-HPLC using a acetonitrile gradient (6% – 20% in 40 min) with column temperature set to 55°C to avoid aggregation and lyophilised.

Special oligonucleotides were first purified 'trityl-on' (still protected at the 5 ' position with the dimethyl-trityl group, DMT) applying an acetonitrile gradient 15% – 40% in 25 min before deprotection and

subsequent 'trityl-off' purification. Cleaving the oligo from the solid support was performed by incorporation with 1 mL 32% ammonia at 55°C for 8 hours. Subsequently, the samples were cooled to -20°C and then concentrated to dryness. The oligos could now be dissolved in water and the beads removed by using a 0.45,µm syringe filter. For the detritylation, 200 µL 80% aqueous acetic acid was added to the dried oligonucleotide. After 20 min shaking at room temperature, 50 µL 3 M aqueous sodium acetate solution and 800 µL *iso*–propanol were added, the mixture was vortexed, cooled to below 0°C in the freezer, centrifuged for 15 min at 13200 g and the supernatant removed. The pellet was washed twice with 500 µL *iso*–propanol including centrifugation for 15 min and removal of the supernantant and subsequently lyophilized the pellet to dryness.
Special nucleotides like 1'-(β) 1-Pyrenyl-5'-*O*-dimethoxytrityl-2'-deoxy-D-ribose-3'-*O*-[(2-cyanoethyl)-*N,N*-diisopropylphosphoramidite] or an abasic site were incorporated using standard conditions on 0.2 µmol columns but with an increased coupling time of 10 to 15 min instead of 5 min.

5.2.3 Thermal Denaturation Studies: DNA Melting Temperatures and annealing of double strands

Solutions for the thermal denaturation studies contained a 1:1 ratio of two complementary oligomers. The buffer contained 10 mM sodium citrate and 100 mM NaCl at pH 5.0. The solutions were heated to 90°C for 5 min and allowed to cool to room temperature during at least 2 h. Melting studies were carried out in a Teflon–stoppered 1 cm path length quartz cell. Absorbance was monitored at 260 nm and ploted versus temperature while temperature was raised from 5 to 95 °C at a rate of 1.0 °C/min. The melting point was retrieved from the maximum of the the first deviation. A sample curve is depicted in Figure 5.6.

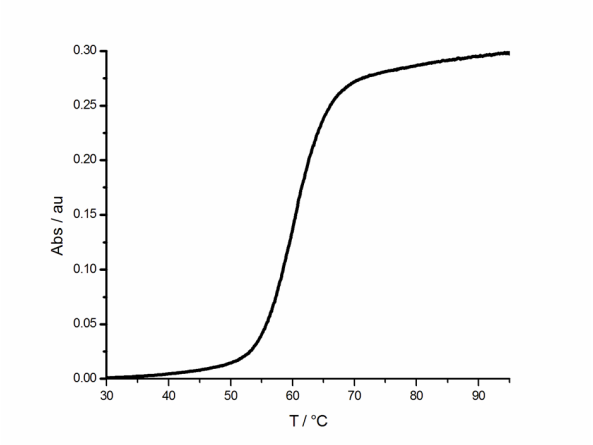

Figure 5.6: DNA melting curve sample

5.2.4 Photolysis of Oligonucleotides

In general, 1 nmol of the investigated oligonucleotide was dissolved in 200–230 µL citrate buffer (20 mM sodium citrate, 100 mM NaCl, pH 5.0) as single strand or as double strand, annealed with 1.1 nmol of complementary strand. The solution was placed in an airtight PMMA cuvette and was flushed with argon for 5 min. Then argon was bubbled through the solution for 10 min to remove dissolved oxygen. During the irradiation, the cuvette was thermostated to 5°C for T* experiments or 15°C for pyrene irradiations. This are reference irradiations for the T* project and the Häner strand irradiations. When using SDCs, about 100 – 300 µL methanol was added extra, because during the removal of oxygen, about this amount of solvent evaporated.

5.2.5 Annealing of Oligonucleodites

5.2.6 Quantification of Oligonucleotides by UV Absorption

The concentration c of an aqueous oligo solution was determinated applying the Lambert–Beer law A=ε·c·d. The absorption A was measured at 260 nm in a cuvette with a path length d of 1 cm. The molar extinction coefficient ε $\left[\mathrm{M}^{-1}\mathrm{cm}^{-1}\right]$ was calculated by adding the increments in the table below for each single base and multiplying the sum by 0.9.[98,99]

Nucleobase	$\varepsilon_{260}{}^{a}$
Adenine	15400
Cytosine	7400
Guanine	11500
Thymine	8700
Pyrene	9560

[a] in $\mathrm{M}^{-1}\,\mathrm{cm}^{-1}$

5.2.7 T* Building Block

For the synthesizer, a 5'-dimethyltrityl protecting group and a phosphoramidite at the 3' position was introduced. The phosphoramidite **9** is very sensitive to oxidation. It is not possible to store it even at -20°C for more than a few days. The diol is stable and was used as storable intermediate. In Figure 5.7 see the amidite, ready for incorporation.

5.2.8 Formation of T* SDCs

T* strand: counter strand = 1:1.2. Surfactant DMDTAB 2.0 eq. used to ensure full encapsulation. Addition of surfactant to annealed ds solution.

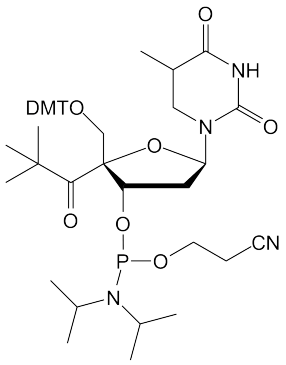

Figure 5.7: T Phosphoramidite ready for DNA Synthesis*

5.2.8.1 Smaller strands get discriminated in complexation and release - material unfinished

To find the experimental error caused by the complexation and the release of the 20mer containing the $\mathbf{T}^*$ modification and the produced fragments during the irradiation, the double-stranded SDC **s4/ cs1** with DMDTAB as surfactant (one 11mer, one 26mer) were HPLC tested before complexation and after release. The ratio shows that the amount of **s4** dropped by 18% throughout the whole treatment (69.01.01).

5.2.9 Analysis of irradiated Oligonucleotides

HPLC prg, MALDI-ToF. The integrated areas of the peaks were divided by the ε of the corresponding strand to make them compairable. Identification through compairing the retention time on the HPLC and the mass using MALDI-ToF. Yields always refer to the conversion of the modified starting material.

5.2.10 Calculation of 3'–phosphate$_{inject}$ in $\mathbf{T}^*$ Experiments

For numbering overview see Theoretical Part Chapter 1.1.2. Irradation of $\mathbf{T}^*$ yield in the injection step the radical cation **4**. This produces also 5'–phosphate **2** and 3'–phosphate$_{inject}$. The amount of formed **4** is equal to the sum of 5'–phosphate **2** and 3'–phosphate$_{inject}$. Then, **4** is trapped by water (3'–phosphate$_{trap}$) or undergoes charge transfer (**6**). The equations 5.1 and 5.2 are shown below.

$$\text{radical cation } \mathbf{4} = \text{5'–phosphate} + \text{3'–phosphate}_{inject} \tag{5.1}$$

$$\text{radical cation } \mathbf{4} = \text{3'–phosphate}_{trap} + \text{enolether} \tag{5.2}$$

In the reaction pathways of $\mathbf{T}^*$ modified strands are two possibilies of **3** formation. The observed **3** is formed at two steps (cf. Equation 5.3).

$$\text{3'–phosphate } \mathbf{3} = \text{3'–phosphate}_{inject} + \text{3'–phosphate}_{trap} \tag{5.3}$$

The resulting Equation 5.4 was used for the calculation.

$$2 \times \text{3'–phosphate}_{trap} = \text{5'–phosphate} + \text{3'–phosphate} - \text{enolether} \tag{5.4}$$

The irradiation of SDC **s2/cs2** in 2-propanol yielded no enolether **6** and there was more 3'–phosphate **3** than 5'–phosphate **2**. As no **6** was formed, all formed **4** reacted with water to yield 3'–phosphate$_{trap}$. The values for the calculation were taken from Table 1.1.

5.2.11 Genomic DNA

We used commercially available genomic DNA isolated from salmon or herring testes (Aldrich). It was used either without further purification or dissolved in TRIS·HCl buffer (10 mM) pH 8.5, and precipitated form 70% ethanol by adding pure ethanol. After centrifugation the supernatant was removed and additional washing with 70% ethanol was performed. The pellet was dried in a speed-vac for storage or application.

For quantification and calculation, an average ε_{260} = 8300 $M^{-1}cm^{-1}$ per base and therefore per negatively charged phosphate was assumed. From the specification of the supplier (A_{260} = 1.0 for 50 µg of double-stranden DNA), the average ε_{260} was calculated. It was confirmed by own measurements prior to application to reduce the error range. To confirm the double-stranded structure, melting experiments were performed.

5.2.12 DNA Fragments by Sonification

Procedure: 11 mg genomic Salmon DNA were dissolved in 20 mL TRIS·HCl buffer (10 mM) at pH 8.5 in a 50 mL falcon tube. The sonification was performed in three times for 20 seconds and cooling of the sample with ice inbetween. The fragments were purified from buffer and salt by sequential preciption in 70% 2-propanol and removal of the supernatant. Here the UV/vis spectrum of the T_m measurement of sonicated genomic DNA, yielding in 400 – 500 bp fragments (Figure 5.8) in TRIS·HCl buffer (10 mM) at pH 8.5. As a clear T_m of about 60°C can be determined, the two strands are still annealed. The structure is not damaged due to sonification.

For the sonification the following device was used. Sonicator W-380 Ultrasonic Processor by Heat Systems Ultrasounds Inc., LSL SECFROID.

The length of the fragment has been checked by 1.2% agarose gel (Eurogenetic, ref.EP-0010-01, molecular biology grade) in TBE buffer (89 mM Tris-borate, 89 mM boric acid, 2 mM ETDA in 0.75 L water) at 100 V for 1.5 h, using a 1 kbp and a 100 bp ladder (commercial) as comparison.

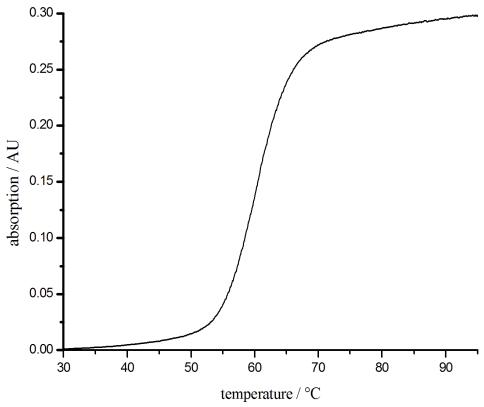

Figure 5.8: Melting curve of 400 – 500 base pair fragements of genomic DNA as proof of the conserved double-strand structure

5.2.13 Circular Dichroism

CD spectra of SDC DMDTAB **s3/cs1** in 2-propanol (solid line) and as ds DNA in buffer (dashed line) are depicted in Figure 5.9.

CD spectra were recorded using a Chirascan spectrometer with a spectral bandwidth of 1 nm at 25°C with a time constant of 3 s and a step resolution of 1 nm. CD data are given as mean residual molar ellipticities (Φ_{MRW} in deg·cm^2·dmol^{-1}). A quartz cell with a path length of 1 cm was used.

5.2.14 Dissolving Aromatic Surfactant-DNA Complexes

In Chapter 4.2.4 in the Theoretical Part, the dissolving of aromatic surfactant-DNA complexes was described with benzyl alcohol being the only possible solvent. The following list contains tested solvents and mixtures, that have not the ability to dissolve this kind of complexes.

Methanol, 2-propanol, n-butanol, i-butanol, tetrahydrofuran (THF), 1,4-dioxane, 1,2 dimethoxy-methane, acetone, acetophenone, 2-hexanone, 3-heptanone, 4-heptanone, 1-hexanol, pyridine, cyclohexane, chloroform, dichloromethane, toluene, benzene, 1,2-dichlorobenzene, acetonitrile, γ-butyrolactone, ethyl acetate, methyl acetate, benzaldehyde, pentane, ethylene glycol monomethyl ether, 2-methoxyethanol, ethyl-methyl-ketone, nitroethane, 2,2,2-trifluoroethanol, 2-propanol:water mixtures, acetonitrile:water mixtures, acetonitrile:dichloromethane mixtures, aceonitrile:methanol mixtures, toluene:methanol mixtures.

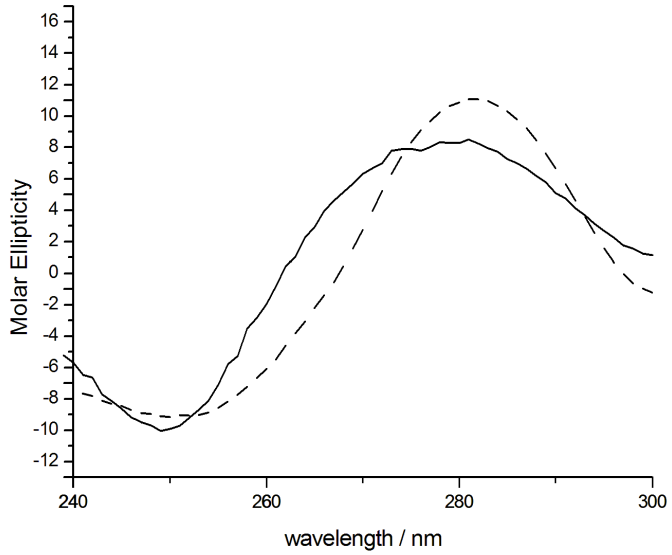

*Figure 5.9: CD of SDC **s3/cs1** in 2-propanol (solid line) and DNA double-strand in buffer (dashed line)*

5.2.15 Optical Tweezers

The surfactant **30** was provided as 135 μM solution in a buffer containing 150 mM NaCl, 10 mM HEPES, 1.0 mM EDTA and 1.5 mM NaN_3.

5.2.16 Electrospinning

We worked with a potential difference of 30 kV ± 2 kV. At lower values, the solution only produced droplets and at higher values, a current was measured between the electrodes. Details: Potential at the needle: +18.0 kV and at the target -12.0 kV. The distance between the electrodes was 17 cm. Temperature 20°C, humidity 41%.

Chapter 6

Syntheses

6.1 Synthesis Part

6.1.1 General Procedures

6.1.1.1 Amination of Alkyl Bromides Using Trimethylamine

A solution of excess trimethylamine (50 eq., 4.2 M) in ethanol was added to the alkyl bromide together with approx. 5 mL dry ethanol per mmol bromide.[100,101,39] The flask was sealed and kept at 55°C for 14 hrs. The solvent and unreacted trimethylamine was removed under reduced pressure. No further purification was required due to total conversion of the educt.

6.1.1.2 Impregnated Silica Gel

103 g silica gel 60 from Merck (40 – 63 µm) were dispersed in 200 mL dichloromethane. 251 mg (1.10 mmol) picric acid were added and the solvent carefully removed under reduced pressure.[102,103,104]

6.1.2 Oligonucleotides

6.1.2.1 Strand s1

Sequence: 5'-TGC ATC ATT GT*T ATC AGA GC-3'
MW: 6255 g·mol^{-1}
ε_{260} = 192200 M^{-1}cm^{-1}
Expected Strand Break Fragments of **s1**:
5'–phosphate:
MW: 2786 g·mol^{-1}
ε_{260} = 91100 M^{-1}cm^{-1}

3'–phosphate:
MW: 3082 g·mol^{-1}
ε_{260} = 93400 M^{-1}cm^{-1}
enolether:
MW: 3305 g·mol^{-1}
ε_{260} = 101900 M^{-1}cm^{-1}
ketoaldehyde:
MW: 3180 g·mol^{-1}
ε_{260} = 93400 M^{-1}cm^{-1}

6.1.2.2 cs1

5'-CT TGC TCT GAT AAC AAT GAT GCA TTC-3'
MW: 7920 g·mol^{-1}
ε_{260} = 244500 M^{-1}cm^{-1}

6.1.3 T* Irradiation Results

6.1.3.1 SDC s1/cs1

Calculating the ratio of 5'–phosphate:3'–phosphate$_{inject}$ after the irradiation of SDC s1/cs1 in 2-propanol. Starting with [radical cation] = [CT products] + [water trapping products]
and [radical cation] = [5'–phosphate],
we get [water trapping products] = [5'–phosphate] − [CT products].
From the chromatogram we conclude [ketoaldehyde] ≈ [enolether] ≈ negligible.
Therefore [3'–phosphate$_{trap}$] = [5'–phosphate]

The observed ratio 5'–phosphate:3'–phosphate = 1:2
⇒ charge injection ratio 5'–phosphate:3'–phosphate$_{inject}$ = 1:1.

6.1.3.2 SDC s2/cs2

Calculating the ratio of 5'–phosphate:3'–phosphate$_{inject}$ after the irradiation of SDC s2/cs2 in methanol. Equations as above. Enolether is not negligible, therefore:
[3'–phosphate$_{trap}$] = [5'–phosphate] − [enolether]
0.8 = 1.3 - 0.5 = 3'–phosphate$_{trap}$; 100% charge injection = 1.3 + 0.2; ⇒ charge injection ratio 5'–phosphate:3'–phosphate$_{inject}$ = 87:13.

6.2 Structural Confirmations

T_m of ds **s6/ cs6** is 53.5°C in irradiation buffer.
Done reference CD spectrum with **s7/ cs6**. This is **s7** strand as **s6** but with a T instead of the pyrene nuc. and the normal counterstrand with the abasic site. The spectrum is with substracted background. Extrema at 250, 264 (zero) and 279 nm. The **s6/ cs6**CD spectrum. Also done in citrate buffer like irradiations. Extrema at 246, 260 (zero) and 274 nm.

6.3 Phosphoramidite of Pyrene deoxyribose nucleotide (14)

6.3.1 1'-(β) 1-Pyrenyl-3',5'-di-*O*-(p-toluoyl)-2'-deoxy-D-ribose (12)

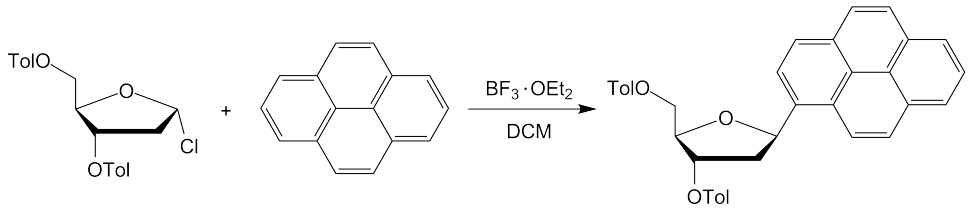

12

To a solution of 342 mg (880 µmol) Hoffer's chlorosugar 1 -(β) chloro-3,5-di-*O*-(p-toluoyl)-2-deoxy-D-ribose and 356 mg (1.76 mmol, 2.0 eq.) pyrene in 12 mL dry dichloromethane was added 167 µL (1.32 mmol, 1.5 eq.) boron trifluoride etherate at 0°C.[69] After stirring for 2 hours the reaction mixture was treated with saturated aqueous sodium bicarbonate and extracted three times with dichloromethane. The combined organic layers were dried over anhydrous $MgSO_4$ and concentrated *in vacuo*. Two times flash chromatography (H/EA 10:1) yielded in 304 mg (62%) of the desired **12**. As a side product the α–epimer could be isolated.
$C_{37}H_{30}O_5$, MW: 554.63 g·mol^{-1}

TLC: R_f = 0.33 (H/EA 6:1)

^{1}H NMR ($CDCl_3$, 400 MHz, δ/ppm, J/Hz)
8.34 (d, J = 7.8, 1H, H_{Ar}), 8.28 (d, J = 9.3, 1H, H_{Ar}), 8.21 – 7.96 (m, 3H, H_{Ar}), 8.11 – 7.95 (m, 11H, H_{Ar}), 7.34 (d, J = 8.1, 2H, H_{Ar}), 7.20 (d, J = 8.1, 2H, H_{Ar}), 7.20 (dd, J = 10.9, J = 5.1, 1H, H-1'β), 5.75 (d, J = 7.0, 1H, H-3'), 4.88 – 4.78 (m, 2H, H-4'), 4.77 – 4.72 (m, 1H, H-5'), 2.91 (dd, J = 5.3, J = 13.9, 1H, H-2'α), 2.48 (s, 3H, Ar-CH_3), 2.47 – 2.38 (m, 1H, H-2'β), 2.38 (s, 3H, Ar-CH_3)

^{13}C NMR ($CDCl_3$, 101 MHz, δ/ppm)
166.6 (q, -COOR), 166.4 (q, -COOR), 144.4 (q, C_{Ar}), 144.0 (q, C_{Ar}), 134.3 – 122.4 (C_{Ar}), 83.1, 78.3, 77.4, 65.0, 41.8, 21.9 (p, Ar-CH_3), 21.8 (Ar-CH_3)

MS (ESI, m/z)
594.0 (43), 577.6 (100), 555.3 (36)
α–epimer
TLC: R_f = 0.29 (H/EA 6:1)

6.3.2 α to β Epimerisation

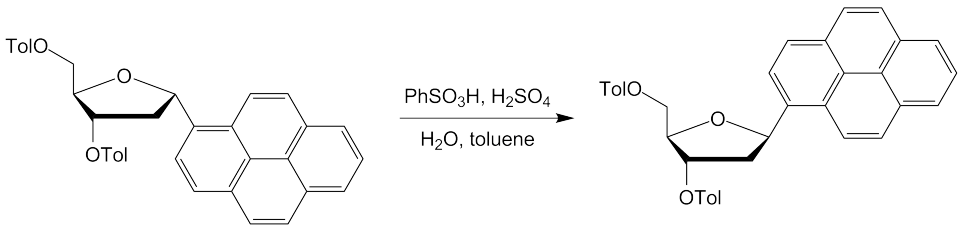

12

To a solution of 36.0 mg (64.9 µmol) α–epimer of **12** in 2.3 mL toluene were added a catalytic amount of benzenesulfonic acid (approx. 10 mg), one small drop of concentrated sulfuric acid, and 2 drops of water.[51] The reaction mixture was refluxed under vigorous stirring for 14 hours. The mixture was then poured into saturated aqueous sodium bicarbonate solution and extracted with ethyl acetate. The combined organic layers were dried over anhydrous magnesium sulfate and evaporated. Flash column chromatography (H/EA 8:1 to 2:1) yielded in 29.9 mg (83%) of the desired β–epimer.

6.3.3 1'-(β) 1-Pyrenyl-2'-deoxy-D-ribose (11)

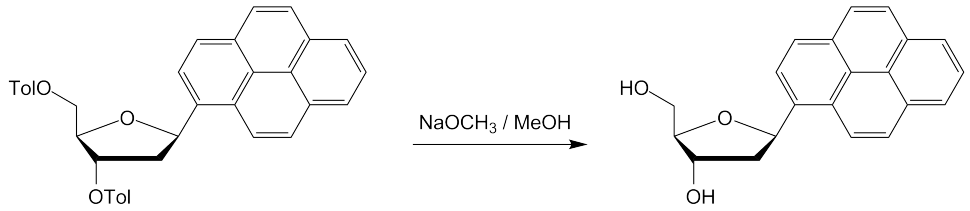

12 **11**

To a solution of 30.4 mg (61.0 µmol) **12** in 1.0 mL methanol was added 366 µL (0.5 M, 3.0 eq.) sodium methoxide solution in methanol.[51] The reaction mixture was stirred at room temperature for 5 hours. Solid ammonium chloride was added until the pH was 8. The mixture was then poured into water and extracted three times with ethyl acetate. The combined organic layers were dried over anhydrous magnesium sulfate and evaporated. Flash column chromatography (pure EA) of the crude mixture gave 15.4 mg (79%) of the deprotected diol.

$C_{21}H_{18}O_3$, MW: 318.37 g·mol^{-1}

TLC: R_f = 0.39 (EA)

^{1}H NMR ($CDCl_3$, 400 MHz, δ/ppm, J/Hz)
8.31 (d, J = 9.3, 1H, H_{Ar}), 8.19 (t, J = 4.0, 4H, H_{Ar}), 8.06 (s, 2H, H_{Ar}), 8.01 (t, J = 7.6, 1H, H_{Ar}), 6.23 (dd, J = 5.8, J = 10.3, 1H), 4.62 – 4.54 (m, 1H), 4.25 – 4.21 (m, 1H), 4.02 – 3.88 (m, 2H), 2.62 (ddd, J = 2.0, J = 5.6, J = 13.4, 1H)

6.3.4 1'-(β) 1-Pyrenyl-5'-*O*-dimethoxytrityl-2'-deoxy-D-ribose (13)

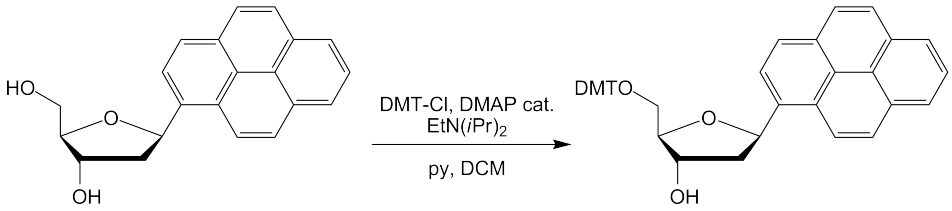

11 **13**

The synthesized unprotected diol **11** was coevaporated with dry dichloromethane twice and 30.0 mg (94.2 µmol) were dissolved in 905 µL dry pyridine and 724 µL dry dichloromethane.[51] To the above mixture were added catalytic amounts of 4-(*N,N*-dimethylamino)-pyridine (DMAP), 24.6 µL (141.3 µmol, 1.5 eq.) diisopropylethylamine (Hünig's base) and 57.5 mg (170 µmol, 1.8 eq.) 4,4 '-dimethoxytrityl chloride. The mixture was stirred at room temperature for 6 hours. 905 µL hexane was added, and the mixture was loaded onto a flash column (pre–equilibrated with 5% triethylamine in hexane) and eluted (H/EA 6:1 to 2:1). The product was obtained as 44.3 mg (76%) white foam.
$C_{42}H_{36}O_5$, MW: 620.73 g·mol^{-1}

TLC: R_f = 0.77 (EA)

^{1}H NMR ($CDCl_3$, 400 MHz, δ/ppm, J/Hz)
8.31 (dd, J = 9.4, J = 13.6, 2H, H_{Ar}), 8.20 – 8.14 (m, 3H, H_{Ar}), 8.07 (t, J = 9.4, 1H, H_{Ar}), 8.05 (s, 2H, H_{Ar}), 8.00 (t, J = 7.6, 2H, H_{Ar}), 7.53 (dm, J = 7.0, 2H, H_{Ar}), 7.41 (dm, J = 8.1, 4H, H_{Ar}), 7.33 – 7.20 (m, 3H, H_{Ar}), 6.86 – 6.80 (m, 4H, H_{Ar}), 6.21 (dd, J = 5.8, J = 9.6, 1H), 4.57 (quint., J = 3.0, 1H), 4.24 (q, J = 5.1, 1H), 3.55 – 3.43 (m, 2H), 2.64 – 2.58 (m, 1H, H-2'), 2.30 – 2.22 (m, 1H, H-2')

MS (ESI, m/z)
662.5 (57), 644.3 (100), 643.0 (94), 609.6 (49), 604.2 (47), 495.5 (48), 434.1 (50)

6.3.5 1'-(β) 1-Pyrenyl-5'-*O*-dimethoxytrityl-2'-deoxy-D-ribose-3'-*O*-[(2-cyanoethyl)-*N,N*-diisopropylphosphoramidite] (14)

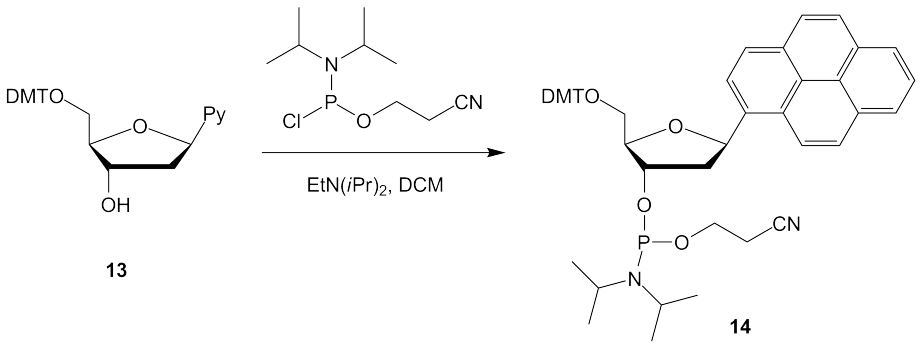

To a solution of 97 mg (156 µmol) dry (coevaporation with dichloromethane) **13** in 2 mL anhydrous dichloromethane, 108 µL (620 µmol, 4.0 eq.) Hünig's base and 54.0 µL (242 µmol, 1.6 eq.) 2-cyanoethyl-

N,N-(diisopropyl)-chlorophosphoramidite were added.[51] The reaction mixture was stirred at room temperature for 6 hours. Subsequent flash chromatography (H/EA/Et_3N 4:1:0.05) on a pre-equilibrated column (EA with 5% triethylamine) yielded in 113.1 mg (88%) of the final building block **14**.

$C_{51}H_{53}N_2O_6P$, MW: 820.95 g·mol^{-1}

TLC: R_f = 0.85 (EA)

^{1}H NMR ($CDCl_3$, 400 MHz, δ/ppm, J/Hz)
8.44 – 8.33 (m, 2H), 7.62 – 7.22 (m, 9H), 6.92 – 6.79 (m, 4H), 6.28 – 6.20 (m,1H), 4.69 (m, 1H), 4.45 (m, 1H), 4.0 – 3.2 (m, 12H), 2.80 (m, 1H), 2.69 (t, 2H), 2.32 (m, 1H), 1.15 (m, 12H)

MS (ESI, m/z)
843.3 (100)

6.3.6 Oligonucleotide containing 11

6.3.6.1 Strand s6

5'- TGC ATC AT**11** TTT ATC AGA GC-3'
MW: 6158 g·mol^{-1}
ε_{260} = 190400 M^{-1}cm^{-1}
Expected Strand Break Fragments of **s6**:
5'–phosphate:
MW: 3411 g·mol^{-1}
ε_{260} = 106920 M^{-1}cm^{-1}
3'–phosphate:
MW: 2465 g·mol^{-1}
ε_{260} = 74880 M^{-1}cm^{-1}
counter strand: **cs6** MW: 8450 g·mol^{-1}
ε_{260} = 260190 M^{-1}cm^{-1}

6.4 Pyrene Diamide 15

6.4.0.2 Synthesis and Incorporation of 15

The synthesis of the building block and the incorporation into an oligonucleotide was performed by coworkers of *Häner*.

Starting from pyrene-1,8-dicarboxylic acid, a asymmetric disubstitution was performed under basic conditions.[5,77,105] The dimethyltrityl (DMT) protected alcohol function will later be the 5' attachment point. The phosphorylation under standard conditions with 2-cyanoethyl-*N,N*-(diisopropyl)-chlorophosphoramidite of the unprotected alcohol group gave the desired pyrene phosphoramidite **41** (labeled as **15** when incorporated into an oligonucleotide) as shown in Scheme 6.1.

Oligonucleotide **s8** was prepared via automated oligonucleotide synthesis by a standard synthetic pro-

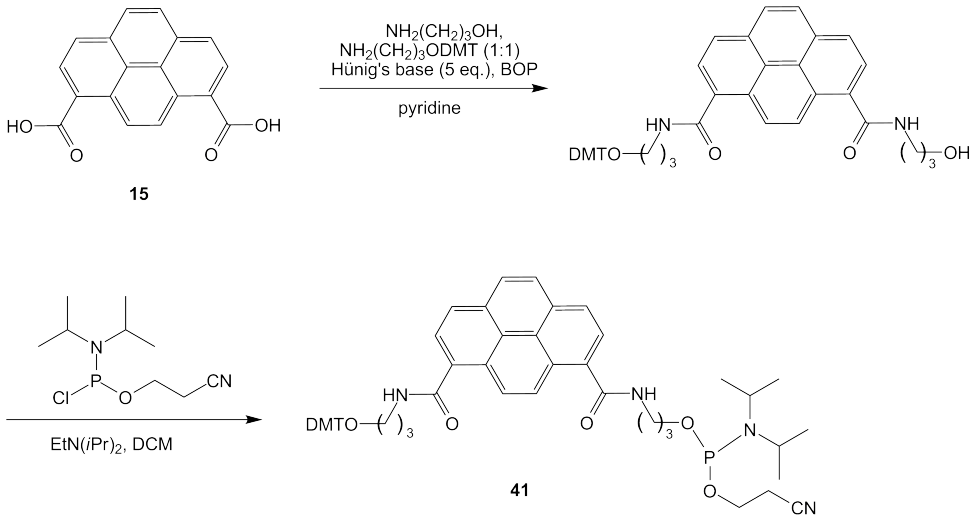

*Scheme 6.1: Synthesis of the pyrene building block **41** of Häner*

cedure ('trityl-off' mode) on a 394-DNA/RNA synthesizer (Applied Biosystems).[79] Cleavage from the solid support and final deprotection was done by treatment with 30% NH_4OH solution at 55°C overnight. The oligonucleotide was purified by reverse phase HPLC (LiChrospher 100 RP-18, 5 µm, Merck), Bio-Tek Instruments Autosampler 560); eluent A = $(Et_3NH)OAc$ (0.1 M, pH 7.4); eluent B = MeCN; elution at 40°C; gradient 5 – 20% B over 30 min. Characterization by electrospray ionisation time-of-flight (ESI-TOF) mass spectrometry.

Incorporation of **15** proceeded without any difficulties, coupling yields being equal to those of unmodified nucleotide bases.

A UV/vis scan of the double-strand **s8/ cs8** in Figure 6.1. Local maxima can be found at 261 nm and 360 nm.

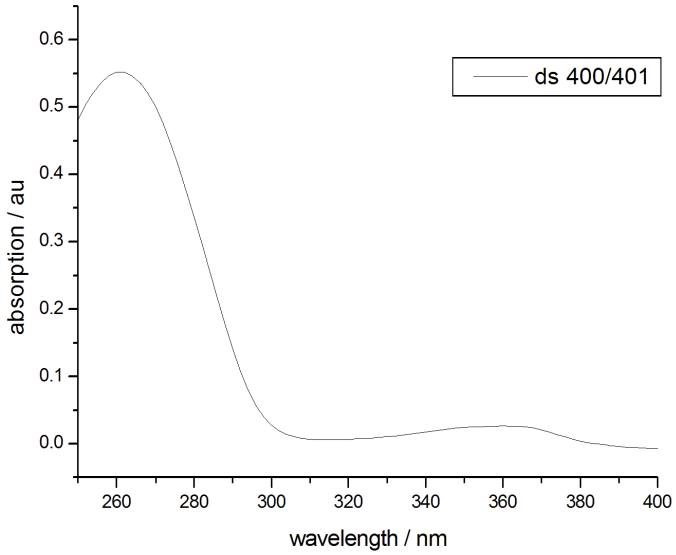

Figure 6.1: ds 400 / 401 annealed

The figure 6.2 shows the UV/vis of **15** in irradiation buffer. Here one can see the absorption.

6.5 12-(Coumarin-7'-yl)-oxydodecyl-trimethylammonium bromide (38)

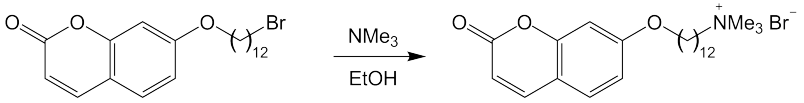

36 **38**

The substance has been synthesized following the general procedure given in section 6.1.1.1. The converted alkyl bromide was **36**. This yielded in 134 mg (286 µmol) white powder.

$C_{24}H_{38}BrNO_3$ x1/2 H_2O, MW: 468.47 g·mol^{-1}

TLC: R_f = 0.00 (DCM/MeOH 9:1)

mp: 157 – 159 °C

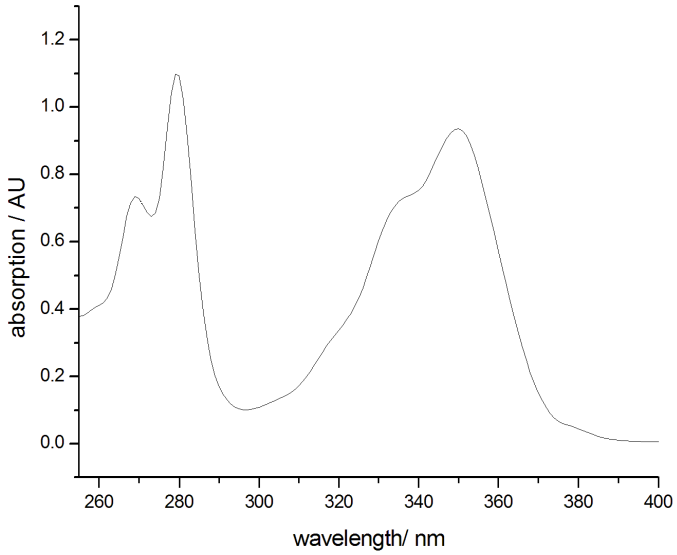

*Figure 6.2: UV/vis of **15** in irradiation buffer*

^{1}H NMR (MeOH-d_4, 400 MHz, δ/ppm, J/Hz)
7.90 (d, J = 9.3, 1H, H-4'), 7.54 (d, J = 8.6, 1H, H-5'), 6.93 (dd, J = 6.3, J = 2.2, 1H, H-6'), 6.88 (d, J = 2.3, 1H, H-8'), 6.25 (d, J = 9.3, 1H, H-3'), 4.07 (t, J = 6.3, 2H, H-12), 3.35 – 3.32 (m, 2H, H-1), 3.13 (s, 9H, $N(CH_3)_3$), 1.85 – 1.76 (m, 4H, CH_2), 1.53 – 1.45 (m, 2H,, CH_2), 1.44 – 1.29 (m, 14H, CH_2)

^{13}C NMR (MeOH-d_4, 101 MHz, δ/ppm):
164.1 (q, C-2'), 163.4 (q, C-7'), 157.2 (q, C-8a'), 145.8 (t, C-4'), 130.5 (t, C-5'), 114.2 (t, C_{Ar}), 113.9 (q, C-4a'), 113.2 (t, C_{Ar}), 102.2 (t, C-8'), 69.8 (s, C-12), 67.9 (s, C-1), 53.5 (p, $N(CH_3)_3$), 30.6 (s, CH_2), 30.6 (s, CH_2), 30.5 (s, CH_2), 30.4 (s, CH_2), 30.2 (s, CH_2), 30.1 (s, CH_2), 27.4 (s, CH_2), 27.0 (s, CH_2), 23.9 (s, CH_2)

IR (KBr, $\tilde{\nu}$/cm^{-1})
3425, 2923 (s), 2853 (s), 1725 (s), 1617 (s), 1554, 1476, 1401, 1292, 1239, 1131 (s), 1028, 849

MS (FAB, m/z)
389 (21), 388 (100), 244 (11), 163 (9), 162 (6), 89 (6), 77 (9), 65 (6), 60 (17), 59 (47), 58 (38), 57 (7), 55 (16), 51 (6), 41 (13), 39 (11)

UV/vis (10 mM TRIS buffer, pH 8.5, ε_λ/M^{-1}cm^{-1})

$\varepsilon_{219} = 7570$, $\varepsilon_{324} = 9360$

EA

calculated:	C: 60.37	H: 8.23	N: 2.93
found:	C: 60.46	H: 8.25	N: 2.72

6.5.1 1-Bromo-12-(coumarin-7'-yloxy)-dodecane (36)

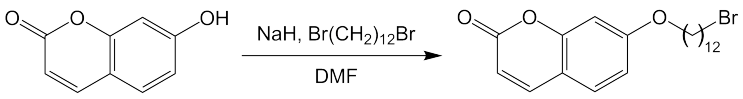

36

A solution of 1.00 g (6.17 mmol) umbelliferone and 2.43 g (7.40 mmol, 1.2 eq.) 1,12-dibromododecane in 25 mL anhydrous DMF was cooled to 0°C under argon.[106] After the addition of 283 mg (6.48 mmol, 1.05 eq.) sodium hydride (55% dispersion in mineral oil) the suspension was stirred for 1 hour at 0°C and 10 hours at room temperature. After quenching with water and extraction with ethyl acetate, the organic layer was washed three times with water and dried over magnesium sulfate. After flash column chromatography (P/DE 20:1 → 3:1) using silica gel prepaired according to the procedure 6.1.1.2, 1.91 g (76%) of the product was isolated.

$C_{21}H_{29}BrO_3$, MW: 409.36 g·mol^{-1}

TLC: R_f = 0.62 (P/DE 1:1)

mp: 79 – 81 °C

^{1}H NMR ($CDCl_3$, 400 MHz, δ/ppm, J/Hz)

7.63 (d, J = 9.6, 1H, H-4'), 7.34 (d, J = 8.4, 1H, H-5'), 6.84 (dd, J = 8.6, J = 2.3, 1H, H-6'), 6.80 (d, J = 2.3, 1H, H-8'), 6.23 (d, J = 9.2, 1H, H-3'), 4.00 (t, J = 6.7, 2H, H-12), 3.40 (t, J = 6.8, 2H, H-1), 1.88 – 1.76 (m, 4H, H-2, H-11), 1.49 – 1.26 (m, 16H, H-3 – H-10)

^{13}C NMR ($CDCl_3$, 101 MHz, δ/ppm)

162.6 (q, C-2'), 161.4 (q, C-7'), 156.1 (q, C-8a'), 143.6 (t, C-4'), 128.8 (t, C-5'), 113.1 (t, C_{Ar}), 113.0 (t, C_{Ar}), 112.5 (q, C-4a'), 101.4 (t, C-8'), 68.8 (s, C-12), 34.2 (s, C-1), 33.0 (s, C-2), 29.6 (s, CH_2), 29.5 (s, CH_2), 29.4 (s, CH_2), 29.1 (s, CH_2), 28.9 (s, CH_2), 28.3 (s, CH_2), 26.1 (s, CH_2)

IR (KBr, $\tilde{\nu}/\mathrm{cm}^{-1}$)
2919 (s), 2854 (s), 1722 (s), 1622 (s), 1472, 1397, 1291 (s), 1237, 1135 (s), 1029, 828 (s), 718, 639

MS (EI, m/z)
410 (8), 408 (8), 329 (6), 163 (20), 162 (100), 134 (19), 57 (7), 55 (14), 53 (10), 41 (12)

EA

calculated:	C: 61.62	H: 7.14	N: 0.00
found:	C: 61.62	H: 7.26	N: 0.00

6.6 6-(Coumarin-7'-yl)-oxyhexyl-trimethylammonium bromide (37)

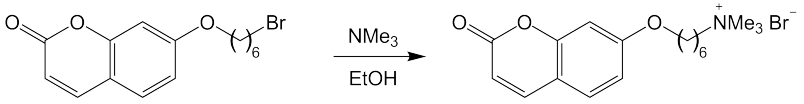

35 **37**

The substance has been synthesized following the general procedure given in section 6.1.1.1. The converted alkyl bromide was **35**. This yielded in 157 mg (409 µmol) of white powder.

$C_{18}H_{26}BrNO_3$, MW: 384.31 g·mol^{-1}

TLC: R_f = 0.00 (DCM/MeOH 9:1)

mp: 176 – 179 °C

^{1}H NMR (MeOH-d$_4$, 400 MHz, δ/ppm, J/Hz)
7.90 (d, J = 9.6, 1H, H-4'), 7.54 (d, J = 8.6, 1H, H-5'), 6.93 (d, J = 8.6, 1H, H-6'), 6.88 (s, 1H, H-8'), 6.25 (d, J = 9.6, 1H, H-3'), 4.12 (t, J = 6.3, 2H, H-6), 3.41 – 3.34 (m, 2H, H-1), 3.15 (s, 9H, N(CH$_3$)$_3$), 1.91 – 1.80 (m, 4H, H-2, H-5), 1.66 – 1.57 (m, 4H, H-3 or H-4), 1.52 – 1.43 (m, 4H, H-3 or H-4)

^{13}C NMR (MeOH-d$_4$, 101 MHz, δ/ppm):
164.0 (q, C-2'), 163.3 (q, C-7'), 157.1 (q, C-8a'), 145.8 (t, C-4'), 130.5 (t, C-5'), 114.1 (t, C$_{Ar}$), 113.9 (t, C$_{Ar}$), 113.2 (q, C-4a'), 102.2 (t, C-8'), 69.5 (s, C-6), 67.8 (s, C-1), 53.6 (p, N(CH$_3$)$_3$), 29.8 (s, C-5), 27.0 (s, C-3), 26.6 (s, C-4), 23.9 (s, C-2)

IR (KBr, $\tilde{\nu}/\mathrm{cm}^{-1}$)
3426 (s), 3008, 2947 (s), 2875, 1724 (s), 1617 (s), 1553, 1512, 1480, 1405, 1296 (s), 1242 (s), 1195, 1132 (s), 1005, 961, 890, 851, 571, 466

MS (ESI, m/z)
305 (16), 304 (100)

UV/vis (10 mM TRIS buffer, pH 8.5, $\varepsilon_\lambda/\mathrm{M}^{-1}\mathrm{cm}^{-1}$)
$\varepsilon_{218} = 9380$, $\varepsilon_{324} = 12160$

EA

calculated:	C: 56.26	H: 6.82	N: 3.64
found:	C: 55.40	H: 6.86	N: 3.62

6.6.1 1-Bromo-6-(coumarin-7'-yloxy)-hexane (35)

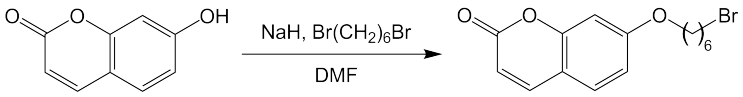

35

A solution of 2.00 g (12.3 mmol) umbelliferone and 3.77 mL (24.7 mmol, 2.0 eq.) 1,6-dibromohexane in 15 mL anhydrous DMF was cooled to -68°C under argon.[106] After the addition of 566 mg (13.0 mmol, 1.05 eq.) sodium hydride (55% dispersion in mineral oil) the suspension was stirred for 1 hour at 0°C and 10 hours at room temperature. After quenching with water and extraction with dichloromethane, the organic layer was washed three times with saturated ammonium chloride solution, three times with water to remove remaining DMF and dried over magnesium sulfate. After flash column chromatography (P/DE 20:1 → 3:1) using silica gel prepaired according to the procedure 6.1.1.2 3.16 g (79%) of the product was isolated from hexane as thin white needles.

$C_{15}H_{17}BrO_3$, MW: 325.20 g·mol^{-1}

TLC: R_f = 0.49 (P/DE 1:1)

mp: 66 – 67 °C

^{1}H NMR ($CDCl_3$, 400 MHz, δ/ppm, J/Hz)
7.64 (d, J = 9.6, 1H, H-4'), 7.37 (d, J = 8.4, 1H, H-5'), 6.84 (dd, J = 8.3, J = 2.5, 1H, H-6'), 6.80 (d, J = 2.3, 1H, H-8'), 6.25 (d, J = 9.6, 1H, H-3'), 4.02 (t, J = 6.3, 2H, H-6), 3.43 (t, J = 6.6, 2H, H-1), 1.94 – 1.79 (m, 4H, H-2, H-5), 1.57 – 1.47 (m, 4H, H-3, H-4)

^{13}C NMR ($CDCl_3$, 101 MHz, δ/ppm)
162.4 (q, C-2'), 161.3 (q, C-7'), 155.9 (q, C-8a'), 143.5 (t, C-4'), 128.8 (t, C-5'), 113.0 (t, C_{Ar}), 113.0 (t, C_{Ar}), 112.5 (q, C-4a'), 101.4 (t, C-8'), 68.4 (s, C-6), 33.8 (s, C-1), 32.7 (s, C-2), 29.8 (s, C-5), 28.9 (s, C-3), 27.9 (s, C-3), 25.3 (s, C-4)

IR (KBr, $\tilde{\nu}$/cm^{-1})
2940 (s), 2864, 1724 (s), 1622 (s), 1556, 1510, 1470, 1397, 1292 (s), 1239 (s), 1195, 1136 (s), 1100, 1034, 1003, 892, 828 (s), 718, 639

MS (EI, m/z)
326 (19), 324 (19), 163 (14), 162 (100), 134 (49), 105 (5), 89 (5), 83 (16), 77 (4), 55 (19),41 (13)

EA

calculated:	C: 55.40	H: 5.27	N: 0.00
found:	C: 55.44	H: 5.14	N: 0.00

6.7 Nonyl-trimethylammonium bromide (40)

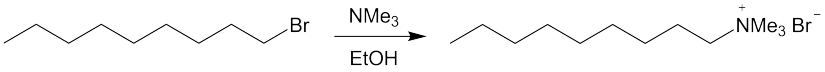

40

The substance has been synthesized following the general procedure given in section 6.1.1.1. The converted alkyl bromide was 1-bromononane. In this way 1.39 g (5.22 mmol) of white foam was received.

$C_{12}H_{28}BrN$, MW: 266.26 g·mol^{-1}

TLC: R_f = 0.00 (DCM/MeOH 9:1)

mp: 239 – 242 °C

^{1}H NMR ($CDCl_3$, 400 MHz, δ/ppm, J/Hz)
3.58 – 3.52 (m, 2H, H-1), 3.43 (s, 9H, $N(CH_3)_3$), 1.75 – 1.66 (m, 2H, H-2), 1.38 – 1.28 (m, 4H, H-3, H-4), 1.28 – 1.16 (m, 8H, H-5, H-6, H-7, H-8), 0.83 (t, J = 6.6, 3H, H-9)

^{13}C NMR ($CDCl_3$, 101 MHz, δ/ppm)
67.0 (s, C-1), 53.4 (p, $N(CH_3)_3$), 31.8 (s, CH_2), 29.4 (s, CH_2), 29.3 (s, CH_2), 29.1 (s, CH_2), 26.2 (s, CH_2), 23.2 (s, CH_2), 22.7 (s, C-8), 14.1 (p, C-9)

IR (KBr, $\tilde{\nu}$/cm^{-1})
3015, 2930 (s), 2854 (s), 1483 (s), 1402, 967, 910, 724

MS (ESI, m/z)
186.3 (100)

6.8 1-Bromo-4-(anthr-9'-yl)-butane (27)

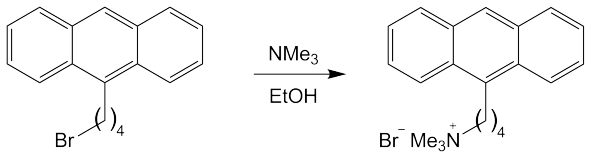

24 **27**

The substance has been synthesized following the general procedure given in section 6.1.1.1. The converted alkyl bromide was **24**. This yielded in 129 mg (346 µmol) of white powder.

$C_{21}H_{26}BrN$, MW: 372.34 g·mol^{-1}

TLC: R_f = 0.00 (DCM/MeOH 9:1)

mp: 238 °C

^{1}H NMR ($CDCl_3$, 400 MHz, δ/ppm, J/Hz)
8.20 (s, 1H, H-10'), 8.13 (d, J = 8.8, 2H, H-1', H-8'), 7.87 (d, J = 8.3, 2H, H-4', H-5'), 7.46 – 7.40 (m,

2H, H-2', H-7'), 7.34 (t, J = 8.4, 2H, H-3', H-6'), 3.53 (t, J = 7.6, 2H, H-4), 3.38 (t, J = 7.6, 2H, H-1), 3.13 (s, 9H, $N(CH_3)_3$), 1.79 – 1.62 (m, 4H, H-2, H-3)

^{13}C NMR ($CDCl_3$, 101 MHz, δ/ppm)
133.3 (q, C-9'), 131 (q, C_{Ar}), 129.5 (q, C_{Ar}), 129.2 (t, C_{Ar}), 126.1 (q, C_{Ar}), 126.0 (t, C_{Ar}), 125.0 (t, C_{Ar}), 124.2 (t, C_{Ar}), 58.1 (s, C-1), 53.2 (p, $N(CH_3)_3$), 27.3 (s, CH_2), 27.0 (s, CH_2), 23.1 (s, CH_2)

6.8.1 1-Bromo-4-(anthr-9'-yl)-butane (24)

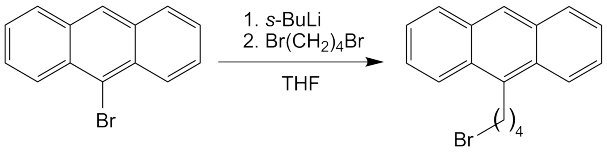

24

In a dry flask, 600 mg (2.24 mmol) 9-bromoanthracene was dissolved in 25 mL dry THF at room temperature.[107] After cooling to -75°C (EtOH, solid CO_2), 3.45 mL (1.3 M in hexane, 4.48 mmol, 2.0 eq.) *s*-BuLi was added slowly. The yellow suspension was stirred for 20 minutes before adding 1.35 mL (11.2 mmol, 5.0 eq.) 1,6-dibromobutane. The reaction was allowed to warm to 0°C after 20 minutes and was stirred for another 50 minutes before quenching with water. Extraction with diethyl ether and washing with water followed by drying over magnesium sulfate and evaporation of the solvent gave the crude product. Filtration of the orange oily suspension dispersed in hexane through cotton wool removed the majority of the by-product anthracene. Purification was performed by careful flash column chromatography (pure H → H/DE 99:1, after anthracene elution) using 70 g silica gel. Dissolving the product in dichloromethane and adding slowly hexane yielded in 175 mg (25%) white crystals of pure **24**.
$C_{18}H_{17}Br$, MW: 313.23 g·mol^{-1}

TLC: R_f = 0.25 (H)

mp: 123 °C

^{1}H NMR ($CDCl_3$, 400 MHz, δ/ppm, J/Hz)
8.35 (s, 1H, H-10'), 8.27 (d, J = 9.1, 2H, H-1', H-8'), 8.02 (d, J = 8.3, 2H, H-4', H-5'), 7.55 – 7.44 (m, 4H, H-2', H-3', H-6'H-7'), 3.65 (t, J = 8.1, 2H, H-1), 3.50 (t, J = 6.8, 2H, H-4), 2.13 (quint., J = 7.3, 2H, H-2), 2.03 – 1.94 (m, 2H, H-3)

^{13}C NMR ($CDCl_3$, 101 MHz, δ/ppm)
134.3 (q, C-9'), 131.7 (q, C-4a', C-10a'), 129.7 (q, C-8a', C-9a'), 129.4 (t, C-1', C-8'), 126.0 (q, C-10'), 125.7 (t, C_{Ar}), 125.0 (t, C_{Ar}), 124.4 (t, C_{Ar}), 33.7 (s, CH_2), 33.2 (s, CH_2), 29.8 (s, CH_2), 27.1 (s, CH_2)

IR (KBr, $\tilde{\nu}/\mathrm{cm}^{-1}$)
2924 (s), 2856 (s), 1655, 1621 (s), 1447 (s), 1350, 1224 (s), 1155, 1012, 887, 842, 734 (s), 651

6.9 8-(10'-Butyl-anthr-9'-yl)-octyl-trimethylammonium bromide (30)

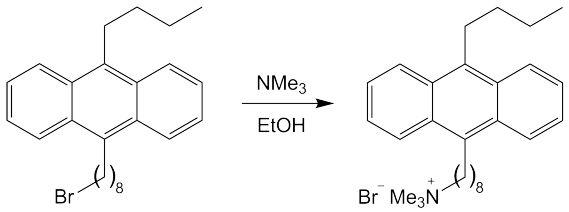

29 **30**

The substance has been synthesized following the general procedure given in section 6.1.1.1. The converted alkyl bromide was **29**. In this way 56.5 mg (117 µmol) of yellow solid was received.

$C_{29}H_{42}BrN$, MW: 484.55 g·mol^{-1}

TLC: R_f = 0.00 (DCM/MeOH 9:1)

mp: 162 – 176 °C

^{1}H NMR ($CDCl_3$, 400 MHz, δ/ppm, J/Hz)
8.32 – 8.24 (m, 4H, H-1', H-4', H-5', H-8'), 7.52 – 7.46 (m, 4H, H-2', H-3', H-6', H-7'), 3.65 – 3.57 (m, 6H, H-1, H-8, H-9), 3.44 (s, 9H, $N(CH_3)_3$), 1.83 – 1.74 (m, 4H, H-7, H-10), 1.74 – 1.65 (m, 2H, H-2), 1.63 – 1.53 (m, 4H, H-6, H-11), 1.43 – 1.34 (m, 6H, H-3, H-4, H-5), 1.03 (t, J = 7.3, H-12)

^{13}C NMR ($CDCl_3$, 101 MHz, δ/ppm)
134.1 (q, C-9'), 133.7 (q, C-10'), 129.5 (q, C-4a', C-8a', C-9a', C-10a'), 125.4 (t, C_{Ar}), 125.3 (t, C_{Ar}),

125.0 (t, C_{Ar}), 124.9 (t, C_{Ar}), 53.5 (p, $N(CH_3)_3$), 33.7 (s, C-8), 31.5 (s, C-9), 30.2 (s, CH_2), 29.5 (s, CH_2), 29.3 (s, CH_2), 28.2 (s, CH_2), 28.1 (s, CH_2), 26.3 (s, CH_2), 23.6 (s, CH_2), 23.3 (s, CH_2), 14.2 (p, C-12)

IR (KBr, $\tilde{\nu}/\mathrm{cm}^{-1}$)
3011, 2925 (s), 2854 (s), 1622, 1478 (s), 1372, 1100, 1028, 967, 906, 756 (s), 650

MS (FAB, m/z)
405 (33), 404 (100), 191 (8), 114 (6), 60 (19), 59 (42), 58 (49)

MS (ESI, m/z)
404.3 (100), 367 (9)

6.9.1 1-Bromo-8-(10'-butyl-anthr-9'-yl)-octane (29)

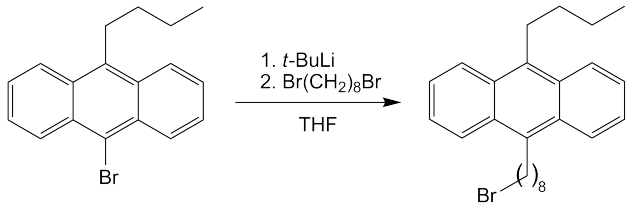

28 **29**

To a yellow suspension of 211 mg (674 µmol) **28**in 10 mL dry THF at -65°C, 539 µL (1.5 M in hexane, 808 µmol, 1.2 eq.) *t*-BuLi was added. The orange suspension was allowed to warm to 0°C after 1 hour and was cooled again to -65°C for the addition of 134 µL (741 µmol, 1.1 eq.) 1,8-dibromooctane. 10 minutes later the suspension was warmed up to 0°C and stirred for 2 1/2 hours. Stirring over night at room temperature completed the reaction. Diethyl ether and water was added to the solution. The organic layer was washed three times with water and dried over magnesium sulfate. The solvent was removed under reduced pressure and flash column chromatography (pure H) with excess silica gel yielded in 94.6 mg (33%) pure product.

$C_{26}H_{33}Br$, MW: 425.44 g·mol^{-1}

TLC: R_f = 0.36 (H)

mp: 50 – 52 °C

^{1}H NMR ($CDCl_3$, 400 MHz, δ/ppm, J/Hz)
8.37 – 8.29 (m, 4H, H-1', H-4', H-5', H-8'), 7.54 (dt, J = 10.1, J = 3.3, 4H, H-2', H-3', H-6', H-7'), 3.66 – 3.58 (m, 4H, H-8, H-9), 3.43 (t, J = 6.8, 2H, H-1), 1.92 – 1.79 (m, 6H, H-2, H-7, H-10), 1.69 – 1.58 (m, 4H, H-6, H-11), 1.51 – 1.33 (m, 6H, H-3, H-4, H-5), 1.07 (t, J = 7.4, 3H, H-12)

^{13}C NMR ($CDCl_3$, 101 MHz, δ/ppm)
134.0 (q, C-9'), 133.9 (q, C-10'), 129.5 (q, C-8a', C-9a'), 129.5 (q, C-4a', C-10a'), 125.4 (t, C_{Ar}), 125.3 (t, C_{Ar}), 124.9 (t, C_{Ar}), 124.9 (t, C_{Ar}), 34.2 (s, CH_2), 33.7 (s, CH_2), 32.9 (s, CH_2), 31.5 (s, CH_2), 30.4 (s, CH_2), 29.5 (s, CH_2), 28.9 (s, CH_2), 28.3 (s, CH_2), 28.0 (s, CH_2), 23.6 (s, CH_2), 15.4 (s, CH_2), 14.2 (p, C-12)

IR (KBr, $\tilde{\nu}$/cm^{-1})
3082, 3049, 2923 (s), 2851 (s), 1619, 1463 (s), 1373, 1252, 1026, 751 (s), 653 (s)

MS (EI, m/z)
426 (73), 425 (19), 424 (73), 383 (18), 381 (18), 248 (12), 247 (61), 191 (100)

6.9.2 9-Bromo-10-butyl-anthracene (28)

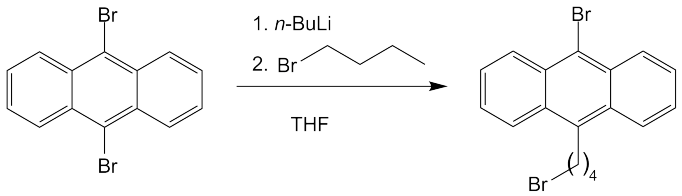

28

In a dry flask, 1.76 g (5.13 mmol) 9,10-dibromoanthracene was suspended in 40 mL dry THF at room temperature.[108] After cooling to -78°C, 2.76 mL (25.6 mmol, 5.0 eq.) 1-bromobutane, followed by 3.20 mL (1.6 M in hexane, 5.13 mmol, 1.0 eq.) *n*-BuLi were added to form an orange suspension at once. After 50 minutes stirring, the reaction was allowed to warm to 9°C and water was added to quench the reaction. The majority of the solvents was removed under reduced pressure, extraction with diethyl ether and washing with water followed by drying over magnesium sulfate and evaporation of the solvent gave the crude product. Filtration of the brown oily suspension dispersed in hexane through cotton wool

removed the majority of the by-product anthracene. Purification was performed by careful flash column chromatography (pure H) to yield 1.06 g (66%) pure **28**.
$C_{18}H_{17}Br$, MW: 313.23 g·mol^{-1}

TLC: R_f = 0.74 (H/DE 9:1)

mp: 54 – 56 °C

^{1}H NMR ($CDCl_3$, 400 MHz, δ/ppm, J/Hz)
8.61 (d, J = 8.6, 2H, H-1, H-8), 8.30 (d, J = 8.6, 2H, H-4, H-5), 7.62 – 7.51 (m, 4H, H-2, H-3, H-6, H-7), 3.60 (t, J = 8.1, 2H, H-11), 1.85 – 1.76 (m, 2H, H-12), 1.67 – 1.56 (m, 2H, H-13), 1.04 (t, J = 8.0, 2H, H-14)

^{13}C NMR ($CDCl_3$, 101 MHz, δ/ppm)
136.3 (q, C-9), 130.5 (q, C_{Ar}), 130.5 (q, C_{Ar}), 128.8 (q, C-1, C-8), 126.8 (t, C_{Ar}), 125.7 (t, C_{Ar}), 125.0 (t, C_{Ar}), 121.8(q, C-10), 33.7 (s, C-11), 28.2 (s, C-12), 23.5 (s, C-13), 14.2 (p, C-14)

IR (KBr, $\tilde{\nu}$/cm^{-1})
3078, 3044, 2956 (s), 2911 (s), 2856 (s), 1620, 1443 (s), 1333 (s), 1251, 1028, 893 (s), 746 (s), 640, 573

MS (EI, m/z)
314 (45), 312 (46), 271 (99), 269 (100), 190 (14), 189 (41)

6.10 6-(Anthr-9'-yl)-hexyl-trimethylammonium bromide (26)

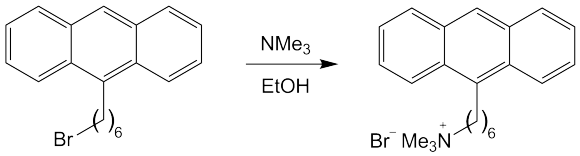

23 **26**

The substance has been synthesized following the general procedure given in section 6.1.1.1. The converted alkyl bromide was **23**. In this way 393 mg (982 µmol) of bright white solid was received.

$C_{23}H_{30}BrN$, MW: 400.40 g·mol^{-1}

TLC: R_f = 0.00 (DCM/MeOH 9:1)

^{1}H NMR ($CDCl_3$, 400 MHz, δ/ppm, J/Hz)
8.32 (s, 1H, H-10'), 8.22 (d, J = 8.8, 2H, H-1', H-8'), 7.99 (d, J = 8.3, 2H, H-4', H-5'), 7.51 (t, J = 6.8, 2H, H-2', H-7'), 7.44 (t, J = 7.8, 2H, H-3', H-6'), 3.60 (t, J = 7.8, 2H, H-1), 3.50 (t, J = 8.7, 2H, H-6), 3.37 (s, 9H, $N(CH_3)_3$), 1.85 – 1.74 (m, 2H, CH_2), 1.74 – 1.63 (m, 2H, CH_2), 1.63 – 1.52 (m, 2H, CH_2), 1.57 – 1.37 (m, 2H, CH_2)

^{13}C NMR ($CDCl_3$, 101 MHz, δ/ppm)
134.8 (q, C-9'), 131.7 (q, C-4a', C-10a'), 129.7 (q, C-8a', C-9a'), 129.4 (t, C-4, C-5), 125.8 (q, C-10'), 125.7 (t, C_{Ar}), 125.0 (t, C_{Ar}), 124.5 (t, C_{Ar}), 53.5 (p, $N(CH_3)_3$), 31.0 (s, CH_2), 29.5 (s, CH_2), 27.7 (s, CH_2), 26.2 (s, CH_2), 23.1 (s, CH_2), 18.6 (s, CH_2)

MS (FAB, m/z)
321 (28), 320 (100), 191 (12), 114 (10), 60 (18), 59 (34), 58 (49)

UV/vis (water, λ_{max}/nm, rel. height)
255 (100), 350 (4), 368 (6), 388 (6)

6.10.1 1-Bromo-6-(anthr-9'-yl)-hexane (23)

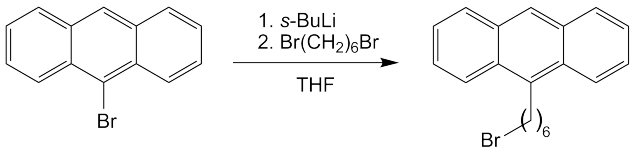

23

In a dry flask, 600 mg (2.24 mmol) 9-bromoanthracene was dissolved in 28 mL dry THF at room temperature.[107] After cooling to -75°C (EtOH, solid CO_2), 3.45 mL (1.3 M in hexane, 4.48 mmol, 2.0 eq.) *s*-BuLi was added slowly to the yellow suspension. 1.76 mL (11.2 mmol, 5.0 eq.) freshly distilled 1,6-dibromohexane was added and 20 minutes later the temperature was allowed to rise to 0°C, followed by stirring for 3 hours. After quenching the reaction with water, extraction with diethyl ether and washing with saturated sodium chloride solution, the organic layer was separated, dried over magnesium sulfate and the solvent removed under reduced pressure. Flash column chromatography (pure H) yielded in

313 mg (41%) pure **23**.
$C_{20}H_{21}Br$, MW: 341.28 g·mol^{-1}

TLC: R_f = 0.26 (H)

mp: 58 – 59 °C

^{1}H NMR ($CDCl_3$, 400 MHz, δ/ppm, J/Hz)
8.34 (s, 1H, H-10'), 8.27 (d, J = 8.8, 2H, H-1', H-8'), 8.02 (d, J = 8.4, 2H, H-4', H-5'), 7.54 – 7.43 (m, 4H, H-2', H-3', H-6'H-7'), 3.62 (t, J = 8.1, 2H, H-1), 3.43 (t, J = 6.8, 2H, H-6), 1.94 – 1.79 (m, 4H, H-2, H-5), 1.65 – 1.51 (m, 4H, H-3, H-4)

^{13}C NMR ($CDCl_3$, 101 MHz, δ/ppm)
135.2 (q, C-9'), 131.8 (q, C-4a', C-10a'), 129.6 (q, C-8a', C-9a'), 129.4 (t, C_{Ar}), 125.7 (q, C-10'), 125.5 (t, C_{Ar}), 124.9 (t, C_{Ar}), 124.5 (t, C_{Ar}), 34.1 (s, CH_2), 32.9 (s, CH_2), 31.3 (s, CH_2), 29.5 (s, CH_2), 28.3 (s, CH_2), 28.0 (s, CH_2)

IR (KBr, $\tilde{\nu}$/cm^{-1})
3049, 2918 (s), 2851 (s), 1620, 1445 (s), 1340 (s), 1261, 1210, 1154, 1010, 887, 842, 734 (s), 639

MS (EI, m/z)
342 (19), 340 (20), 192 (16), 191 (100)

EA
× 1 H_2O

calculated:	C: 70.39	H: 6.20	N: 0.00
found:	C: 70.38	H: 6.25	N: 0.00

6.11 4-(Phthalimid-*N'*-yl)-butyl-trimethylammonium bromide (39)

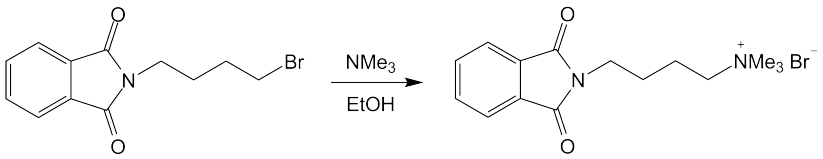

39

*4-(Phthalimid-N'-yl)-butyl-trimethylammonium bromide (**39**)*

The substance has been synthesized following the general procedure given in section 6.1.1.1. The converted alkyl bromide was the commercially available *N*-(4-bromobutyl)phthalimide. In this way 587 mg (1.72 mmol) of white needles has been isolated.

$C_{15}H_{21}BrN_2O_2$, MW: 341.24 g·mol^{-1}

TLC: R_f = 0.00 (DCM/MeOH 9:1)

mp: 173 – 174 °C

^{1}H NMR (DMSO-d$_6$, 400 MHz, δ/ppm, J/Hz)
7.90 – 7.83 (m, 4H, H_{Ar}), 3.62 (t, J = 7.1 2H, H-4), 3.32 (t, J = 8.3, 2H, H-1), 3.03 (s, 9H, $N(CH_3)_3$), 1.78 – 1.69 (m, 2H, CH_2), 1.61 (quint., J = 7.1, 2H, CH_2)

^{13}C NMR (DMSO-d$_6$, 101 MHz, δ/ppm):
168.0 (q, C-1', C-3'), 134.4 (t, C_{Ar}), 131.7 (q, C_{Ar}), 123.0 (t, C_{Ar}), 64.7 (s, C-1), 52.2 (p, $N(CH_3)_3$),36.8 (s, C-4), 24.9 (s, C-3), 19.6 (s, C-2)

IR (KBr, $\tilde{\nu}$/cm^{-1})
3013, 2945, 1768, 1710 (s), 1612, 1484, 1462, 1436, 1406 (s), 1049, 967, 917, 726 (s)

MS (FAB, m/z)
262 (18), 261 (100), 160 (9), 58 (17)

UV/vis (water, λ_{max}/nm, rel. height)
220 (100), 223 (100), 233 (36), 242 (26), 300 (5.2)

EA
$\times$ 1 H_2O

calculated:	C: 50.15	H: 6.45	N: 7.80
found:	C: 50.84	H: 6.24	N: 7.86

6.12 8-(Anthr-9'-yl)-octyl-trimethylammonium bromide (25)

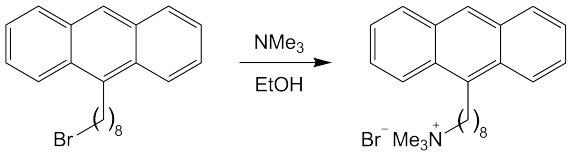

22 **25**

The substance has been synthesized following the general procedure given in section 6.1.1.1. The converted alkyl bromide was **22**. By using 9.7 mL of ethanol, 381 mg (889 µmol) of white powder has been isolated.

$C_{25}H_{34}BrN$, MW: 428.45 g·mol^{-1}

TLC: R_f = 0.00 (DCM/MeOH 9:1)

mp: 199 – 200 °C

^{1}H NMR ($CDCl_3$, 400 MHz, δ/ppm, J/Hz)
8.32 (s, 1H, H-10'), 8.25 (d, J = 8.8, 2H, H-1', H-8'), 8.00 (d, J = 8.3, 2H, H-4', H-5'), 7.53 – 7.42 (m, 4H, H-2', H-3', H-6', H-7'), 3.59 (t, J = 8.1, 2H, H-1), 3.55 – 3.49 (m, 2H, H-8), 3.42 (s, 9H, $N(CH_3)_3$), 1.83 – 1.74 (m, 2H, CH_2), 1.73 – 1.65 (m, 2H, CH_2), 1.58 – 1.51 (m, 2H, CH_2), 1.41 – 1.33 (m, 6H, CH_2)

^{13}C NMR ($CDCl_3$, 101 MHz, δ/ppm)
135.3 (q, C-9'), 131.7 (q, C-4a', C-10a'), 129.6 (q, C-8a', C-9a'), 129.3 (t, C-4', C-5'), 125.6 (q, C-10'), 125.5 (t, C_{Ar}), 124.9 (t, C_{Ar}), 124.6 (t, C_{Ar}), 67.1 (s, C-1), 53.5 (p, $N(CH_3)_3$), 31.4 (s, CH_2), 30.2 (s, CH_2), 29.4 (s, CH_2), 29.3 (s, CH_2), 28.1 (s, CH_2), 26.2 (s, CH_2), 23.3 (s, CH_2)

IR (KBr, $\tilde{\nu}$/cm^{-1})
3012, 2925 (s), 2853 (s), 1623, 1481 (s), 964, 908, 792, 735 (s), 672, 646

MS (FAB, m/z)
349 (30), 348 (100), 307 (13), 191 (12), 154 (82), 136 (59), 58 (52)

UV/vis (water, ε_λ/$M^{-1}cm^{-1}$)
$\varepsilon_{255} = 79121$, $\varepsilon_{350} = 3490$, $\varepsilon_{368} = 5250$, $\varepsilon_{388} = 4760$

6.12.1 1-(Anthr-9'-yl)-8-bromo-octane (22)

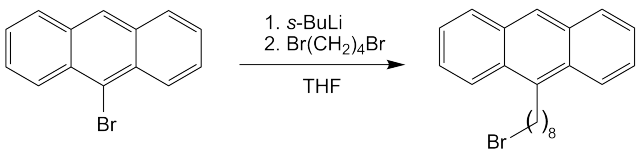

22

In a dry flask, 497 mg (1.93 mmol) 9-bromoanthracene was dissolved in 15 mL dry THF at room temperature.[107] After cooling to -65°C (acetone, solid CO_2), 1.63 mL (1.3 M in hexane, 2.12 mmol, 1.1 eq.) *s*-BuLi was added slowly to the yellow suspension. 322 µL (1.74 mmol, 0.9 eq.) 1,8-dibromooctane was added dropwise and 5 minutes later the temperature was allowed to rise to 0°C, followed by stirring for 10 hours. After quenching the reaction with water, extraction with diethyl ether and washing with saturated sodium chloride solution, the organic layer was separated, dried over magnesium sulfate and the solvent removed under reduced pressure. Flash column chromatography (P/DE 150:1) yielded in 342 mg (53%) pure **22**.
$C_{22}H_{25}Br$, MW: 369.34 g·mol^{-1}

TLC: R_f = 0.26 (P/DE 100:1)

mp: 57 – 59 °C

^{1}H NMR ($CDCl_3$, 400 MHz, δ/ppm, J/Hz)
8.34 (s, 1H, H-10'), 8.28 (d, J = 8.6, 2H, H-1', H-8'), 8.01 (d, J = 8.3, 2H, H-4', H-5'), 7.54 – 7.44 (m, 4H, H-2', H-3', H-6'H-7'), 3.61 (t, J = 8.1, 2H, H-8), 3.42 (t, J = 6.8, 2H, H-1), 1.91 – 1.78 (m, 4H, H-2, H-7), 1.64 – 1.53 (m, 2H, CH_2), 1.50 – 1.41 (m, 4H, CH_2), 1.40 – 1.31 (m, 2H, CH_2)

^{13}C NMR ($CDCl_3$, 101 MHz, δ/ppm)
135.5 (q, C-9'), 131.8 (q, C-4a', C-10a'), 129.6 (q, C-8a', C-9a'), 129.3 (t, C-4a', C-5a'), 125.6 (q, C-10'), 125.5 (t, C_{Ar}), 124.9 (t, C_{Ar}), 124.6 (t, C_{Ar}), 34.2 (s, CH_2), 32.9 (s, CH_2), 31.5 (s, CH_2), 30.3 (s, CH_2), 29.5 (s, CH_2), 28.9 (s, CH_2), 28.3 (s, CH_2), 28.2 (s, CH_2)

IR (KBr, $\tilde{\nu}/\mathrm{cm}^{-1}$)
3048, 2924 (s), 2851 (s), 1620, 1445, 1348, 1247, 1155, 1008, 887, 843, 733 (s)

MS (EI, m/z)
370 (26), 368 (25), 192 (14), 191 (100)

6.13 8-(1', 8'-Naphthalimid-*N'*-yl)-octyl-trimethylammonium bromide (17)

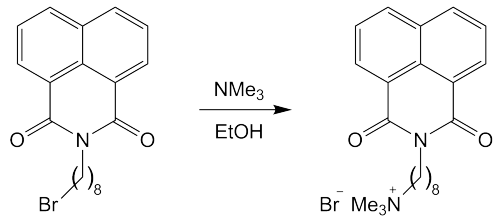

16 **17**

The substance has been synthesized following the general procedure given in section 6.1.1.1. The converted alkyl bromide was **16**. In this way 19.5 mg (43.6 µmol) of white powder has been isolated.

$C_{23}H_{31}BrN_2O_2$, MW: 447.41 g·mol^{-1}

TLC: R_f = 0.05 (DCM/MeOH 9:1)

^{1}H NMR (MeOH-d_4, 400 MHz, δ/ppm, J/Hz)
8.50 (d, J = 7.3, 2H, H-2', H-7'), 8.32 (d, J = 8.4, 2H, H-4', H-5'), 7.78 (t, J = 8.1, 2H, H-3', H-6'), 4.11 (t, J = 7.3, 2H, H-1) , 3.39 – 3.37 (m, 2H, H-8), 3.15 (s, 9H, $N(CH_3)_3$), 1.85 – 1.76 (m, 2H, CH_2), 1.75 – 1.67 (m, 2H, CH_2), 1.44 (s, 8H, H-3, H-4, H-5, H-6)

^{13}C NMR ($CDCl_3$, 101 MHz, δ/ppm)
165.4 (q, C-9', C-10'), 135.4 (t, C_{Ar}), 133.0 (q, C_{Ar}), 131.9 (t, C_{Ar}), 129.0 (q, C_{Ar}), 128.0 (t, C_{Ar}), 123.4 (q, C_{Ar}), 67.7 (s, C-1), 53.4 (p, $N(CH_3)_3$), 41.0 (s, C-8), 29.8 (s, CH_2), 29.8 (s, CH_2), 28.7 (s, CH_2), 27.7 (s, CH_2), 27.0 (s, CH_2), 23.7 (s, C-2)

6.13.1 1-Bromo-8-(1', 8'-Naphthalimid-*N'*-yl)-octane (16)

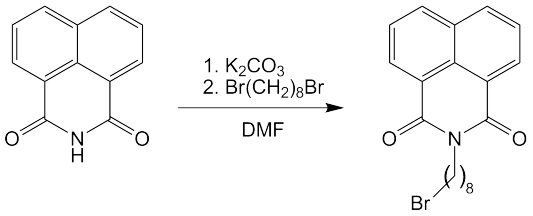

16

A suspension of 407 mg (2.06 mmol) 1,8-naphthalimide, 1.02 g (6.19 mmol, 3.0 eq) potassium carbonate and 1.15 mL (6.36 mmol, 1.03 eq.) 1,8-dibromooctane was stirred at 50°C for 1 hour in 6 mL anhydrous DMF.[109,110] After stirring at room temperature for 16 hours, water was added and the crude product was extracted with dichloromethane and dried over magnesium sulfate. Dissolving in dichloromethane, addition of 2.0 g silica gel and removal of the solvent was performed with sequential flash column chromatography (P/EA 4:1). The purification yielded in 696 mg (87%) pure **16**.

$C_{20}H_{22}BrNO_2$, MW: 388.30 g·mol^{-1}

TLC: R_f = 0.76 (P/EA 4:1)

^{1}H NMR ($CDCl_3$, 400 MHz, δ/ppm, J/Hz)
8.54 (dd, J = 7.3, J = 1.0, 2H, H-2', H-7'), 8.15 (dd, J = 8.4, J = 1.0, 2H, H-4', H-5'), 7.69 (t, J = 7.7, 2H, H-3', H-6'), 4.11 (t, J = 7.6, 2H, H-1), 3.33 (t, J = 7.1, 2H, H-8), 1.78 (quint., J = 7.4, 2H, H-2), 1.67 (quint., J = 7.6, 2H, H-7), 1.41 – 1.23 (m, 8H, H-3, H-4, H-5, H-6)

^{13}C NMR ($CDCl_3$, 101 MHz, δ/ppm)
164.5 (q, C-9', C-10'), 134.2 (t, C_{Ar}), 131.9 (q, C-4'), 131.5 (t, C_{Ar}), 128.5 (q, C_{Ar}), 127.2 (t, C-3', C-6'), 123.1 (q, C_{Ar}), 40.7 (s, C-8), 34.4 (s, C-2), 33.1 (s, C-1), 29.4 (s, CH_2), 29.0 (s, CH_2), 28.4 (s, CH_2), 28.4 (s, CH_2), 27.3 (s, CH_2)

6.14 8-(Carbazol-9'-yl)-octyl-trimethylammonium bromide (19)

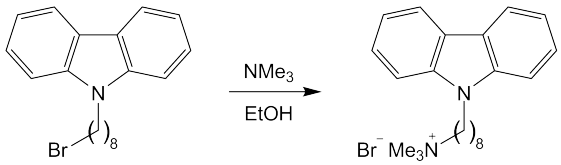

18 **19**

The substance has been synthesized following the general procedure given in section 6.1.1.1. The converted alkyl bromide was **18**. In this way 375 mg (898 µmol) of white powder has been isolated.

$C_{23}H33BrN_2$, MW: 417.43 g·mol^{-1}

TLC: R_f = 0.00 (DCM/MeOH 9:1)

^{1}H NMR (MeOH-d_4, 400 MHz, δ/ppm, J/Hz)
8.09 (d, J = 7.8, 2H, H-4', H-5'), 7.50 (d, J = 8.1, 2H, H-1', H-8'), 7.43 (t, J = 8.1, 2H, H-2', H-7'), 7.18 (t, J = 7.1, 2H, H-3', H-6'), 4.39 (t, J = 6.8, 2H, H-8), 3.24 – 3.19 (m, 2H, H-1), 3.06 (s, 9H, N(CH_3), 1.93 – 1.84 (m, 2H, H-7), 1.71 – 1.61 (m, 2H, H-2), 1.38 – 1.22 (m, 8H, H-3, H-4, H-5, H-6)

^{13}C NMR ($CDCl_3$, 101 MHz, δ/ppm)
141.8 (q, C-8a', C-9a'), 126.6 (t, C-2', C-7'), 124.1 (q, C-4a', C-4b'), 121.1 (t, C-4', C-5'), 119.8 (t, C-3', C-6'), 109.9 (t, C-1', C-8'), 53.5 (s, C-1), 53.4 (p, N(CH_3)$_3$), 43.6 (s, CH_2), 30.2 (s, CH_2), 29.9 (s, CH_2), 29.9 (s, CH_2), 28.0 (s, CH_2), 27.0 (s, CH_2), 23.8 (s, CH_2)

MS (MALDI–ToF, m/z)
337.8 (cation) Matrix: 2,5-Dihydroxy-benzoic acid

6.14.1 1-Bromo-8-(carbazol-9'-yl)-octane (18)

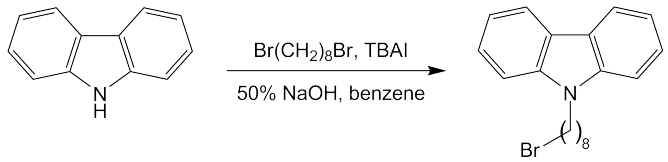

18

A mixture of 502 mg (3.00 mmol) carbazole, 834 µL (4.61 mmol, 1.5 eq.) 1,8-dibromooctane, 30.0 mg (81 µmol, 2.7 mol–%) tetrabutylammonium iodide (TBAI) in 1.5 mL 50% (wt/wt) and 1.5 mL benzene was stirred vigorously at room temperature for 16 hours.[111] The solvent of the organic layer was removed after addition of dichloromethane and three time washing with water. After addition of diehtyl ether and filtration, 822 mg (76%) of the desired product was isolated by flash column chromatography (P/DE 100:1) as an oil.

C_{20}H24BrN, MW: 358.32 g·mol^{-1}

TLC: R_f = 0.32 (H/DCM 5:1)

^{1}H NMR ($CDCl_3$, 400 MHz, δ/ppm, J/Hz)
8.10 (d, J = 7.8, 2H, H-4', H-5'), 7.45 (t, J = 7.1, 2H, H-2', H-7'), 7.40 (d, J = 8.1, 2H, H-1', H-8'), 7.22 (t, J = 7.6, 2H, H-3', H-6'), 4.28 (t, J = 7.1, 2H, H-8), 3.35 (t, J = 6.8, 2H, H-1), 1.89 – 1.75 (m, 4H, H-2, H-7), 1.40 – 1.19 (m, 8H, H-3, H-4, H-5, H-6)

^{13}C NMR ($CDCl_3$, 101 MHz, δ/ppm)
140.5 (q, C-8a', C-9a'), 125.7 (t, C-2', C-7'), 122.9 (q, C-4a', C-4b'), 120.5 (t, C-4', C-5'), 118.8 (t, C-3', C-6'), 108.7 (t, C-1', C-8'), 43.1 (s, C-8), 34.1 (s, C-2), 32.8 (s, C-1), 29.3 (s, CH_2), 29.0 (s, CH_2), 28.7 (s, CH_2), 28.1 (s, CH_2), 27.3 (s, CH_2)

IR (NaCl, $\tilde{\nu}$/cm^{-1})
3053, 2928, 2856, 1922, 1887, 1769, 1626, 1597, 1449, 1456, 1375, 1332, 1233, 1153, 1124, 1066, 1019, 748, 724

MS (EI, m/z)
359 (21), 357 (21), 181 (14), 180 (100), 152 (6)

6.15 8-(Pyren-1'-yl)-octyl-trimethylammonium bromide (34)

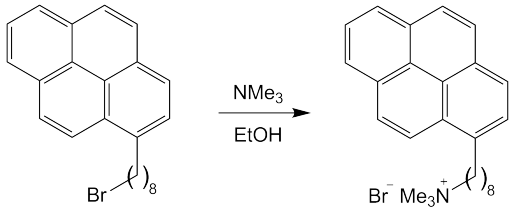

32 **34**

The substance has been synthesized following the general procedure given in section 6.1.1.1. The converted alkyl bromide was **32**. In this way 259 mg of white powder has been isolated.

$C_{27}H_{34}BrN$, MW: 452.47 g·mol^{-1}

TLC: R_f = 0.00 (DCM/MeOH 9:1)

^{1}H NMR (DMSO-d$_6$, 400 MHz, δ/ppm, J/Hz)
8.36 (d, J = 9.3, 1H, H$_{Ar}$), 8.30 – 8.25 (m, 2H, H$_{Ar}$), 8.24 – 8.20 (m, 2H, H$_{Ar}$), 8.16 – 8.10 (td, J = 11.1, J = 2.0, 2H, H$_{Ar}$), 8.06 (t, J = 7.6, 1H, H$_{Ar}$), 7.96 (d, J = 7.8, 1H, H$_{Ar}$), 3.36 – 3.31 (m, 2H, H-8), 3.25 – 3.19 (m, 2H, H-1), 3.00 (s, 9H, N(CH$_3$)$_3$), 1.80 (qunit., J = 7.3, 2H, H-7), 1.64 (qunit., J = 7.1, 2H, H-2), 1.47 – 1.20 (m, 8H, CH$_2$)

MS (ESI, m/z)
372.6 (100)

UV/vis (water, λ_{max}/nm, rel. height)
233 (61), 242 (100), 265 (36), 276 (67), 313 (17), 326 (39), 342 (55)

EA

calculated:	C: 71.67	H: 7.57	N: 3.10
found:	C: 70.19	H: 7.57	N: 3.09

6.15.1 1-Bromo-8-(pyren-1'-yl)-octane (32)

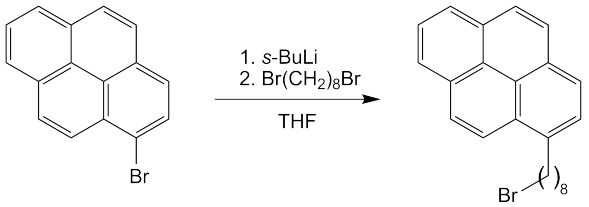

32

A solution of 498 mg (1.94 mmol) 1-bromopyrene in 10 mL anhydrous THF was cooled to -78°C. To the white suspension 3.13 mL (1.3 M in hexane, 4.07 mmol, 2.1 eq.) *s*-BuLi was slowly added to form a orange suspension. After 15 min, 431 µL (2.32 mmol, 1.2 eq.) 1,8-dibromooctane in 5 mL THF was added and the suspension turned curry-coloured. After stirring for 2 hours the reaction was allowed to warm to room temperature and stirring was continued for 2 hours. Quenching with water, addition of dichloromethane and three times washing with water resulted in the crude product. Flash column chromatography (pure P) yielded in 567 mg (74%) of pure **32**.
$C_{24}H_{25}Br$, MW: 393.36 g·mol^{-1}

TLC: R_f = 0.34 (P)

^{1}H NMR ($CDCl_3$, 400 MHz, δ/ppm, J/Hz)
8.17 (d, J = 9.4, 1H, H_{Ar}), 8.05 (dd, J = 7.6, J = 3.3, 2H, H_{Ar}), 7.99 (dd, J = 7.6, J = 2.8, 2H, H_{Ar}), 7.91 (dd, J = 9.0, J = 3.0, 2H, H_{Ar}), 7.87 (t, J = 7.8, 1H, H_{Ar}), 7.75 (d, J = 7.8, 1H, H_{Ar}), 3.27 (t, J = 7.1, 2H, H-8), 3.21 (t, J = 7.6, 2H, H-1), 1.77 – 1.67 (m, 4H, CH_2), 1.40 – 1.15 (m, 8H, CH_2)

^{13}C NMR ($CDCl_3$, 101 MHz, δ/ppm)
137.2 (q, C-1'), 131.4 (q, C_{Ar}), 130.9 (q, C_{Ar}), 129.7 (q, C_{Ar}), 128.5 (q, C_{Ar}), 127.5 (t, C_{Ar}), 127.2 (t, C_{Ar}), 127.1 (t, C_{Ar}), 126.4 (t, C_{Ar}), 125.7 (t, C_{Ar}), 125.0 (q, C_{Ar}), 125.0 (q, C_{Ar}), 124.7 (t, C_{Ar}), 124.7 (t, C_{Ar}), 124.6 (t, C_{Ar}), 123.4 (t, C_{Ar}), 34.0 (s, CH_2), 33.5 (s, CH_2), 32.7 (s, CH_2), 31.8 (s, CH_2), 29.6 (s, CH_2), 29.3 (s, CH_2), 28.7 (s, CH_2), 28.1 (s, CH_2)

6.16 12-(Pyren-1'-yl)-dodecyl-trimethylammonium bromide (33)

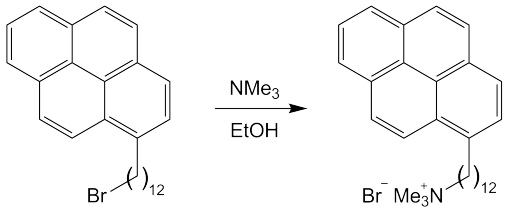

31 **33**

The substance has been synthesized following the general procedure given in section 6.1.1.1. The converted alkyl bromide was **31**. In this way 34.2 mg of white powder has been isolated.

$C_{31}H_{42}BrN$, MW: 508.58 g·mol^{-1}

TLC: R_f = 0.00 (DCM/MeOH 9:1)

mp: 209 – 218 °C

^{1}H NMR ($CDCl_3$, 400 MHz, δ/ppm, J/Hz)
8.27 (d, J = 9.4, 1H, H_{Ar}), 8.15 (dd, J = 9.3, J = 3.0, 2H, H_{Ar}), 8.08 (dd, J = 8.8, J = 3.3 2H, H_{Ar}), 8.04 – 7.95 (m, 3H, H_{Ar}), 7.87 (d, J = 7.8, 2H, H_{Ar}), 3.51 – 3.45 (m, 2H, H-1), 3.38 (s, 9H, $N(CH_3)_3$), 3.32 (t, J = 7.6, 2H, H-12), 1.84 (quint., J = 7.8, 2H, H-2), 1.68 – 1.60 (m, 2H, H-11), 1.47 (q, J = 7.6, 2H, CH_2), 1.37 – 1.21 (m, 8H, CH_2)

^{13}C NMR (MeOH-d_4, 101 MHz, δ/ppm):
139.3 (q, C-1'), 133.7 (q, C_{Ar}), 133.2 (q, C_{Ar}), 129.4 (t, C_{Ar}), 129.3 (t, C_{Ar}), 129.3 (t, C_{Ar}), 129.0 (q, C_{Ar}), 128.4 (t, C_{Ar}), 127.9 (q, C_{Ar}), 127.8 (q, C_{Ar}), 126.9 (t, C_{Ar}), 126.7 (t, C_{Ar}), 126.6 (t, C_{Ar}), 125.4 (t, C_{Ar}), 68.7 (s, C-1), 54.4 (p, $N(CH_3)_3$), 35.2 (s, CH_2), 33.9 (s, CH_2), 31.5 (s, CH_2), 31.4 (s, CH_2), 31.4 (s, CH_2), 31.3 (s, CH_2), 31.1 (s, CH_2), 31.0 (s, CH_2), 28.2 (s, CH_2), 24.8 (s, CH_2), 24.7 (s, CH_2)

MS (ESI, m/z)
249.3(89), 248.5 (100), 367.4 (37), 365.3 (38), 321.4 (28), 271.6 (10)

6.16.1 1-Bromo-12-(pyren-1'-yl)-dodecane (31)

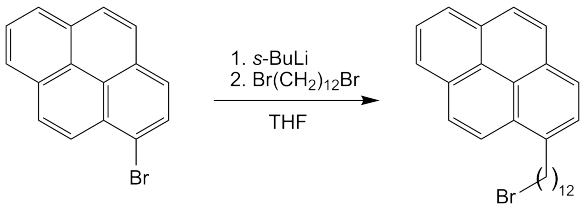

31

A solution of 128 mg (454 µmol) 1-bromopyrene in 5 mL anhydrous THF was cooled to -78°C. To the white suspension 420 µL (1.3 M in hexane, 549 µmol, 1.2 eq.) *s*-BuLi was slowly added to form a orange suspension. After 15 min, 164 µL (499 µmol, 1.1 eq.) 1,12-dibromodecane in 2 mL THF was added and the suspension turned curry-coloured. After stirring for 2 hours the reaction was allowed to warm to room temperature and stirring was continued for 2 hours. Quenching with water, addition of diethyl ether and three times washing with water resulted in the crude product. Flash column chromatography (pure P) yielded in 94.6 mg (46%) of pure **31**.

$C_{28}H_{33}Br$, MW: 449.47 g·mol^{-1}

TLC: R_f = 0.35 (P)

^{1}H NMR ($CDCl_3$, 400 MHz, δ/ppm, J/Hz)
8.29 (d, J = 9.3, 1H, H_{Ar}), 8.16 (dd, J = 9.2, J = 3.0, 2H, H_{Ar}), 8.11 (dd, J = 9.4, J = 3.0, 2H, H_{Ar}), 8.05 – 7.96 (m, 3H, H_{Ar}), 7.88 (d, J = 7.8, 1H, H_{Ar}), 3.40 (t, J = 6.8, 2H, H-1), 3.34 (t, J = 7.6, 2H, H-12), 1.89 – 1.80 (m, 4H, CH_2), 1.51 – 1.45 (m, 2H, CH_2), 1.44 – 1.35 (m, 4H, CH_2), 1.31 – 1.24 (m, 10H, CH_2)

^{13}C NMR ($CDCl_3$, 101 MHz, δ/ppm)
140.6 (q, C-1'), 137.7 (q, C_{Ar}), 131.9 (q, C_{Ar}), 131.3 (q, C_{Ar}), 130.1 (q, C_{Ar}), 129.0 (q, C_{Ar}), 127.9 (t, C_{Ar}), 127.7 (t, C_{Ar}), 127.5 (t, C_{Ar}), 126.9 (t, C_{Ar}), 126.1 (t, C_{Ar}), 125.5 (q, C-10a'), 125.2 (t, C_{Ar}), 125.0 (t, C_{Ar}), 123.9 (t, C_{Ar}), 34.5 (s, C-2), 34.0 (s, C-12), 33.2 (s, C1), 32.4 (s, C-11), 30.2 (s, CH_2), 30.0 (s, CH_2), 29.9 (s, CH_2), 29.8 (s, CH_2), 29.1 (s, CH_2), 28.6 (s, CH_2)

6.17 Surfactant-DNA Complexes

6.17.1 Procedure for the Formation of DMDTAB SDC

82 µL (164 nmol, 2.0 eq.) of aqueous DMDTAB solution in a safe-twist 1.5 mL tube was placed in a thermoshaker at 35°C with 700 rpm. The DNA solution was added slowly over a period of 2 min to the DMDTAB solution. The tube was stirred in a vortex mixer and placed back in the thermoshaker, which was tuned to 1200 rpm. After 24 h the tube was placed in a centrifuge with 16100 g for 10 min and the supernatant was removed. After addition of 300 µL of nanopure water and another 10 min in the thermoshaker, the tube was centrifuged again for 15 min. The supernatant was removed and the tube was lyophilized/dry-frozen for 2 h or over night. In this form the SDC is stable at ambient temperature and can be stored over months at -18°C.

Acknowledgements

I want to thank my thesis supervisor Prof. Dr. Bernd Giese for providing me a very interesting project and giving me the opportunity to work in his laboratory under his guidance and support. Thanks also to Prof. Dr. Helma Wennemers for accepting to co-referee my PhD thesis and for excellent support during my work as practical course assistant.
I am grateful to Prof. Antonietti and Sascha General, Prof. Bickle and Fabienne Hamburger, Dr. Martin Hegner and Sudhir Husale, Thomas Kaufmann and Prof. Wendorff and Markus Rudisile for fruitful collaborations.
I want to thank my lab mates Meike Cordes and Michael Graber for always having a good time. Special thanks to Meike Cordes for proof-reading the manuscript. Special thanks to Gary Larson for daily emotional support. Thanks also to the Giese and Wennemers group for support and fun.
Finally, I want to thank the Swiss National Science Fond (SNF), the National Center of Competence in Research (NCCR) and the University of Basel for financial support.

List of Schemes

List of Figures

Bibliography

1. Bernd Giese and Martin Spichty. Long distance charge transport through DNA: Quantification and extension of the hopping model. *Chem. Phys. Chem.*, 1:195–198, 2000.

2. Ralf Dahm. Friedrich Miescher and the discovery of DNA. *Developmental Biology*, 278:274 – 288, 2005.

3. Lubert Stryer. *Biochemie*. Spektrum Verlag, 4th edition, 1996. ISBN 3-86025-346-8.

4. J. D. Watson and F. H. Crick. A structure for deoxyribose nucleic acid. *Nature*, 171:737 – 738, 1953.

5. Simon M. Langenegger. *Non–nucleosidic Polyaromatic Buiding Blocks as DNA Base Surrogates*. PhD thesis, University of Bern, Mai 2005.

6. J. Sambrook, E.F. Fritsch, and T. Maniatis. *Molecular Cloning - A Laboratory Handbook*. Cold Spring Harboratory Press, 2nd edition, 1989.

7. F. Samain, V.L. Malinovskii, S. M. Langenegger, and R. Häner. Spectroscopic properties of pyrene-containing DNA mimics. *Bioorg. Med. Chem.*, 16(1):27 – 33, 2008.

8. Francoise M. Winnik. Photophysics of preassociated pyrenes in aqueous polymer solutions and in other organized media. *Chem. REv.*, 93:587 – 614, 1993.

9. S. L. Beaucage and M. H. Caruthers. Deoxynucleoside phosphoramidites – a new class of key intermediates for deoxypolynucleotdie synthesis. *Tetrahedron Letters*, 22:1859 – 1862, 1981.

10. Eric T. Kool. Replacing the nucleobases in dna with designer molecules. *Accounts of Chemical Research*, 35(11):936 – 943, 2002.

11. Claus A. M. Seidel, Andreas Schulz, and Markus H. M. Sauer. Nucleobase-specific quenching of fluorescent dyes. 1. nucleobase one-electron redox potentials and their correlation with static and dynamic quenching efficiencies. *J. Phys. Chem.*, 100(13):5541 – 5553, 1996.

12. Kazuhiko Nakatani, Chikara Dohno, and Isao Saito. Modulation of dna-mediated hole-transport efficiency by changing superexchange electronic interaction. *J. Am. Chem. Soc.*, 122(24):5893 – 5894, 2000.

13. Bernd Giese. Long-distance charge transport in DNA: The hopping mechanism. *Acc. Chem. Res.*, 33(9):631 – 636, 2000.

14. R. A. Marcus and Norman Sutin. Electron transfer in chemistry and biology. *Biochim. Biophys. Acta*, 811:265 – 322, 1985.

15. Bernd Giese, Eric Meggers, Stefan Wessely, Martin Spormann, and Andreas Biland. DNA as a supramolecule for long-distance charge transport. *Chimia*, 54(10):547 – 551, 2000.

16. Erich Meggers, Adrian Dussy, Thomas Schäfer, and Bernd Giese. Electron transfer in DNA from guanine and 8-oxoguanine to a radical cation of the carbohydrate backbone. *Chem. Eur. J.*, 6(3): 485 – 492, 2000.

17. Eric Meggers, Maria E. Michel-Beyerle, and Bernd Giese. Sequence dependent long range hole transport in dna. *Journal of the American Chemical Society*, 120(49):12950–12955, 1998.

18. Bernd Giese, Barbara Carl, Thomas Carl, Thomas Carell, Christoph Behrens, Ulrich Hennecke, Olav Schiemann, and Emiliano Feresin. Excess electron transport through DNA: a single electron repairs more than one UV-induced lesion. *Angew. Chem. Int. Ed.*, 43(14):1848 – 1851, 2004.

19. Miral Dizdaroglu, Clemens Von Sonntag, and Dietrich Schulte-Frohlinde. Strand breaks and sugar release by γ-irradiation of dna in aqueous solution. *J. Am. Chem. Soc.*, 97(8):2277 – 2278, 1975.

20. Adrian P. Dussy. *Synthese und Anwendung photolabiler DNA-Bausteine*. PhD thesis, University of Basel, 1998.

21. Senn Martin. *Kinetische Untersuchungen zum redikalinduzierten DNA-Strangbruch*. PhD thesis, University of Basel, 1997.

22. Cornelia Bohne, Katja Faulhaber, Bernd Giese, Angelika Häfner, Andrea Hofmann, Heiko Ihmels, Anne-Kathrin Köhler, Saana Perä, Friedemann Schneider, and Molina A. L. Sheepwash. Studies on the mechanism of the photo-induced DNA damage in the presence of acridizinium salts-involvement of singlet oxygen and an unusual source for hydroxyl radicals. *J. Am. Chem. Soc.*, 127 (1):76 – 85, 2005.

23. Eric Meggers. *Zum Elektronentransfer in DNA*. PhD thesis, University of Basel, St. Johanns-Ring 19, 4056 Basel, Switzerland, 5 1999.

24. Andeas Simon Biland-Thommen. *Elektronentransfer in der DNS: Der Einfluss des Donors und der Brücke*. PhD thesis, University of Basel, St. Johanns-Ring 19, 4056 Basel, Switzerland, 2002.

25. Shana O. Kelley and Jacqueline K. Barton. Dna–mediated electron transfer from a modified base to ethidium: π–stacking as a modulator of reactivity. *Chem. Biol.*, 5(8), 1998.

26. Chaozhi Wan, Torsten Fiebig, Shana O. Kelley, Christopher R. Treadway, Jacqueline K. Barton, and Ahmed H. Zewail. Femtosecond dynamics of DNA–mediated electron transfer. *Proc. Natl. Acad. Sci. USA*, 96:6014 – 6019, 1999.

27. Nicole Amann, Robert Huber, and Hans-Achim Wagenknecht. Phenanthridinium as an artificial base and charge donor in DNA. *Angewandte Chemie, International Edition*, 43(14):1845–18474, 2004.

28. Milton J. Rosen. *Surfactants and Interfacial Phenomena*. John Wiley & Sons, New York, 2nd edition, 1989.

29. Tetsuyuki Akao and Akio Ito. Stacking and mobility of cationic amphiphiles in the complex with DNA and DNA transfection activity of the complex. *J. Chem. Soc., Perkin Trans. 2*, (2):213–218, 1997.

30. Débora B. Vieira and Ana M. Carmona-Ribeiro. Cationic lipids and surfactants as antifungal agents: mode of action. *Journal of Antimicrobial Chemotherapy*, 58:760 – 767, 2006.

31. Priya V. Jaiswal, Vijaykumar S. Ijeri, and Ashwini K. Srivastava. Voltammetric behavior of certain vitamins and their determination in surfactant media. *Analytical Sciences*, 17 Supplement:i741–i744, 2001.

32. V. G. Sergeyev, O. A. Pyshkina, M. O. Gallyamov, I. V. Yaminsky, A. B. Zezin, and V. A. Kabanov. DNA-surfactant complexes in organic media. *Progress in Colloid & Polymer Science*, 106:198–203, 1997.

33. P. Smith, R.M. Lynden-Bell, and W. Smith. Surfactant structure around DNA in aqueous solution. *Phys. Chem. Chem. Phys.*, 2:1305–1310, 2000.

34. Lili Wang, Jonichi Yoshida, and Naoya Ogata. Self-assembled supramolecular films derived from marine deoxiribonucleic acid (DNA) - cationic surfactant complexes: Large-scale preparation and optical and thermal properties. *Chem. Mater.*, 13(4):1273–1281, 2001.

35. Zhenhua Sun. Importance of minor groove functional groups for the stability of DNA duplexes. *Biopolymers*, 65(3):211–217, 2002.

36. Michael Feig and B Montgomery Pettitt. Crystallographic water sites from a theoretical perspective. *Structure*, 6(11), 1998.

37. A. R. Bellamy and R. K. Ralph. *Recovery and Purification of Nucleic Acid by Means of Cetyltrimethylammonium Bromide*, volume 12, B of *Methods in Enzymology*, chapter Isolation of Total Nucleic Acids, pages 156–160. Grossman, L. and Moldave, K. and Sidney, P. and Colowick Kaplan, 1968.

38. Santanu Bhattacharya and Subhrangsu S. Mandal. Evidence of interlipidic ion-pairing in anion-induced DNA release from cationic amphiphile–DNA complexes. mechanistic implications in transfection. *Biochemistry*, 37(21):7764–7777, 1998.

39. Santanu Bhattacharya and Subhrangsu S. Mandal. Interaction of surfactants with DNA. role of hydrophobicity and surface charge on intercalation and DNA melting. *Biochimica et Biophysica Acta*, 1323(1):29–44, 1997.

40. Dino Guerritore and Luciano Bellelli. Interaction between nucleic acid and a cationic detergent. *Nature*, 184:1638, 1959.

41. R. Sharma, H. R. Mahla, T. Mohapatra, S. C. Bhargava, and M. M. Sharma. Isolating plant genomic dna without liquid nitrogen. *Plant Molecular Biology Reporter*, 21(1):43 – 50, 2003.

42. A. Reineke, P. Karlovsky, and C. P. W. Zebitz. Preparation and purification of DNA from insects for AFLP analysis. *Insect molecular biology*, 7(1):95–99, 1998.

43. Sascha General. *Polyelektrolyt-Tensid-Komplexe – nanostrukturierte biomimetische Arzneistoffträger*. PhD thesis, Humboldt-Universität zu Berlin, 10 2001.

44. Sascha General and Markus Antonietti. Supramolekulare organisation von oligopeptiden mit tensiden. *Angew. Chem.*, 114(16):3081 – 3084, 2002.

45. Wolfgang Hillen, Thomas C. Goodman, and Robert D. Wells. Circular dichroism spectra of twelve short DNA restriction fragments of known sequence: a comparison of measured and calculated spectra. *Nucleic Acid Research*, 9(13):3029 – 3045, 1981.

46. Walter A. Baase and W.Curtis Johnson Jr. Circular dichroism and DNA secondary structure. *Nuc. Acid Res.*, 6(2):797 – 814, 1979.

47. Olivier Boss. *Untersuchungen zur pyrenmodifizierten DNA*. PhD thesis, University of Basel, 2004.

48. Kevin M. Guckian, Barbara A. Schweitzer, Rex X.-F. Ren, Charles J. Sheils, Deborah C. Tahmassebi, and Eric T. Kool. Factors contributing to aromatic stacking in water: Evaluation in the context of dna. *J. Am. Chem. Soc.*, 122(10):2213 – 2222, 2000.

49. Eric T. Kool, Juan C. Morales, and Kevin M. Guckian. Mimicking the structure and function of dna: Insights into dna stability and replication. *Angew. Chem. Int. Ed.*, 39:990 – 1009, 2000.

50. Jean Lhomme, Jean-Francois Constant, and Martine Demeunynck. Abasic dna structure, reactivity, and recognition. *Biopolymers*, 52:65 – 83, 1999.

51. Rex X.-F. Ren, Narayan C. Chaudhuri, Pamela L. Paris, Squire Rumney IV, and Eric T. Kool. Naphthalene, phenanthrene, and pyrene as dna base analogues: Synthesis, structure, and fluorescence in dna. *J. Am. Chem. Soc.*, 118(33):7671 – 7678, 1996.

52. Matray Tracy J. and Eric T. Kool. Selective and stable dna base pairing without hydrogen bonds. *J. Am. Chem. Soc.*, 120(24):6191 – 6192, 1998.

53. Tracy J. Matray and Eric T. Kool. A specific partner for abasic damage in dna. *Nature*, 399(6737): 704 – 708, 1999.

54. Serge Smirnov, Tracy J. Matray, Eric T. Kool, and Carlos de los Santos. Integrity of duplex structures without hydrogen bonding: DNA with pyrene paired at abasic sites. *Nuc. Ac. Res.*, 30(24): 5561 – 5569, 2002.

55. Eric T. Kool. Hydrogen bonding, base stacking, and steric effects in DNA replication. *Annu. Rev. Biophys. Biomol. Struct.*, 30:1 – 22, 2001.

56. Liping Sun, Mu Wang, Eric T. Kool, and John-Stephen Taylor. Pyrene nucleotide as a mechanistic probe: Evidence for a transient abasic site–like intermediate in the bypass of dipyrimidine photoproducts by t7 dna polymerase. *Biochemistry*, 39(47):14603 – 14610, 2000.

57. Nicole Amann, Evgeni Pandurski, Torsten Fiebig, and Hans-Achim Wagenknecht. Electron injection into dna: Synthesis and spectroscopic properties of pyrenyl-modified oligonucleotides. *Chem. Eur. J.*, 8(21):4877 – 4888, 2002.

58. Vladimir Ya. Shafirovich, Scott H. Courtney, Naiqi Ya, and Nicholas E. Geacintov. Proton-coupled photoinduced electron transfer, deuterium isotope effects, and fluorescence quenching in noncovalent benzo[a]pyrenetetraol-nucleoside complexes in aqueous solutions. *J. Am. Chem. Soc.*, 117 (17):4920 – 4929, 1995.

59. Nicole Amann, Evgeni Pandurski, Torsten Fiebig, and Hans-Achim Wagenknecht. Ein modellnucleosid für die elektroneninjektion in die DNA: 5-pyrenyl-2'-desoxyribose. *Angew. Chem.*, 114 (16):3084 – 3087, 2002.

60. Nicole Amann, Evgeni Pandurski, Torsten Fiebig, and Hans-Achim Wagenknecht. *Angew. Chem. Int. Ed.*, 41(16):2978 – 2980, 2002.

61. Peter Kaden, Elke Mayer-Enthart, Anton Trifonov, Torsten Fiebig, and Hans-Achim Wagenknecht. Real–time spectroscopic and chemical probing of reductive electron transfer in DNA. *Angew. Chem. Int. Ed.*, 44:1636 – 1639, 2005.

62. Thomas L. Netzel, Min Zhao, Kambiz Nafisi, Jeb Headrick, Matthew S. Sigman, and Eaton Bruce E. Photophysics of 2'-deoxyuridine (du) nucleosides covalently substituted with either 1 -pyrenyl or 1 -pyrenoyl: Observation of pyrene–to–nucleoside charge–transfer emission in 5–(1–pyrenyl)–du. *J. Am. Chem. Soc.*, 117(36):9119 – 9128, 1995.

63. T. Kubota, K. Kano, B. Uno, and T. Konse. Energetics of the sequential electroreduction and electrooxidation steps of benzenoid hydrocarbons. *Bulletin of the Chemical Society of Japan*, 60 (11):3865–3877, 1987. Times Cited: 38 Article English Cited References Count: 70 L0565.

64. S. Steenken, J. P. Telo, H. M. Novais, and L. P. Candeias. One-electron-reduction potentials of pyrimidine bases, nucleosides, and nucleotides in aqueous solution. consequences for DNA redox chemistry. *J. Am. Chem. Soc.*, 114(12):4701 – 4709, 1992.

65. Tadao Takada, Kiyohiko Kawai, Sachiko Tojo, and Tetsuro Majima. Kinetics of multistep hole transfer in dna by monitoring the transient absorption of the pyrene radical cation. *Journal of Physical Chemistry B*, 107(50):14052 – 14057, 2003.

66. Kiyohiko Kawai, Tadao Takada, Sachiko Tojo, Nobuyuki Ichinose, and Tetsuro Majima. Observation of hole transfer through dna by monitoring the transient absorption of pyrene radical cation. *J. Am. Chem. Soc.*, 123(50):12688 – 12689, 2001.

67. Takahiro Kawai, Masashi Ikegami, and Tatsuo Arai. Exciplex formation between pyrene and guanine in highly polar solvents. *Chem. Commun.*, pages 824 – 825, 2004.

68. Simon M. Langenegger and Robert Häner. Selectivity in DNA interstrand-stacking. *Bioorg. Med. Chem. Lett.*, 16:5062 – 5065, 2006.

69. Sven Hainke, Sebastian Arndt, and Oliver Seitz. Concise synthesis of aryl-*C*-nucleosides by friedel–crafts alkylation. *Org. Biomol. Chem.*, 3:4233 – 4238, 2005.

70. Max Hoffer. α–thymidin. *Chem. Ber.*, 93:2777 – 2781, 1960.

71. Péter Várnai and Richard Lavery. Base flipping in DNA: Pathways and energentics studied with molecular dynamic simulations. *Journal of the Americal Chemical Society*, 124:7272–7273, 2002.

72. U. B. Christensen and E. B. Pedersen. Intercalating nucleic acids containing insertions of 1-o-(1-Pyrenylmethyl)Glycerol: Stabilisation of dsDNA and discrimination of DNA over RNA. *Nucleic Acids Research*, 30(22):4918–4925, 2002. 1362-4962 Journal Article.

73. Kazuhiro Sasa Yukinori Ohtoshi Kenji Kanaori1 Haruhisa Hayashi Hidehiko Nakano Mitsunobu Nakamura, Yudai Fukunaga and Kazushige Yamana. Pyrene is highly emissive when attached to the rna duplex but not to the dna duplex: the structural basis of this difference. *Nucleic Acids Research*, 33(18):5887 – 5895, 2005.

74. S. Kanvah and G. B. Schuster. One-electron oxidation of DNA: The effect of replacement of cytosine with 5-methylcytosine on long-distance radical cation transport and reaction. *J. Am. Chem. Soc.*, 126(23):7341–7344, 2004. 0002-7863 Journal Article.

75. Michael Hutter and Timothy Clark. On the enhanced stability of the guanine-cytosine base-pair radical cation. *J. Am. Chem. Soc.*, 118(32):7574 – 7577, 1996.

76. Simon M. Langenegger and Robert Häner. A DNA mimic made of non–nucleosidic phenanthrene building blocks. *Chem. Bio. Chem.*, 6:2149 – 2152, 2005.

77. Simon M. Langenegger and Robert Häner. Excimer formation by interstrand stacked pyrenes. *Chem. Comm.*, 24:2792 – 2793, 2004.

78. Häner Robert Langenegger, Simon M. DNA containing phenanthroline– and phenanthracene–derived, non–nucleosidic base surrogates. *Tet. Let.*, 45:9273 – 9276, 2004.

79. Florent Samain, Vladimir L. Malinovskii, Simon M. Langenegger, and Robert Häner. Spectroscopic properties of pyrene–containing dna mimics. *Bioorg. Med. Chem.*, page in press, 2007.

80. Hiromu Kashida, Hiroyuki Asanuma, and Makoto Komiyama. Insertion of two pyrene moieties into oligodeoxyribonucleotides for the efficient detection of deletion polymorphisms. *Chem. Comm.*, pages 2768 – 2770, 2006.

81. Simon M. Langenegger, Gapian Bianké, Rolf Tona, and Robert Häner. DNA mimics containing non-nucleosidic base surrogates. 59(11):794 – 797, 2005.

82. S. M. Langenegger and R. Häner. Remarkable stabilization of duplex DNA containing an abasic site by non-nucleosidic phenanthroline and pyrene building blocks. *Chem. Bio. Chem.*, 6(5):848 – 851, 2005.

83. Robert Häner. Patent PCT wo 2006/032487 a3, 30.03.2006.

84. Kentaro Tanaka and Mitsuhiko Shionoya. Bio-inspired programmable self-assembly on dna templates. *Chem. Lett.*, 35(7):694 – 699, 2006.

85. Chengde Mao, Weiqiong Sun, Zhiyong Shen, and Nadrian C. Seeman. A nanomechanical device based on the b – z transition of DNA. *Nature*, 397(67):144 – 146, 1999.

86. Markus Ahlskog, Christophe Laurent, Mark Baxendale, and Maria Huhtala. Electronic properties and applications of carbon nanotubes. *Encyclopedia of Nanoscience and Nanotechnology*, 3(23): 139 – 161, 2004.

87. C. Joachim, J. K. Gimzewski, and A. Aviram. Electronics using hybrid-molecular and monomolecular devices. *Nature*, 405:541 – 548, 2000.

88. Tom Bickle. 400 – 500 bp ds DNA production, 2005. 500 bp DNA by sonication. see exp. 315.01.01 for details or facts.tex.

89. Sudhir Husale, Wilfried Grange, Marc Karle, Stephan Bürgi, and Martin Hegner. Interaction of cationic surfactants with dna: a single-molecule study. *Nucleic Acids Research*, pages 1 – 7, January 2008.

90. Sudhir C. Husale. *Single biomolecule studies using optical tweezers*. PhD thesis, University of Basel, June 2005.

91. Antonin Formhals. Us patent, 1-975-504, 1934.

92. Audrey Frenot and Ioannis S. Chronakis. Polymer nanofibers assembled by electrospinning. *Current Opinion in Colloid and Interface Science*, 8:64 – 75, 2003.

93. R. Dersch, Taiqi Liu, A. K. Schaper, A. Greiner, and Joachim. H. Wendorff. Electro-spun nanofibers: Internal structure and intrinsic orientation. *Journal of Polymer Science, Part A: Polymer Chemistry*, 41(4):545 – 553, 2003.

94. Jayesh Doshi and Darrell H. Reneker. Electrospinning process and applications of electrospun fibers. *Journal of Electrostatics*, 35:151 – 160, 1995.

95. X. Fang and D. H. Reneker. Dna fibers by electrospinning. *Journal of Macromolecular Science, Physics*, B36(2):169 – 173, 1997.

96. Hugo E. Gottlieb, Vadim Kotlyar, and Abraham Nudelman. NMR chemical shifts of common laboratory solvents as trace impurities. *J. Org. Chem.*, 62(21):7512 – 7515, 1997.

97. R. Goscinny and A. Uderzo. *Der Sohn des Asterix*, volume 27. Ehapa, dt. 1st ed. edition, 1983.

98. Charles R. Cantor, Myron M. Warshaw, and Shapiro Herman. Oligonucleotide interactions. III. circular dichroism studies of the conformation of deoxyoligonucleotides. *Biopolymers*, 9:1059 – 1077, 1970.

99. N. D. Sinha, J. Biernat, J. McManus, and H. Koester. Polymer support oligonucleotide synthesis. XVIII: use of β-cyanoethyl-*N,N*-dialkylamino-*N*-morpholino phosphoramidite of deoxynucleosides for the synthesis of dna fragments simplifying deprotection and isolation of the final product. *Nucleic Acids Research*, 12(11):4539 – 4557, 1984.

100. Charles D. Hurd and Lewis R. Drake. Validity of the structure assigned to cyclo.ovrddot.octatetraene: Pyrolysis of bisquaternary ammonium hydroxides related to 1,2- and 2,3-butenes. *JACS*, 61:1943–1945, 1939.

101. Michèle Calas, Marie L. Ancelin, Cordina Gérard, Philippe Portefaix, Gilles Piquet, Valérie Vidal-Saihan, and Henri Vial. Antimalarial activity of compounds interfering with plasmodium falciparum phospholipid metabolism: Comparison mono- and bisquaternary ammonuim salts. *J. Med. Chem.*, 43:505 – 516, 2000.

102. *Houben-Weyl: Methoden der Organischen Chemie*, volume V of *Houben-Weyl*. Georg Thieme Verlag, 4th edition, 1981.

103. H Kessler and Müller E. Separation of multinucleic aromatic compounds by thin layer chromatography using picric acids as complex forming agent. *J. Chromatog.*, 24(2):469–473, 1966.

104. Timothy J. Wozniak and Ronald A. Bites. Separation of hydroaromatic compounds in synfuels by picric acid columns. *Anal. Chem.*, 55(11):1791–1796, 1983.

105. Thomas H. Keller and Robert Häner. Synthesis and hybridization properties of oligonucleotides containing 2'-o-modified ribonucleotides. *Nucleic Acids Research*, 21(19):4499 – 4505, 1993.

106. C. Cornelissen, W. Rettig, Desvergne J.-P., and H. Bouas-Laurent. Multiple emitting species and competing intramolecular fluorescence quenching in 9,9'-dianthrylmethanol and model compounds. *Chemical Physics Letters*, 239:290–298, 1995.

107. Chishio Hosokawa, Masakazu Funehashi, Hisayuki Kawamura, Hiromasa Arai, Hidetoshi Koga, and Hidetsugu Ikeda. Organic electroluminescent devices, 20000706 2000.

108. Shigehiro Yamaguchi, Toshiaki Shirasaka, and Kohei Tamao. Synthesis, structures, and uv-visible absorption spectra of tri(9-anthryl)bismuthine derivatives. *Organometallics*, 21(12):2555–2558, 2002.

109. Lisbet Xuarez Marill, Rolando F. Pellon Comdom, and Miriam Mesa Hernandez. Influence of the reaction conditions in the *N*-alkylation of acridone-2-carboxylic acids. *Synthetic Communications*, 31(14):2159–2167, 2001.

110. John C. Sheehan and Wm A. Bolhofer. An improved procedure for the condensation of potassium phthalimide with organic halides. *Journal of the American Chemical Society*, 72:2786 – 2788, 1950. Copyright 2004 ACS on SciFinder (R)) CAPLUS CAN 45:19053 10 Organic Chemistry JACSAT 0002-7863 language unavailable. Condensation, chemical (of halides with potassium phthalimide); Halogen compounds (reactions of, with K phthalimide).

111. Xiang Li, Eric A. Mintz, R. Bu Xiu, Olivier Zehnder, Christian Bosshard, and Peter Günter. Phase transfer catalysis for tandem alkylation of azo dyes for the synthesis of novel multifunctional molecules. *Tetrahedron*, 56(32):5785–5791, 2000.

The following lecturers contributed to my education at the University of Basel (in alphabetical order):

T. Bickle, Th. Boller, E. Constable, W. Gehring, G. Gescheidt, G. Giese, P.C. Hauser, C. Housecraft, H. Huber, H.-C. Im Hof, U. Jenal, M. Jungen, T.A. Kaden, A. Keller, J.P. Maier, M. Major, W. Meier, M. Neuburger-Zehnder, M. Oehme, A. Pfalz, G. Schatz, P. Schiess, J. Seelig, U. Séquin, I. Sick, H. Sigel, P. Strazewski, L. Tauscher, C. Ullrich, H. Wennemers, T. Wirth, J. Wirz, W.-D. Woggon, A.D. Zuberbühler